EXPERIMENTAL STUDY OF PHOTON INDUCED GAMMA EMISSION OF $^{178}Hf^{m2}$ BY NUCLEAR SPECTROSCOPY METHODS

by

NICOLAE CATALIN ZOITA, B. S., M. S.

DISSERTATION

Presented to the Faculty of

The University of Texas at Dallas

in Partial Fulfillment

of the Requirements

for the Degree of

DOCTOR OF PHILOSOPHY IN PHYSICS

THE UNIVERSITY OF TEXAS AT DALLAS

May, 2005

UMI Number: 3163267
ISBN: 9780496971367

ProQuest Information and Learning Company
300 North Zeeb Road
P.O. Box 1346
Ann Arbor, MI 48106-1346

PREFACE

This dissertation could not have been completed without the guidance and help that I received over the years from all my teachers, professors and colleagues. I would like to thank all of them and express my sincerest appreciation, especially to Prof. Dr. Carl B. Collins of the University of Texas at Dallas for his support, invaluable guidance and instruction. I would also like to express my appreciation to the other members of my dissertation committee for their contributions to the completion of this work. I extend my gratitude to Acad. Prof. Dr. Ioan I. Popescu, Prof. Dr. Iancu Iova and Dr. Geavid Musa for their continuous support and guidance from the time I were undergraduate student of the Faculty of Physics from University of Bucharest, Romania. I am also deeply grateful to Dr. Mariana Braic and Dr. Viorel Braic of the National Institute of Optoelectronics (INOE-2000), Bucharest, Romania who have supervised my first steps in the experimental physics research.

I am deeply grateful to the entire international collaborators, who contribute in different ways to make this round of experiments a success. I wish to express my thanks namely to Dr. Farzin Davanloo, Claudiu Rusu, Tiberius Camase and Mugurel Iosif of the University of Texas at Dallas, Dr. Jean-Michel Pouvesle and Dr. Remi Dussart of the GREMI, CNRS - Universite d'Orleans, Orleans, France, Prof. Shuichi Emura of the University of Osaka, Japan; Dr. Yoshitaka Yoda and Dr. Tomoya Uruga of the SPring-8 - JASRI, Japan; Prof. Bruce Patterson and Dr. Bernd Schmitt of the SLS - Paul Scherrer Institut, Villigen, Switzerland; Dr. Calin Ur of the National Institute of Physics and Nuclear Engineering (IFIN-HH), Romania; Dr. Vladimir I. Kirischuk and Dr. Nicolai V. Strilchuk of the Institute for Nuclear Research,

Kiev, Ukraine; Dr. Forrest J. Agee of the Air Force Office of Scientific Research (AFOSR), Arlington, USA; Dr. Martin Stickley of the Defense Advanced Research Projects Agency (DARPA), Arlington, USA.

Grateful thanks for the guidance given to me are due to Mrs. Margie Renfrow, the Graduate Counselor and Student Coordinator of the Physics Department.

Finally, I wish to thank my family for their continued love and support during this long trip: my mother, my parents-in-low, my sister, my sister-in-low and my good cousin. My deepest gratitude goes to my best friend who has given me hope and support to finish this work. She is my wife, Carmen Angela Zoita.

This dissertation was produced in accordance with guidelines which permit the inclusion as part of the dissertation the text of an original paper, or papers, submitted for publication. The dissertation must still conform to all other requirements explained in the *Guide for the Preparation of Master's Theses, Doctoral Dissertations, and Doctor of Chemistry Practica Reports at The University of Texas at Dallas*. It must include a comprehensive abstract, a full introduction and literature review, and a final overall conclusion. Additional material (procedural and design data as well as descriptions of equipment) must be provided in sufficient detail to allow a clear and precise judgment to be made of the importance and originality of the research reported.

It is acceptable for this dissertation to include as chapters authentic copies of papers already published, provided these meet type size, margin, and legibility requirements. In such cases, connecting texts which provide logical bridges between different manuscripts are mandatory. Where the student is not the sole author of a manuscript, the student is required to

make an explicit statement in the introductory material to that manuscript describing the student's contribution to the work and acknowledging the contribution of the other author(s). The signatures of the Supervising Committee which precede all other material in the dissertation attest to the accuracy of this statement.

November, 2004

EXPERIMENTAL STUDY OF PHOTON INDUCED GAMMA EMISSION OF $^{178}Hf^{m2}$ BY NUCLEAR SPECTROSCOPY METHODS

Publication No._____

Nicolae Catalin Zoita, Ph.D.

The University of Texas at Dallas, 2005

Supervising Professor: Carl B. Collins

The induced release of the energy stored in nuclear isomers in the form of an incoherent gamma burst is of great scientific and technological importance. Powerful sources of induced gamma-ray radiation could be obtained, which would be an intermediary step to the development of a gamma-ray laser. High-energy nuclear isomers with very long lifetimes of the order of years and higher can serve as good active media. For instance, a macroscopic sample of $^{178}Hf^{m2}$ isomer stores about 1 *GJ/g* as excitation energy of the isomeric state. Photonuclear reactions induced by real or virtual photons are the most promising mechanisms to release the energy stored by $^{178}Hf^{m2}$ nuclei. The isomeric nucleus is excited to an intermediate level from which cascade to the ground state emitting γ-photons. The nuclear level density approaches one per *keV* at those excitation energies. Experimental investigations by nuclear spectroscopy methods conducted in this work revealed that the decay of $^{178}Hf^{m2}$ is

accelerated when the energies of the incident photons were tuned at about 20,825 *keV*, 11.15 *keV* or near the L_3 photoionization threshold of atomic hafnium at 9561 *keV*. In the first case, the presumed mechanism was the direct photoexcitation of the *m2* isomeric nucleus to a trigger level at about 2466.9 *keV*. There was a strong decay branch from this trigger level to the 11^- level of the 8^- band that caused the accelerated emission of gamma photons from many of the transitions detected in the unperturbed spontaneous decay. In the second case, a trigger level at about 2457.2 *keV*, that meant 11.15 *keV* above the 16^+ isomeric level, was mediating the energy release. The direct transition from this level to ground state was observed. Other branches of its decay enhanced the γ-emission of the ground state band (GSB) members. In the third case, complex electron bridging mechanisms were implied when incident X-ray photons were tuned at energies near the L_3 photoionization threshold. Those phenomena have been largely termed Nuclear-XAFS effects. They could induce a fast release of the energy stored by the isomer. The induced deexcitation cascade was by-passing the 8^- band and included the 130.2 *keV* and 642.5 *keV* transitions, non-members of the spontaneous decay. At about 9567 *eV*, a sharp peak of the excitation function of the induced gammas indicated a nuclear photoexcitation of another trigger level. The results of this research offer a much deeper understanding of the processes governing the induced gamma emission by soft x-ray photons of $^{178}Hf^{m2}$ and bring a step forward to the development of a new generation of energy storage devices at the nuclear scale with controlled release of stored energy.

TABLE OF CONTENTS

LIST OF FIGURES

LIST OF TABLES

CHAPTER 1

INTRODUCTION

The possibility of inducing the gamma rays from excited nuclear states has been studied for more than four decades, and predictions about this possibility are know in the scientific literature from very early times [1]. The use of X-rays to stimulate the decay of nuclear isomers - the Photon Induced Gamma Emission (PIGE) - is at the focus of a great scientific and technological interest, leading to the development of a gamma-ray laser (glaser). This would be the ultimate form of power released as electromagnetic waves characterized by coherence and directionality, the shortest wavelength emitted by the matter, and the highest photon density.

At this time, just a controlled released of nuclear energy in the form of incoherent gamma burst would be of great technological importance while being at the same time an intermediary step to achieve a glaser by providing the means for pumping a gamma-ray laser. Such a device could find its right place in a multitude of applications [2, 3]. Progress in advancing this technology has already taken advantage of the highest electromagnetic energy densities that can arise from phenomena at the atomic scale. To reach higher photon energies and flux densities requires the excitation of states within the nucleus, because the greatest non-nuclear energy may be founded in the movement of the nucleons, the nucleus constituents.

In a similar manner, with atomic electrons, the nucleons may absorb the photons of the electromagnetic waves and make a transition to an excited quantum state of higher energy. The deexcitation of nuclear exited states is usually dominated by spontaneous electromagnetic

emission and the transition probabilities strongly depend on the intrinsic structures of initial and final states. As in the case of atomic metastability, the selection rules may sometimes inhibit the coupling of a nucleon motion to the electromagnetic field, making the lifetime of exited states higher than the usual ($\sim 10^{-12}$ *s*). However, the nuclear metastability phenomena are more complicated and several physical mechanisms are responsible [4, 7], leading to the classification of the long-lived exited states as shape-, spin- and K-isomeric states [5]. They are commonly found to exist in many different nuclides within a wide range of energies (from *KeV* to few *MeV*) with half-lifes ranging from *ns* to years and even thousand of years. In principal, several isomeric states may arise at different excitation energies within the same nucleus due to different mechanisms [6].

For practical realization of an induced gamma emission device, nuclear isomeric materials would be the right active medium. Nuclear isomers with very long lifetimes of order of years and higher will fit best the needs for storing the energies for long period of times. That will allow *ex-situ* input of the energy into the isomeric states through nuclear reaction mechanisms long before the time of use. Because of the high excitation energies of some isomeric states, the amount of energy that can be stored and that is able to be released as a pure electromagnetic emission, can reach remarkable levels. A macroscopic sample of such an isomer will store orders-of-magnitude more energy per gram than that available from chemical compounds [8].

For practical applications, once an active medium of isomeric material is created, efficient techniques must be used for releasing the energy stored in the nuclear isomers. Such a method should be able to supply a controlled release of energy at different levels of power or at least to enhance the natural decay by a constant fraction. That means it could gradually and efficiently modify the half-life of isomeric states [9]. In order to design efficient techniques for modulating of the isomeric decay, detailed theoretical and experimental studies are required to characterize

different isomeric materials and the different processes implied in the mechanism of triggered gamma emission.

Many concepts have been put forward for the developing of an efficient dumping mechanism of the isomeric energy. One of the most promising approaches is the X-ray triggering into an up-conversion scheme [10], which implies the excitation of isomeric nuclei to some higher mediating level with subsequent prompt decay to lower states by emission of gamma radiation or by internal electron conversion. The giant pumping resonance (GPR) [11, 12] - a strong (γ, γ') photonuclear resonance reaction - it is already known [13] as an efficient dumping mechanism of isomeric energy via K-mixing gateway states [7]. Such states are common in the island of masses near 180, usually lying at few *MeV* from the ground state of those nuclei [6, 7]. Long-lived isomers with energy in the proximity of the K-gateways are very attractive candidates for mass storage devices because they require low input energy in order to be excited to the intermediate states. If the required energy is comparable with inner-shell transitions of surrounding electrons, more efficient nuclear excitation mechanisms may be based on higher-order nuclear excitation processes. Most widely known candidates for such effects include second-order non-radiative process of nuclear excitation via resonance electron transition (NEET) [14] with the same multipolarity, via electron capture from the continuum by a vacancy in an electron shell (NEEC) [15] and nuclear excitation via a third-order mechanism which is referred to as the inverse electron bridge (IEB) [16].

Other proposed mechanisms effectively can influence the life-time of the isomeric states. These mechanisms are based on the inter-equilibrium that exists between the electronic-shell structure and the nuclear structure. For example, the probability of the internal conversion process, one of the fundamental nuclear decay channels, depends directly on the presence of

electrons in the corresponding atomic state. Ionization of one of these shells leads to an increase of the nuclear state half-life. Also, there are situations when the ionization results in a sharp increase in the total probability of the nuclear isomer decay. Responsible for that can be the bound internal conversion (BIC) [17] or electron bridge mechanism (EBM) [16].

It may be concluded that there are many possibilities for inducing the energy release of nuclear isomers, one or another mechanism may dominate for a specific isomer. A list of most advantageous isomeric materials was necessary [8, 11], taking into account a set of parameters such as the excitation energy of the isomeric state and its half-life, the cross section for potential mass production and possible mechanisms for inducing the energy release. It was clearly established that $^{178}Hf^{m2}$ [18] is one of the most interesting isomers from the perspective of energy storage. The $I^{\pi} = 16^{+}$ isomeric state has 31-years half-life and is lying at about 2.446 *MeV* [19]. The isomer is not naturally occurring and at present is not available in amounts larger than about 10^{16} atoms in the *m2* state. It was established in 1995 [20, 21] from experimental systematics for the photoexcitation of neighboring isomeric nuclei that it might be possible to trigger gamma emission from $^{178}Hf^{m2}$ in a (γ, γ') reaction using incident X-rays having energies on the order of 300 *keV* or less. This fact is of special technological interest because of the availability of high-intensity flux and low cost X-ray sources, and because of the high energy gain obtained.

The Center for Quantum Electronics (CQE) of The University of Texas at Dallas (UTD) was the first laboratory in the world which reported successful efforts for induced release of the energy stored in the $^{178}Hf^{m2}$ in 1998 [22, 23]. A commercial X-ray generator was used to irradiate a sample containing 6×10^{14} isomeric nuclei. Up to now, continued efforts have been done in order to add new details to the description of the induced deexcitation mechanism.

This thesis summarizes the author's contribution to the recently published papers and it falls into 8 chapters. This introduction is followed by subchapter 2.1 which review the nuclear structure in the 180 mass-region and the nuclear K-isomerism phenomenon. Subchapter 2.2 review the nuclear photoexcitation processes with special emphasize on higher order excitation processes, such as NEET and IEB mechanism. Chapter 3 presents experimental aspects implied in studying of PIGE on $^{178}Hf^{m2}$ by nuclear spectroscopy methods. The first subchapter is a description of the X-ray sources used in this work for irradiation of the isomeric samples, accentuating on the author contribution to the redesigning and characterization of the Bremsstrahlung X-ray device. It follows subchapter 3.2 which review standard methods and instrumentation used in X- and γ-ray spectroscopy. Subchapter 3.3 presents an original data acquisition system designed and implemented by this author for single spectra and γ-γ coincidence measurements, and also for time-resolved measurements in experiments with Bremsstrahlung and synchrotron radiation. The successful results in the inducing of the gamma emission of $^{178}Hf^{m2}$ isomeric nuclei are presented in the chapters 4, 5, 6, and 7, while chapter 8 summarizes the main conclusions of the experiments conducted in this thesis.

CHAPTER 2

REVEW OF GENERAL CONCEPTS

Nuclear Excitations. Nuclear Isomers. NEET/EBM Processes

2.1 The Atomic Nucleus. Collective and Quasiparticle Excitations. Isomers

The concept of the atomic nucleus was first advanced by Rutherford in 1911 [24], who showed that all of the positive charge and almost the entire atomic mass are concentrated on a central nuclear core with radius of the order of 10^{-5} that of the atomic radius. The nucleus is now understood to be a quantum system composed of protons and neutrons. In addition to its atomic and mass numbers, a nucleus is also characterized by its size, shape, binding energy and half-life if it is unstable.

Over time different theoretical models have been developed to explain more or less of the nuclear structure. Two broad classes of models have been proposed: independent particle models and collective models. The Independent Particle Model known as Shell Model or Single Particle Model [25-28] is similar to the atomic model, where electrons arrange themselves into shells (degenerate single particle states) around the nucleus under a central force potential. In the same way, the motion of each nucleon is determined by an average spherical symmetric potential due to the average attractive force of the other nucleons that are considered to be static. The alternative Spherical Shell Model [25-28] best describes spherical nuclei with a spherical Woods-Saxon (WS) potential [29] coupled with a strong spin-orbit potential. This term arises from the coupling between the intrinsic angular momentum ($\boldsymbol{s}$) and orbital angular momentum ($\boldsymbol{\ell}$) of the each individual nucleons, the so called $\boldsymbol{j}$-$\boldsymbol{j}$ coupling, with $\boldsymbol{j} = \boldsymbol{\ell} + \boldsymbol{s}$. The energy levels of each j-shell are $(2j+1)$ degenerate and are

labeled by m_j (the projection of $\boldsymbol{j}$). The WS potential together with the spin orbit term can be expressed as [29, 30]:

$$V_{WS}(r) = -\frac{V_0}{1+e^{(r-R)/a}} + V_{SO}\,\boldsymbol{\sigma}\cdot\boldsymbol{s} \qquad (2.1)$$

where R is the radius of the nucleus, r is the radial distance from the center of potential, a is a parameter that determines how sharply the potential increases to zero and V_0 defines the depth of the potential. The form of this potential is somewhere between a simple harmonic oscillator and a square well potential. The spin-orbit potential gives the proper separation of the subshells.

There are separate energy levels for protons and neutrons, the arrangement of the nucleons on levels respecting the Pauli principle, which require that each nucleon have a unique set of quantum numbers to describe its motion. The ground state of a nucleus has each of its protons and neutrons in the lowest possible energy level. Exited states are then described as promotions of nucleons to higher energy levels. Closed shells occur at proton and neutron "magic numbers" (2, 8, 20, 28, 50, 82, 126, 184) where there are large energy gaps between successive nuclear orbitals. At these shell closures, the binding energy of the last nucleon is much larger then the corresponding value in the neighboring nuclei, double magic nuclei are very stable.

The spherical phenomenological single-particle model succeeds in the explanation of the magic shell closures and of the properties of nuclei nearby, but needs modifying to describe nuclei with many nucleons outside closed shell. The residual interaction between these many valence nucleons may be more simply described in terms of deformed potential, which takes into account the collective behavior of the nucleus.

The Collective Models [26-28, 30] treat a nucleus like a charged incompressible liquid drop of constant density and with a sharp surface whose motion may produce surface oscillations around the

equilibrium shape. Further it may rotate if the nucleus is permanently deformed, that means if it is deformed in its ground state. The nuclear surface may be described by an expansion in spherical harmonics functions with time dependent shape parameters as coefficients [30].

$$R(\theta,\varphi) = R_0\left(1+\sum_{\lambda=2}^{\infty}\sum_{\mu=-\lambda}^{\lambda}\alpha_{\lambda\mu}Y_{\lambda\mu}(\theta,\varphi)\right) \qquad (2.2)$$

where R_0 is the radius of the spherical nucleus and $\alpha_{\lambda\mu}$ (not all independent) are the coefficients of the spherical harmonics $Y_{\lambda\mu}(\theta,\varphi)$. The quadrupole deformations ($\lambda = 2$) predominate, giving the main nuclear shape symmetries: prolate (elongated form), oblate (flattened form) and triaxial, besides the spherical symmetry. Only the first two deformations enumerated above have axial symmetry ($\beta \equiv \alpha_{20} \neq 0$), describing spheroidal nuclei. Octopole deformations ($\lambda = 3$) - the principal asymmetric modes of the nucleus - describe reflection asymmetry in the nuclear shape, that gives the nucleus a shape similar with that of a pear. A direct consequence of deformations to the movement of single nucleons is that the orbital angular momentum and the intrinsic spin are no longer good quantum numbers in axially symmetric nuclei. The energy of the states of each single particle depend on the spatial orientation of the orbit, that means the energy depends on the component (Ω) of angular momentum ***j*** projected along the symmetry axis of the core (figure 2.1). This component becomes a conserved quantum number together with the projection *K* on the symmetry axis of total angular momentum (***I***) of the nucleus. Levels with $\pm\Omega$ have the same energy due to reflection symmetry of axially symmetric nuclei, so that each state is doubly degenerated, The ordering of these levels depends on the particular shape of the nucleus. For prolate nuclei the states with the lowest Ω values are most tightly bound whereas for oblate nuclei, the highest Ω orbital occurs lowest in energy [30].

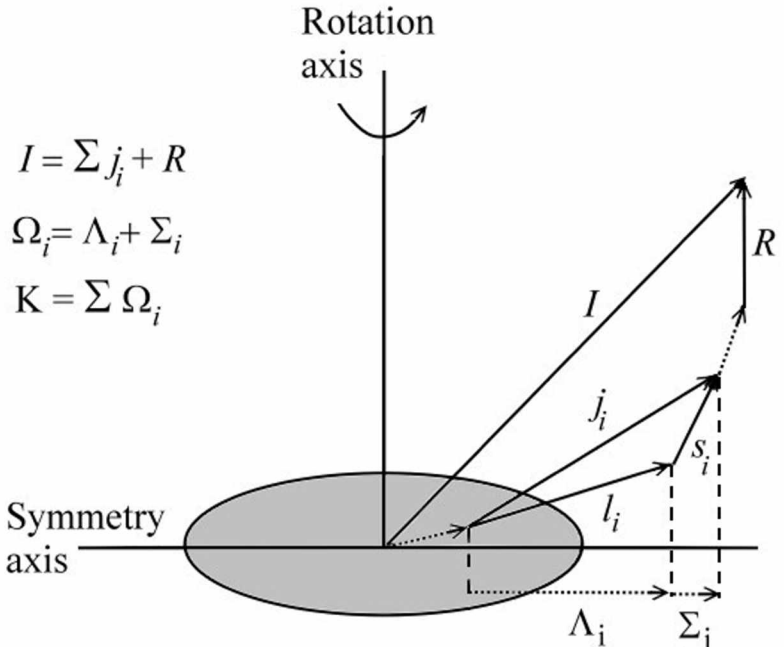

Figure 2.1. Angular momentum coupling in spheroidal deformed nuclei. ***I*** is the total angular momentum of the nucleus, ***R*** is the collective rotation and $\boldsymbol{j_i}$ is the single particle component. *K* is the projection of ***I*** on the symmetry axis. Ω_i denotes the angular momentum projection of the i^{th} particle.

The Collective Model [26-28, 30] describes the nuclear collective vibrations as tridimentional harmonic oscillations of the nuclear surface defined by (2.2), around an equilibrium surface, in this case, the phonon (the vibration quanta) of multipolarity λ, carry the energy. The vibration states are equally spaced, being about 1 *MeV* for medium height nuclei. In addition to the vibration around the equilibrium shape, the nuclei with permanent non-spherical equilibrium shape may rotate as a whole preserving both the deformed shape and the internal structure. While the most common deformed nuclear shape is spheroidal, the Symmetric Rotor approach [26-28, 30] treats the nucleus as having axial symmetry and is rotating around an axis perpendicular on the symmetry axis. Associated with this rotation is a sequence of rotational energy levels with energies described by the $I\,(I+1)$ rule, where I is the total angular quantum number of the nucleus. Such levels are well identified in the mass regions $150 < A < 190$ and $A > 220$, which are both well away from closed shell region. The rotational motion depends on the deformations and is far slower than the vibrational and internal motion. The correct picture of a rotating deformed nucleus is a stable equilibrium shape determined by nucleons in rapid internal motion in the nuclear potential.

Collective excitations dominate the low energy spectra of Z-even, N-even nuclei. In the mass region $A < 150$, the even-even nuclei are generally treated as spherical nuclei with vibration spectra, and a good approach is a model based on quadrupole vibrations about a spherical shape. The mass-regions $150 < A < 190$ and $A > 220$ are characterized by permanently deformed nuclei exhibiting rotational spectra. In fact, vibration and rotation motions coexist in deformed nuclei; the Rotation-Vibration Model describes the even-even spectra as rotational bands built on the vibrational states.

In the odd-odd and odd-A nuclei additional complexity appears from the influence of the individual motion of the unpaired nucleons. The picture is that of a one neutron and/or one proton

added to a collective even-even nucleus so that excitations of both collective and single-particle are possible and in general are coupled. The Particle-Rotor model is widely used to interpret the low-lying spectra of odd-A nuclei. The model includes a single-particle Hamiltonian describing the particle motion in an average deformed nuclear potential, a rotational Hamiltonian describing the rotational motion of the even-even core, and a residual Hamiltonian for adding residual interaction such as pairing.

Many versions of the single-particle Hamiltonian have been tested, these differ either in the form of the potential or in the parameterization of the shape [28]. Such potential may be easily obtained by extending the spherical form of WS potential (2.1) to deformed nuclei by taking into account the parameterization (2.2) [30]. The mostly used potential is the modified harmonic oscillator (MHO) or deformed Nilsson potential [31, 32] which comprise, as the name says, an deformed tridimentional harmonic oscillator potential together with the spin-orbit force and the $\boldsymbol{\ell}^2 - \langle \boldsymbol{\ell}^2 \rangle_N$ term introduced to simulate the fattening of the nuclear potential at the center of the nucleus. The Nilsson single-particle orbitals are labeled by the asymptotic quantum numbers $\Omega^{\pi}[N\ n_z\ \Lambda]$, where N is the principal harmonic oscillator quantum number and n_z is the number of oscillator shell quanta along the symmetry axis. The parity of the state is defined by $\pi = (-1)^N$. The projection of the orbital angular momentum ($\boldsymbol{\ell}$) on the symmetry axis is denoted by Λ (figure 2.1).

The pairing interaction - the most important residual interaction - is treated in terms of BCS model [28]. It reflects the nucleon-nucleon interactions which results in favoring even-even nuclei over odd-N and/or odd-Z nuclei, and thus the binding energy due to pairing is higher for even-even nuclei making them more stable. The net effect is a *compression* of the single-particle-level energies, which can be 1.5 to 2 times. The single-particle-level corrected for pairing is termed as quasiparticle-

level. In the strong-coupling limit, which is associated with large shape deformations, the quasiparticles are coupled separately at the symmetry axis in states characterized by their components of angular momentum Ω_i along the symmetry axis (figure 2.1). Pair-breaking particle excitations are termed as quasiparticle excitations, adding more quasiparticles to the even-even core nucleus. This may result in states with high total spin and high K-projection ($K = \Sigma\, \Omega_i$).

The rotational Hamiltonian adds rotational energy states to the system. The spectrum consists on bands of rotational states built on each quasiparticle state. The spin of the states takes certain restriction when [26-28, 30]

$$K= 0 : I = 2, 4, 6 \qquad (2.3)$$

$$K\neq 0 : I = K, K+1, K+2, \ldots$$

The structure of rotational bands (2.3) shows how the collective picture of the nucleus allows successive levels into a band having a spin difference of one or two units for angular momentum and the same parity. The electromagnetic transitions between such levels should obey the general selection rule which states that the multipolarity L and parity π of a γ- transition $(K_i,,I_i,\pi_i) \rightarrow (K_f,I_f,\pi_f)$ are subject to (2.4) restrictions [26-28, 30]. An additional requirement is that no radiation of null multiple order can occur.

$$\left| I_i - I_f \right| \leq L \leq \left| I_I + I_f \right|, \quad \pi = \pi_i\, \pi_f \qquad (2.4)$$

$$\Delta K = \left| K_i - K_f \right| \leq L$$

The probability of the allowed transitions depends on the energy and the multipolarity of the transition, but more sensitive to the wave functions of the nuclear levels involved. The selection rules permit several multipoles to be emitted; the lowest permitted multipole usually dominates, while the emission of superior multipoles is less probable by orders of magnitude. The electric multipole

emission is usually more probable than the same magnetic multipole (of course it can not exist in the same radiation field). Also, it may be stated that the inter-band electromagnetic collective transitions are most probable than the intra-band transitions, because in the latest case large changes in spins, shapes and quasiparticle configuration may be required. That is why in general, the transitions starting from bandheads are less probable. A low transition probability to any lower energy level results in a higher half-life of the exited state, leading to nuclear isomerism.

There does not exist a strict definition of the minimum half-life that an exited state should have in order to qualify as isomeric state. Practically, the isomeric half-life should be longer than that of the most of the exited states, and this limit is generally considered to be in the order of nanoseconds. An isomer may deexcite by one or more established radioactive decay modes, such as α-, β- or γ-ray emission, but being retarded or hindered because of significant changes in the shapes and angular momentum, that are the basis of the occurrence of the isomers. From this perspective the nuclear isomers can be classified in shape-, spin- and K- isomers [5]. In the shape-isomer class can be found the fission isomers for which decaying back to the ground state by γ-ray emission competes with fission into two lighter nuclei.

A more common form of isomerism is the spin-isomerism [5]. It occurs when the nuclear decay to the lower energy states by electromagnetic processes requires a large change in nuclear spin, strongly lowering the transition probability. If the nucleus is permanently deformed with spheroidal symmetry, the electromagnetic decay probability depends not only on the magnitude of the nuclear angular momentum vector, but also on its orientation relative to symmetry axis, denoted by K quantum number. The K-selection rule (2.4) requires that the multipolarity of the decay radiation to be as large as the change in the K-value, so that a large K-changing transition is strongly hindered,

resulting in a long half-life. This is the K-trap mechanism responsible for the K-isomers in the 150-190 mass region. Isomers with 2- or 4-quasiparticle are common in this region [5, 6, 7] that are significant for modulated PIGE decay.

The experimental identification of K-forbidden transitions demonstrates that there are symmetry-braking processes that make K an approximately good quantum number and that there are mixings of these quantities [6]. The quantity

$$\nu = \Delta K - L \qquad (2.5)$$

expresses the degree of K-forbiddenness, which establishes the degree of hindrance of the corresponding transition [5, 6, 7]. Empirically, each K-forbiddenness unit reduces the transition rate by a factor of 10^2 approximately [6, 7]. For example, the $K^{\pi} = I^{\pi} = 16^{+}$ state of the $^{178}Hf^{m2}$ [18] isomer has 31-years half-life [19]. This state decay predominantly to the $I^{\pi} = 13^{-}$ member of the $K^{\pi} = 8^{-}$ band by an 13 *keV* electric octupole (E3) transition that requires a total orientation change of angular momentum vector of $\Delta K = 8$ units. This leads to a forbiddenness degree $\nu = 5$ units and a hindrance factor is about 10^{10} which explains the long half-life of the isomer. Therefore, the $^{178}Hf^{m2}$ isomer is simultaneously a spin-trap ($L > 1$) and a K-trap ($L < \Delta K$). Its high-K quantum value is the consequence of its 4-quasiparticale structure that is explicitly presented in the subchapter 4.1. If the K-trap was not to occur, a half-life of about 100 *ms* would be expected for the 13 *keV* transition [6].

Different mechanisms such as γ-tunneling [7, 33, 68] or the Coriolis effect [7, 34] have been proposed to explain the decay of the nuclear configuration where a K-forbidden transition takes place. In addition, when two levels of the same spin and parity lie close in energy, the wave-functions of low-K and high-K states can mix, effectively reducing ΔK and resulting in a faster transition. Which permits transitions that otherwise, would be completely forbidden [7].

It indicates that the K-mixing phenomena have an important role in PIGE with high-K isomers. The mixing levels in the higher proximity of the isomeric state will efficiently work as gateways into an up-conversion triggering scheme. On the other side, same factors responsible for the K-mixing of the gateway states may contribute to the K-mixing of the isomeric state increasing the probability of spontaneous emission and so, lowering its long-time energy storage capability. From this perspective, $^{178}Hf^{m2}$ isomer is the most promising media for an energy storage and controlled release device. That is because it has a high excitation energy and long half-life, and indications of K-mixing gateways in the higher proximity of the isomer already exist [63-66].

2.2 Nuclear Excitation Processes

The energy stored in a long-lived nuclear state is usually released spontaneous by gamma-ray emission or internal electron conversion with a total rate determined by the half-life of the corresponding isomeric state. Triggering or “dumping” of an isomeric nucleus implies an induced release of that energy. Isomeric states which differ substantially in spin from the ground state can not be dumped or populated directly in photoinduced reactions due to the low transfer of angular momentum by photons, as presented in previous paragraph. The proposed method is called up-conversion scheme [11] that excites the isomeric nucleus to some higher short-lived intermediate states with subsequent prompt decay to lower states by emission of γ-radiation or by internal conversion processes (figure 2.2). The K-mixed states would work best as triggering gateways of K-isomers. Therefore, the first step of an up-conversion scheme should be one of nuclear excitation starting from an isomeric state, and this process should be externally controlled.

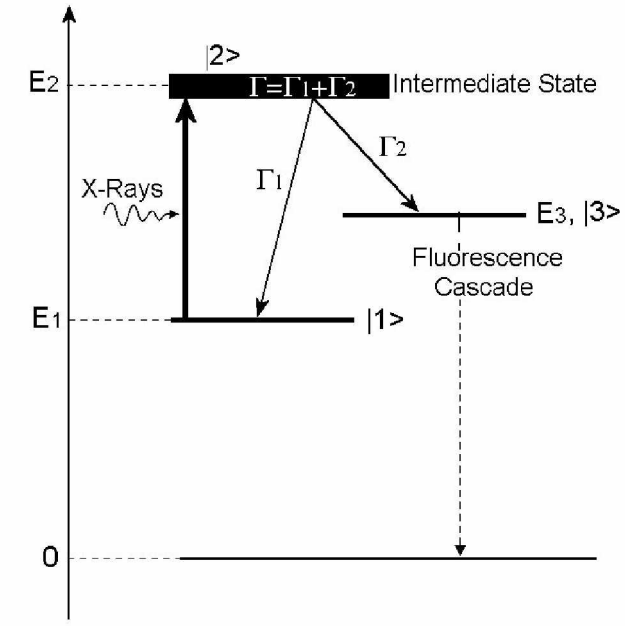

Figure 2.2. The up-conversion scheme for induced gamma emission of nuclear isomers. The resonant absorption of an incident X-ray photon is followed by the release of a fluorescent cascade.

Nuclear excitations may take place due to the interaction of the nucleus with electromagnetic radiation (i.e. radiative excitation by absorption of externally produced X-rays) or with particles and generally are not associated with the atomic electrons outside of the nucleus. However, there are several processes in which the inner-shell electrons take part in the excitation of the nucleus and may become important when the excitation energy is comparable with the binding energy of the atomic electrons [14, 16].

Interaction of photons with atomic systems is complicated and many processes could take place, with one or two dominating interactions in different ranges of incident photon energy. In general, one can assert that the interaction between X-ray or γ-ray and atomic systems are single, identifiable process, characterized by a cross section. Such an interaction may primarily be a scattering event or may essentially be an absorption process, due to both the electronic and nuclear parts [28].

In atoms, as in nuclei, the elementary processes induced by incident photons may be classified into a number of phenomenological distinguishable types. There are coherent scatterings from the atoms (Rayleigh or electron resonance scattering) or from nuclei (nuclear Thomson and nuclear resonance scattering). When the energy of the gamma-rays becomes much greater than the binding energy of electrons or of nucleons, incoherent Compton scattering from the individual nucleons or electrons in the atom will occur. On the other hand, there are two discernable absorption processes in which the energy of the incident photon is completely absorbed. In the first one, designated as resonant absorption, the atom or the nucleus makes a transition to a real or virtual excited state. The second process, in which a nucleon or electron is directly ejected, leaving the residual nucleus or atom into a low-lying state. Besides interacting with electrons and nucleons, gamma-rays can also interact with electric field surrounding electrons or nucleons. The incident photons may be absorbed in

electron-positron pair production or scattered by virtual electron-positron pair (Delbrück scattering) if the photon energy is greater then 1.02 *MeV*. A schematic illustration of the energy dependency of cross sections of the principal elementary processes enumerated above as a function of the incident photon energy is presented in figure 2.3 a), with an expanded view of the total photonuclear cross section in figure 2.3 b).

2.2.1 Nuclear Photoabsorption. (γ, γ') Reaction

In the interaction of γ-rays with nuclei the excitation of nuclear levels occurs either as a result of photoabsorption or in inelastic scattering of photons. A schematic illustration of the energy dependency of the total photonuclear cross-section ($\sigma_{Ph.N}$) as a function of the photon energy is presented in figure 2.3 b). The dominant feature of $\sigma_{Ph.N}$ is the broad peak corresponding to the giant resonances, the most important of which is the giant dipole resonances (GDR) [27, 28], described in the liquid-drop model as collective vibrations of proton fluid against neutron fluid as a whole. The energy of GDR peak is roughly located at $60A^{-1/3}$ *MeV* [28], typical values are in the range of 10 to 20 *MeV*. The continuous shape of GDR begins at energy in the closed proximity of the threshold for particle emission where a compound nucleus may result. This is a state of extreme excitation which may decay by γ-emission, particle emission (protons, neutrons, alpha particles) or fission. Like any other quantum-mechanical system, it can be excited only to its discrete energy levels. If the widths of these levels are larger than the distance between resonances, the total absorption cross section will have a continuous shape. At lower incident photon energies, below the particle emission threshold, collective and single-particle excitation may occur resulting in sharp scattering resonances as shown in figure 2.3 b).

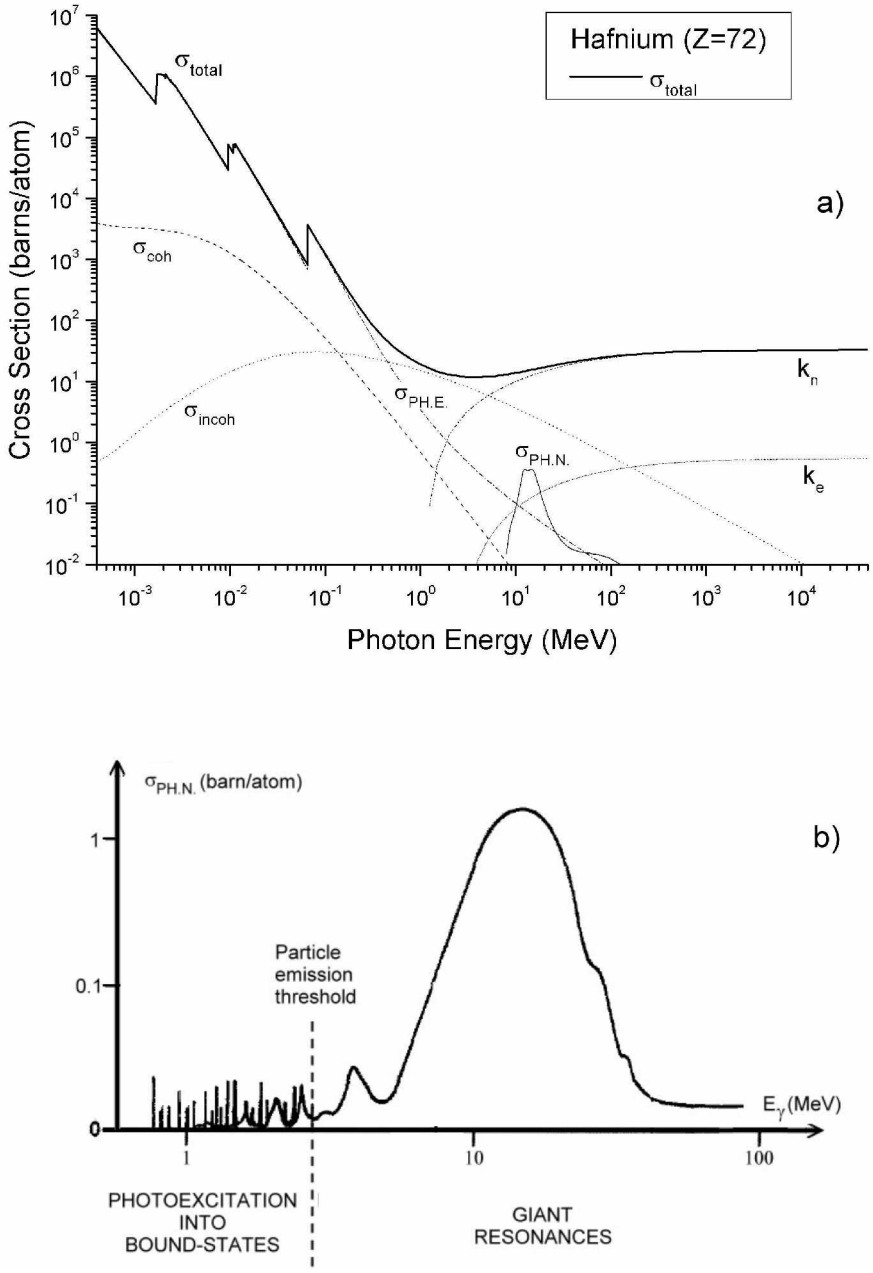

Figure 2.3. a) Contributions to the total photon interaction cross section σ_{tot} of atomic photoeffect, $\sigma_{PH.E}$, coherent scattering, σ_{coh}, incoherent scattering, σ_{incoh}, nuclear-field pair production, k_n, electron-field pair production, k_e, and nuclear photoabsorption, $\sigma_{PH.N}$

b) Total photonuclear cross section, schematic view

Making the assumption that the excited level is isolated from other levels and that it has an total intrinsic width (FWHM) $\Gamma = \Gamma_1 + \Gamma_2$ much less than the transition energy $E_0 = E_2 - E_1$ shown in figure 2.2, the single level resonant absorption cross section of incident gamma radiation with energy E_γ, has a Breit-Wigner (BW) form [28, 30]:

$$\sigma_\gamma(E_\gamma) = g\frac{\pi}{2k^2}\frac{\Gamma_\gamma\Gamma}{(E_\gamma - E_0) + \Gamma^2/4} \qquad (2.6)$$

where k is the wave number of incident radiation and Γ_γ is the corresponding radiative nuclear transition width, coincide with Γ_1 in the context of the up-conversion mechanism shown in figure 2.2. The statistical factor g takes into account the spin-multiplicities of the initial and final states. Replacing in the numerator of equation 2.6 the total intrinsic width Γ with the partial width Γ_2 of the decay from the gateway |2> to the fluorescence level |3>, one may obtain the expression of the cross section for the induced decay to the |3> level via intermediate level |2>. The population transferred from initial state (isomeric state in this case) to the fluorescence level by an incident radiative field with a spectral flux density F(E), can be expressed as $N = N_{iso}\int\sigma(E)F(E)dE$. For narrow resonances, such the levels below the particle evaporation threshold, the BW form may be approximated by a $\delta(E_\gamma - E_0)$ function [28]. In this context, the integrated cross-section becomes $\sigma\Gamma = \int\sigma(E)dE = = (N/N_{iso})*(1/F(E_0))$, which may be determined experimentally from the measured values of the of the fluorescence yield N/N_{iso} and of the irradiation flux density $F(E_0)$.

Such measurements were performed for the first time by the Center for Quantum Electronics of the University of Texas at Dallas [13]. An integrated cross section of 1.2×10^{-25} cm^2keV has been found for the $^{180}Ta^m(\gamma,\gamma')^{180}Ta$ reaction channel via an intermediate state of narrow band of states near 2.8 *MeV* [11]. The absorption mechanism discovered has been called giant pumping resonance (GPR) [11, 13].

2.2.2 Nuclear Excitation Involving Inner-Shell Electrons. NEET. IEBM.

At very low energies, below 150 *keV*, the effects on the atomic structure dominate the interaction of photons with matter, prevailing the photoelectric effect. Photoelectrons may be ejected from any of K, L, M,.. shells of the atom. The ionization cross section of the inner-shell electrons with the binding energy E_i, by incident photons with energy closed to the threshold of ionization, $(E_\gamma - E_i) << E_i$, may be expressed as [35]:

$$\sigma_i^{(r)} \cong 6.27 \times \frac{1}{(Z-\beta)^2}\left(\frac{E_i}{E_\gamma}\right)^{8/3} \times 10^{-18}(cm^2) \qquad (2.7)$$

where β is the number of electrons screening the motion of the considered electron. The photoionization cross section has a maximum near the threshold energy of ionization E_i and it diminishes with an increase in the photon energy (figure 2.3).

When an inner-shell vacancy is created, two fundamental channels may contribute to the deexcitation of these atomic exited states: X-ray and Auger electron emissions. In the first process, as shown in figure 2.4(a), an electron in a higher-energy level transits and fills the hole with a photon emission. In the second process shown in figure 2.4(b), the electron in high level fills the hole and ionizes another outer shell electron via a virtual photon exchange. Also, if there exist free electrons near to the ionized atom, the atom may capture one of the free electrons with emission of radiation. This process is known as radiative-recombination.

In addition to these processes, there is the possibility that the excess energy released in atomic deexcitation or recombination processes to be near-resonantly absorbed by the nucleus conducting to a nuclear resonant excitation. It means that nuclear excitations may follow the electronic transitions

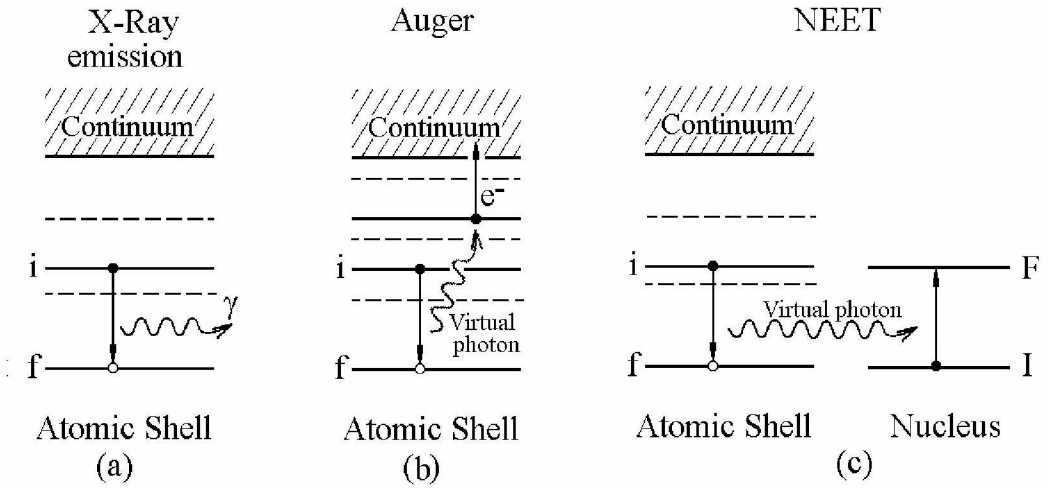

Figure 2.4. The fundamental atomic deexcitation processes. The probability of the NEET process can have upper limits between $10^{-3} – 10^{-2}$ relative to the total deexcitation process. Usual probability of Auger effect is about 10^{-2}, while the X-ray emission channel has a probability close to unity [Y. Ho et al., Phys. Rev. C 48, 2277 (1993)].

between two bound states, the process is known as nuclear excitation by electron transition (NEET) [14], or it may follow a free-to-bound electron transition, such case known as nuclear excitation by electronic capture (NEEC) [36, 37], which is the exactly inverse process of internal conversion. These higher-order processes become important only when the selection rules forbid faster modes or when the transition energy is low. The NEET process was first considered theoretically in 1973 by Morita [14]. He pointed out that an atomic inner-shell vacancy might decay by other than the two usual modes, X-ray and Auger-electron emissions, if the atomic and nuclear states have closely matching transition energies and also involve the same changes in spin and parity. Thus, excitation energy is transferred from the atomic electron system to the nucleus of the same atomic system via a near-field interaction (virtual photon exchange), as shown in figure 2.4(c). It is a non-radiative, rare but fundamental process of atomic deexcitation and also of nuclear excitation.

Using perturbation techniques, Morita [14] developed a first theoretical model to describe the NEET process and to calculate its probability (P_{NEET}), with discussions of NEET applicability to isotope separation. It has been stated that P_{NEET}, defined as the probability that the decay of the initial excited atomic state will result in the excitation of the corresponding nuclear state, is significantly less than unity. The upper limits for the cross section have been established later to reach up to a few 10^{-3} values relative to photoionization process [38, 39], because atomic processes such as X-ray and Auger electron emission, are fast relative to nuclear excitation and also because the emission of characteristic X-rays corresponds to the first-order perturbation process, while the Auger and NEET effects are treated as second order perturbation processes.

It was predicted that the highest NEET probability should be met in processes involving atoms with high atomic number (Z) where the sizes of the atomic orbits are reduced and the resonant

transition condition satisfied [14, 40]: $P_{NEET} \sim Z^8/\Delta^2$, where $\Delta = E_A - E_N$ is the energy mismatch between the atomic (E_A) and nuclear (E_N) transition energies involved in the process. The spin and parity changes of the atomic and nuclear transition must be exactly equal. This necessary condition results from the non-zero matrix element [14, 40] requirement. The physical meaning of resonance, $E_A \approx E_N$, is that even in ordinary atomic transitions, NEET always occurs if the multipolarity condition is satisfied, but the probability will be large enough to be observed only close to resonance. The finite widths of the initial and final states allow transitions to occur when energy matching is not exact.

Unlike NEET, in NEEC process, for a specific nuclear triggering energy, the resonance requirement can be satisfied exactly for some values of incident electrons, because a large number of atomic orbitals with ionization energy smaller that the nuclear transition energy could participate in the NEEC process, the electron capture could occur also into a partly filled electron shell (valence shell). Naturally, the NEEC probability via higher-lying orbitals tends to be less than those for lower-lying ones due to the decrease in coupling between electrons and atomic nucleus. It results that NEEC and NEET may coexist in some experimental conditions such as laser-induced plasma [41, 42, 43], their contribution could be comparable.

Over the years many theoretical and experimental investigations have been devoted to NEET. There were from the beginning big discrepancies between theory and experiments, due to both the imperfect theoretical models and ambiguous experiments.

Almost always the NEET process has been treated separately from the X-ray and Auger electron emission effects, while they take place concurrently in the deexcitations of excited atomic states. There are only two papers [38, 39] from the same group of authors who investigated the three processes together into an unified framework. It was concluded that the interference effects between

NEET and X-ray or Auger electron emission are negligible because of the great difference in magnitude between the NEET matrix element and the other two.

Also, all calculations of P_{NEET} assume that the NEET probability is independent of the electronic excitation or ionization process that generates the initial inner-shell holes, because the timescale for ionization (~ 10^{-19} s) is much shorter than the timescale associated with filling of the shell hole (~ 10^{-17} s) [44]. A quantitative treatment of both ionization and NEET processes in a unified framework is difficult and has not yet been carried out.

The most accepted form of NEET probability is the one that gradually accomplished by improvements performed over the time by different reference groups. Its final form [44] can be expressed as:

$$P_{NEET} = \left(1 + \frac{\Gamma_f + \Gamma_F}{\Gamma_i}\right) \frac{E_{\text{int}}^2 (i \to f, I \to F)}{\Delta^2 + (\Gamma_i + \Gamma_f + \Gamma_F)^2 / 4} \qquad (2.8)$$

where $\Gamma_{i,\, f,\, F}$ are the total widths of the initial and final hole states. The interaction energy (E_{int}) between nucleus and atomic shell is a function of the matrix element of i-to-f 2^L pole atomic transition and of the reduced transition probability associated with the nuclear excitation by the multipole transition from I-to-F. The energy of the current interaction is very sensitive to the values of the atomic matrix elements, i.e. to the calculated accuracy of the atomic functions of the K-, L-, M-,..shells [44]. If the initial atomic holes are generated in photoionization processes, the NEET cross section can be expressed by:

$$\sigma_{NEET} = \sigma_i^{(r)} P_{NEET} \qquad (2.9)$$

with photoionization cross section defined by equation (2.7).

The inverse process of nuclear deexcitation followed by the excitation of a bound electron to a higher-lying bound orbital is also possible and is known in literature as internal conversion between

bound states (BIC) [45] or inversed NEET (INEET) [46]. Its probability can be expressed as a function of NEET probability that occurs between the same atomic and nuclear levels [46]. It is a potential channel of deexcitation of isomeric nuclear levels, which can accelerate the decay of the isomers if vacancies are previously created in the corresponding atomic shell. Thus, it is one of the processes that can offer control over the isomeric decay, without implying an up-conversion scheme. Calculations have shown that, for example, with creating vacancies in the M_1 shell, the probability of the decay of the ($½^+$) isomeric level in ^{197}Au increases by a factor of more than 50 [46]. Experimental evidences of BIC have been found in the studies of the internal electron conversion of highly ionized states (charge state ranging from 44^+ to 48^+) of ^{125m}Te atoms [45]. It has been pointed out as the strong resonant character of BIC process. A change of few *eV* in the atomic excitation energy as a result of changing the charge state may result in a large variation in the nuclear decay rate and nuclear half-life.

In the last years, the NEET process has been generalized to a broader class of third-order processes with respect to the electromagnetic interaction named electron bridging mechanisms [16]. These are additional nuclear γ-excitation and γ-decay channels via electronic shells, which offer promising solutions for modulation of the life-time of nuclear excited states. The surrounding atomic shells act as a mediator of the electromagnetic energy transfer.

The Inverse Electron Bridge (IEB) mechanism is defined as the process of nuclear excitation by external radiation via atomic excited intermediate states. It is known in literature also as Compton excitation of nuclear levels [47, 52] or nuclear excitation by inelastic photoelectric effect [48, 53], because IEB mechanism is similar to the Compton scattering of gamma rays by bound atomic electrons, except that instead of the emission of a scattered gamma-ray there is an excitation of

nucleus via a virtual photon exchange (figure 2.5). The intermediate atomic state |n> can be of a positive energy state (unbound state) or a partially or totally filled bound state [47, 49, 37]. Various sub-shells and shells may participate in the electronic-bridge effect, their contributions being additive. In the single-level approximation of a discrete intermediate state, the cross section for the excitation of nucleus by incident radiation tuned to the atomic transition energy i → n (figure 2.5) by an inverse electronic bridge effect can be expressed in factorized form [50, 51]: the cross section for the resonant excitation of the n^{th} atomic level and the relative probability of the NEET process (n → f, F → I). It results that the IEB cross section, like the NEET process, depends inversely proportional with the square of energy mismatch between the nuclear transition energy and the corresponding virtual atomic transition energy ($\sigma \sim \Delta^{-2}$). Also, the maximum value of σ occurs for nuclear transitions with the lowest possible multipolarity, especially *M1* transitions [52, 53], accompanied by bound-bound atomic virtual transitions (discrete intermediate states), when the nuclear transition energy is comparable with the binding energies of atomic electrons. The relative probability of nuclear excitation by IEB, under the above conditions, has been predicted to reach 10^{-7} to 10^{-9} values per incident X-ray photon [52]. The cross sections are fairly large ~ 10^{-27} cm^2 [52]. For higher incident photon energies, the cross sections are estimated to be much smaller, typically of the order of 10^{-34} cm^2. It is significantly exceeding the cross section for the quadrupole excitation of heavy nuclei (A≈200) in inelastic scattering of the photons, which is about 10^{-40} cm^2. At much lower excitation energy, such as that of $^{229}Th^m$ isomeric state, the IEB mechanism is much more effective, the cross section is predicted to reach sufficiently large values, such as ~10^{-20} cm^2 [54], to produce population inversion.

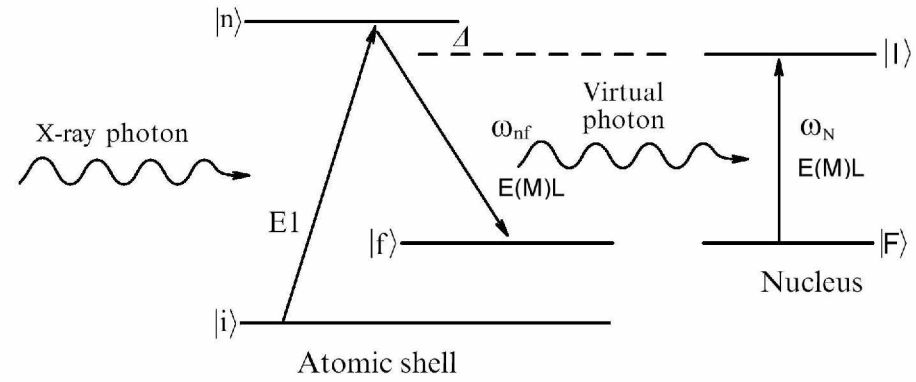

Figure 2.5. Schematic presentation of the Inverse Electrom Bridge (IEB) mechanism.

The direct mechanism - the electron bridge (EB) effect – is similar to the internal Compton effect (ICE) with the difference that the atomic electron suffers a discrete transition, rather than being emitted to the continuum. The energy of nuclear excitation is transferred to the atomic shell emitting monoenergetic gamma rays via atomic excited intermediate states. If the electron is shaken up, gamma lines with energy smaller than nuclear transition energy appear in the deexcitation spectrum of the nucleus. Experimental investigations have established a 7% relative contribution to the total decay probability of $^{93}Nb^{m}$ by the EB channel [55].

Mechanisms like those mentioned above and which depend upon the presence of atomic electrons can mainly be modified by chemical and physical environment of the nucleus, while these factors affect the electronic wave functions. The most pronounced effects can be expected on low-energy transitions which directly involve outer and valence electrons which are most sensitive to the environmental conditions. There are multiple example of the influence on the internal conversion decay rate due to both chemical [57] and physical environments [58]. The magnitude of these effects may be of the order of few percents [59].

Up to now, experimental efforts devoted to the 2^{nd} and 3^{rd} order processes of nuclear excitation have been more concentrated on the distinguish of the NEET process, and have been focused on a few heavy nuclei for which the energy, spin, and parity requirements for atomic and nuclear transitions are simultaneously met. The initial vacancies states were mainly created by irradiation with photons (bremsstrahlung or synchrotron radiation) and by electron bombardment (direct or in plasma condition). Because the NEET effects tend to be small, one must use highly sensitive detection techniques and very intense photon or electron beams. The use of a broad continuous spectral distribution of "white" synchrotron radiation or bremsstrahlung X-rays results in a contribution from direct nuclear photoabsorption into the NEET/IEB nuclear state or indeed into a

range of nuclear levels that can feed that state or lower-lying metastable states of which population is monitored.

More or less, the experimental attempts to distinguish NEET process before 2000 suffered from one or more of these problems. There are significant variations among the experimental results of the same process, which can be ascribed only to the population of excited nuclear states by non-NEET effects. The solution was provided by the improved technologies in emitting and monochromatization of superior ranges of SR energy [77]. Intense monochromatic SR-beams with energy carefully chosen just above the ionization energy of atomic state, not coinciding with the nuclear transition energy, were used in order to obtain more accurate results [60, 61]. For example, during an experiment conducted at Spring-8 SR facility [60] an ^{189}Os target was irradiated with monochromatic and "white" synchrotron radiation in successive runs. It was observed that the 69.5 *keV* level of ^{189}Os was mainly populated via direct nuclear photoabsorption when the isomeric sample was irradiated with "white" SR, explaining the large variations obtained by different experiments up to that time.

Also, an accurate NEET/IEB experiment requires one to certainty establish that the expected nuclear state has been excited. This fact requires the knowledge of the nuclear transition that should take place and thus to observe the characteristic decay radiation from the excited state or from a lower nuclear state to which the NEET/IEB-excited nuclear state decays. The half-life of the nuclear states involved in the deexcitation process can bring additional help in the identification of the nuclear transitions and also in the establishment of a corresponding detection technique. A correlation between the incident radiation or between the photoelectrons which escapes from the atom and the signal measured as a NEET/IEB signature will improve the signal-to-noise ratio. Since the lifetimes of

the nuclear excited states are in general much longer than those of the atomic states, there is the possibility of detecting NEET by combination of an incident beam of very short pulses and a delayed coincidence technique.

This method has been used at SPring-8 SR facility, where Kishimoto *et al.* [61] first combined the advantages of the high energy monochromatic SR beam with its pulsed nature to observe NEET in ^{197}Au. A fast detection system based on a silicon avalanche photodiode (APD) detector, synchronized with the irradiation pulses, was used to distinguish from the intense prompt SR background the weak radiation emitted from excited nuclei. The experiment stands as the first definitive and unambiguous experimental demonstration of the NEET process. The NEET probability was found to be $P_{NEET} = (5.0 \pm 0.6) \times 10^{-8}$, smaller by three orders of magnitude than the previous experimental value [62] and in relatively good agreement with the recently calculated values [44, 46].

At SPring-8 in 2001, the Center for Quantum Electronics group of the University of Texas at Dallas extended the successful results of observation NEET/EBM process in ^{197}Au [61] to the $^{178}Hf^{m2}$ and reported [63] a yield of 0.2% relative to the photoionization process, a value approaching the theoretical maximum. The results were reconfirmed by continuous efforts and new details have been added to the description of the physical processes governing the X-ray induced gamma emission of $^{178}Hf^{m2}$ [64-66, 114, 115] which are the subject of the following chapters.

CHAPTER 3

EXPERIMENTAL METHODS AND INSTRUMENTATION FOR STUDY OF PHOTON INDUCED GAMMA EMISSION OF $^{178}Hf^{m2}$

Irradiation Sources. Nuclear Spectroscopy Instrumentation. Data Acquisition.

The experimental setup required for a PIGE investigation can be divided in four distinctive parts: the isomeric target, the X-ray irradiation source, the photon detection and monitoring system, and the data acquisition and processing system. Each part should be designed in accordance with the specific characteristics of the proposed PIGE experiment. In the particular case of $^{178}Hf^{m2}$ PIGE experimental investigations, the energy of gamma transitions of of ^{178}Hf ranges from few *keV* to few *MeV*. Special attention in this work was on the range of γ-energies from 80 *keV* to 600 *keV*, which cover almost all the natural transitions of the isomeric decay. An X-ray source, emitting a continuous spectrum of photons with energies less than 100 *keV* was required for the first preliminary investigations, in accord with the predictions of the scaling studies [69]. An adjustable endpoint of the continuous X-ray spectrum was necessary, together with the need of a pulsed irradiation structure (pulse width in the range of few *μs* to few *ms)*. Larger irradiation gaps of the order of few tens of seconds were also required in order to detect the relaxation of any intermediate isomeric states that could be populated by the induced decay. It was established by the first experimental efforts [22, 70] that photons with energy less than 20 *keV* are implicated in triggering process, and as a result, intense tunable monochromatic X-ray sources were needed in order to identify the most favorable energies of triggering photons. The synchrotron radiation sources were the right solution from both points of in

view, intensity and monochromatization. It was also established [22, 70] that the induced decay should follow a different path than the spontaneous one, while the members of the GSB were not enhanced the same way. Coincidence measurements were required in order to identify the members of the induced decay, which must use a list-mode data acquisition approach and means for that were found and implemented in this work. The list-mode acquisition was further used as the usual way of data logging in SR experiments. Detailed description of these solutions will be discussed during the next paragraphs of this chapter. While the isomeric targets used in different experimental investigations are described in the chapters 4, 5 and 6, it should be mentioned here that special attention on maximizing the transparency to the incident radiation of the substrate and of the encapsulation material of the isomeric samples was required for the targets used in the SR experiments. The measured fractional absorption in figure 3.1 shows that about 4% of the 9.5 *keV* incident photons are absorbed by the substrate material.

3.1 X-ray Sources

3.1.1 Bremsstrahlung X-ray Generator

In the first experimental investigations of PIGE on $^{178}HF^{m2}$ [22, 70] a commercial GENDEX GX-100 X-ray generator was used for irradiation. Its functionality is based on a Röntgen–type X-ray tube with hooded W-anode, encapsulated in an evacuated sealed-off tube-envelope together with the filament, made of tungsten. The electrical power supply mainly consists of a step-down and a step-up high-voltage (HV) transformer to heat the filament and to accelerate the emitted thermoelectrons toward the W-anode, respectively. A main controller provides measurement, stabilization, and control of the supply. The transformers and the X-ray tube are immersed into an oil tank and comprise the

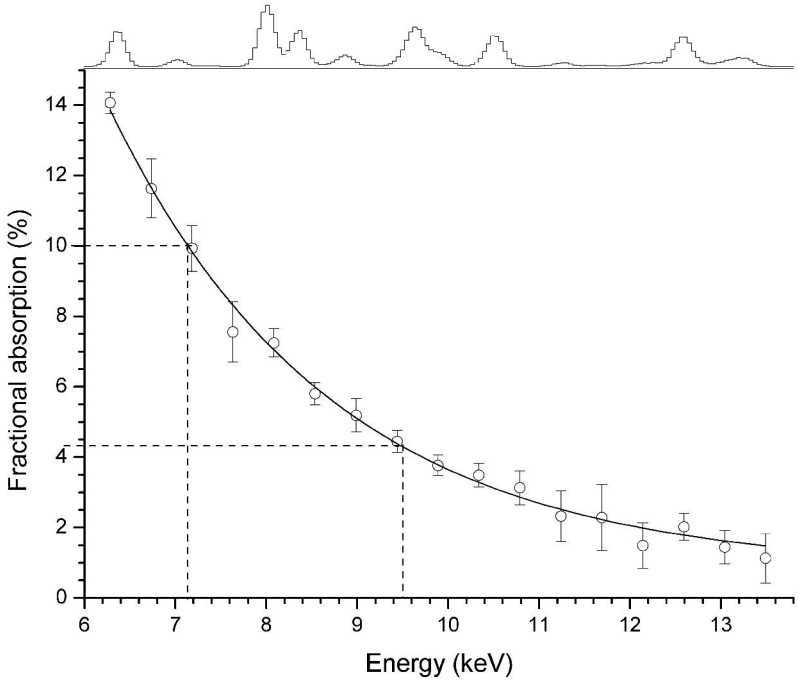

Figure 3.1. Fractional absorption of the incident radiation in the substrate material of the isomeric sample. About 4.2% of the 9.5 *keV* incident radiation is absorbed by the substrate material.

head-tube. Thus, the design assures mobility of the X-ray emitter from the main controller while also assuring the insulation of the high-voltage and heat dissipation. The X-ray tube is connected directly across the secondary winding of the HV transformer, so that the X-rays are emitted during alternate half cycles when the W-anode is positive with respect to the filament-cathode. X-ray lines and Bremsstrahlung photons with maximum 100 *keV* energy endpoint could be produced by up to 45 *mA* peak value of the half-wave rectified electronic current passing through the X-ray tube. The spectral flux of the emitted photons had a maximum of about $5x10^{10}$ *photons/s/cm*^{2}*/keV* at about 25 *keV* [70] when the device was operated at 63 *KV* energy endpoint.

In order to increase the flux of emitted X-ray photons, while preserving the electrical power applied to the X-ray tube during one 60 *Hz* cycle, shorter rectangular pulses of current through the tube were needed for increased emission of thermoelectrons of the filament. The power supplied to the head-tube has been replaced with a computer controlled waveform synthesizer system shown in figure 3.2 that was able to provide a stepped pulse of current which could be programmed to values as great as 80 *mA* for a duration of 2.5 *ms* (figure 3.2 (b)) to excite Bremsstrahlung photons with an energy endpoint of 60 *keV*. The voltage waveform (figure 3.2 (c)) is generated at one of the analog outputs of a multifunction DAQ PC-board (NI PCI–6024E) with a sampling rate of 10^4 *Samples/s*. The voltage is further amplified 40 times by a 5 *kW* amplifier and applied to the input of the primary winding of the HV transformer as shown in figure 3.2 (a), while the filament remained powered by the original controller. The synthesized voltage has been developed to correct for changes of the impedance in the primary of the transformer.

The X-ray source is operated in bursts producing 100 pulses at 60 *Hz*, synchronized with the voltage applied on the filament. One burst is made each minute. The large gap between consecutive bursts is necessary to prevent overheating of the HV transformer and especially of the W-anode.

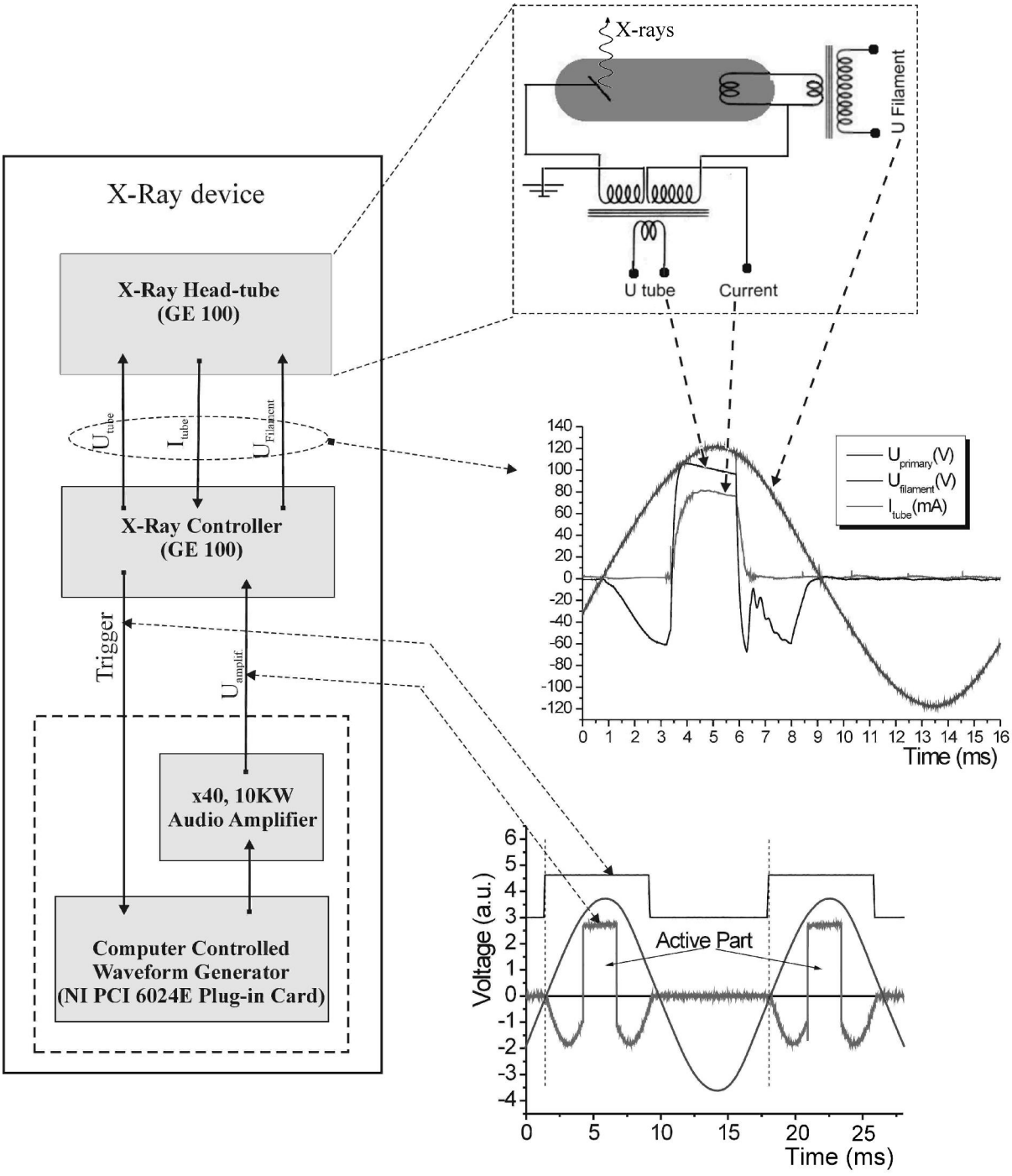

Figure 3.2. Computer controlled Bremsstrahlung X-ray generator. Schematic diagram.

During about the first 10 pulses of an irradiating burst the temperature of the filament is equilibrating, which result in the dropping of impedance of the X-ray diode - the load of the system. That is why the peak current rises to a stable value while the peak voltage developed across the tube is decreasing during the first pulses of an irradiation burst, as can be seen in figure 3.3. However, for the last 90 pulses of a burst, the peak of the current and voltage can be seen to be stabilized. For that region, a typical temporal dependence of the development of a single irradiation pulse within a burst together with the time-dependence of the synthesized voltage developed across the HV transformer are also shown in the inset of figure 3.3. The current in the X-ray source is reasonably constant during more than 1 *ms* in the middle part of the pulses. While the intensity of emitted photons is proportional with the square of the voltage across the X-ray diode [71], it is expected that the flux of emitted photons and the endpoint energies of the bremsstrahlung photons to be much more affected by the increased voltage than by the reduced current during the first pulses. Measurements of the irradiation flux during each X-ray pulse of a burst confirmed these suppositions, as shown in the figure 3.4. In the inset, the endpoint energies are seen to be stable for the last 90 pulses, varying only from 60 *keV* to 61 *keV*. Even if the increased voltage could be corrected by developing the sequence of synthesized waveform of pulses with reduced amplitudes, and thus having constant endpoint over all X-ray pulses, the decision was made to use the entire range of X-ray energies. The actual flux at 80 *mA* peak value of the current is in general two times larger than before [70] as shown in figure 3.5. There is a period of about 2 *ms* in the middle of each of the last 90 pulses of a burst during which the X-ray production is stabilize, as is suggested by the time-resolved measurement of the radiation produced by the device shown in figure 3.6. For investigation of induced gamma emission of $^{178}Hf^{m2}$ with X-ray photons produced by this X-ray device, valuable data should be founded during those 2 *ms* of stability of each X-ray pulse.

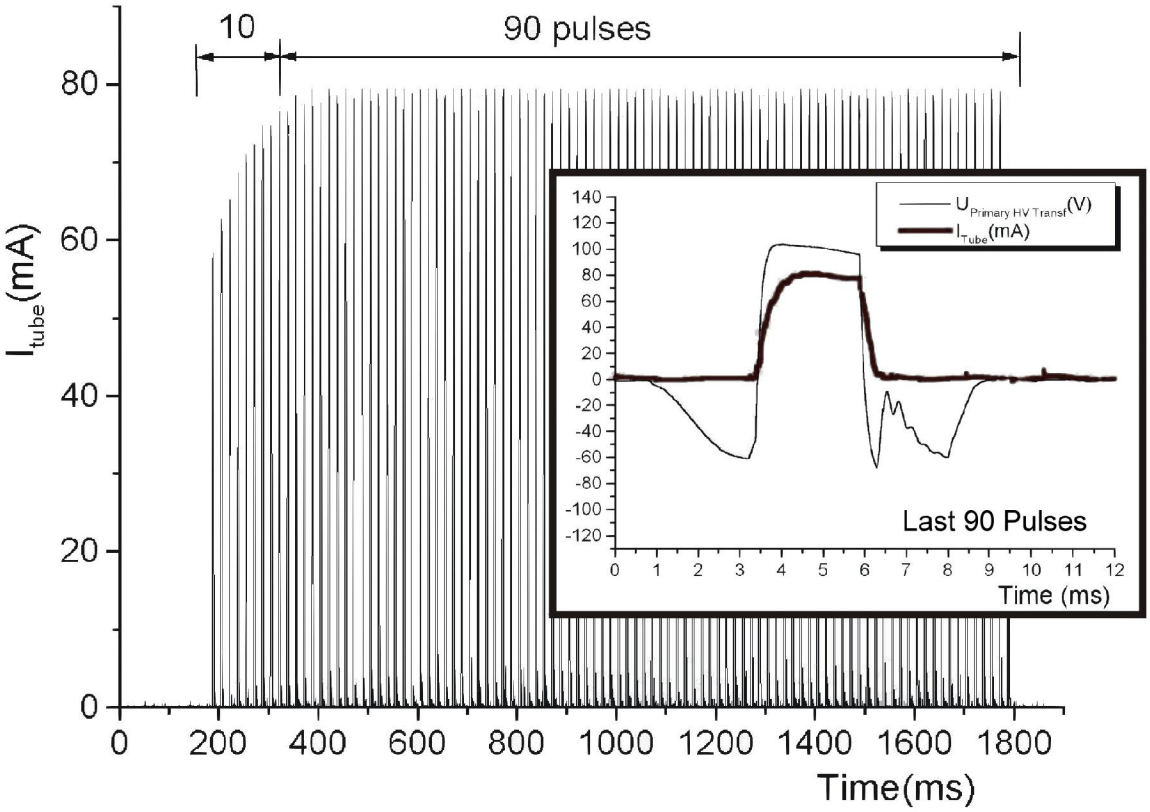

Figure 3.3. Direct measurement of the current passing through X-ray tube during a burst of irradiation. The first 10 pulses are affected by the heating of the filament in the X-ray tube which changed its impedance, but after that currents and voltages remained stable for the last 90 pulses in a burst. The inset shows typical data for the last 90 pulses.

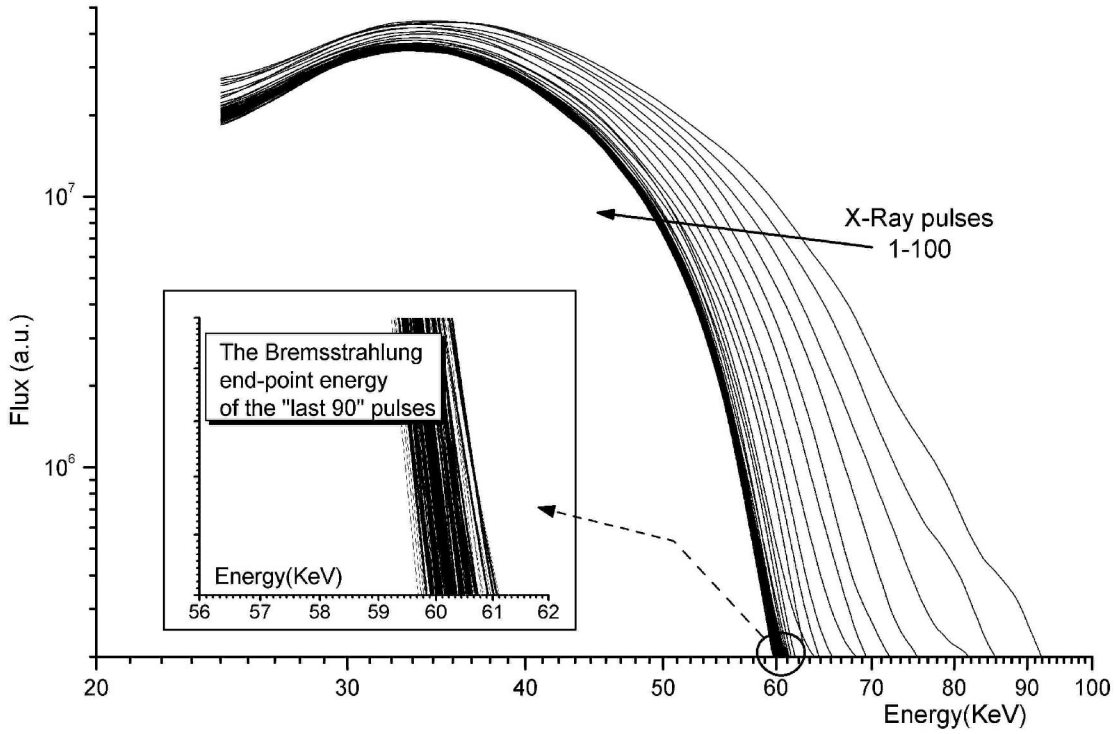

Figure 3.4. Comparison of X-ray flux emitted during each pulse of a burst. Substantial reduction of the end point energy of the bremsstrahlung component of the X-rays is observed during the first 10 pulse of a burst. Higher stability can be seen in the energy endpoints of the last 90 pulses in each burst.

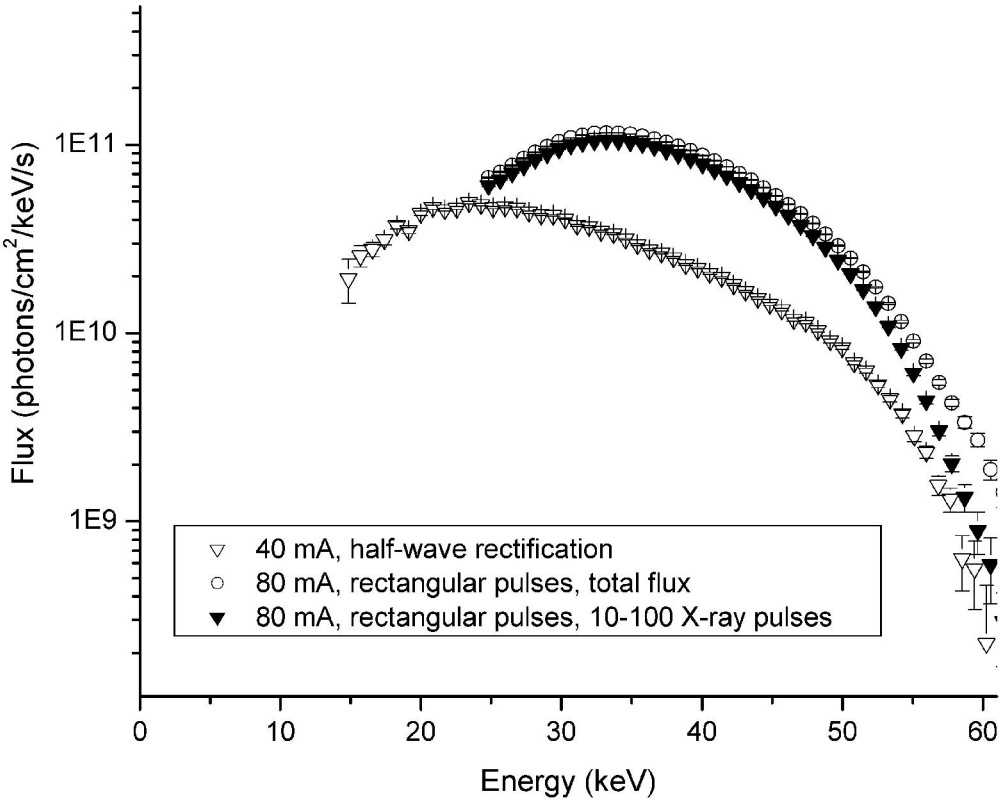

Figure 3.5. Photon flux comparison between the initial and the redesigned X-ray device. The new device is working at 80 *mA*, driven by a waveform synthesizer.

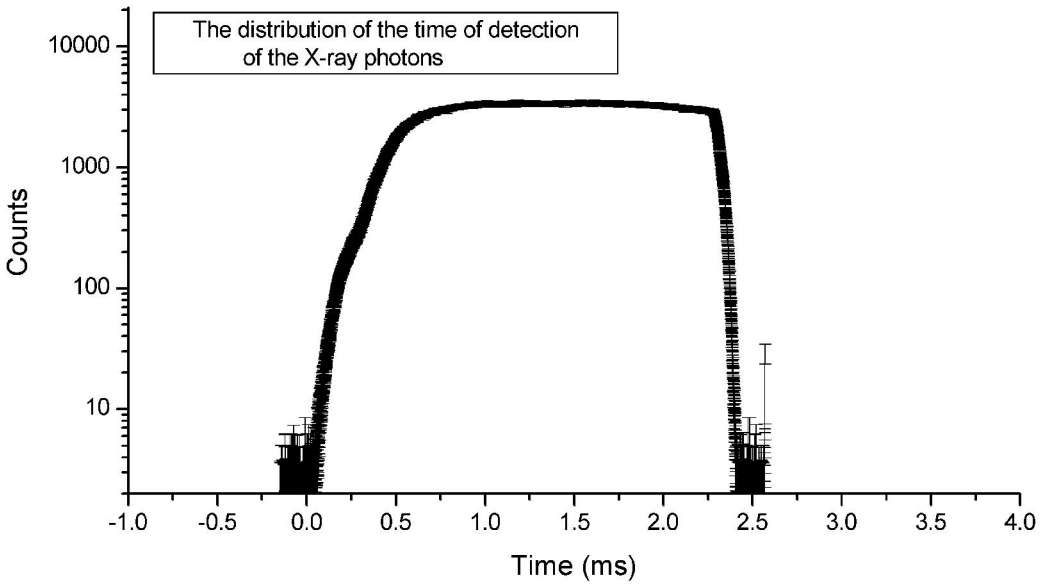

Figure 3.6. The distribution of the time of detection of X-ray photons produced by the X-ray device during one irradiation pulse. It shows that there is a period of 2 *ms* of stabilized X-rays production

3.1.2 Synchrotron Radiation Source

Unlike Bremsstrahlung radiation, which is emitted by a charged particle when is decelerated or deflected in the electric field of other charged particle, the synchrotron radiation is emitted by a relativistic charged particle when its path is bent by a magnetic field [71]. The intense synchrotron light beams are sharply focused and the emitted radiation is concentrated in the forward direction tangential to the trajectory of the particle into a solid angle which becomes smaller as the energy of the particle increases [71]. Usually, electrons are used in the SR facilities. The accelerator complex is composed of three major parts. A linear injection system (LINAC) supplies pre-accelerated electrons to the synchrotron booster, which in successive turns raises the energy of electrons up to the working energy, and then injected into a low emittance storage ring (figure 3.7 (a)). This may happened very often (top-up injection) keeping the intensity of the circulating electron beam constant in the storage ring; or can be much rare, only once or few times per day, with a complete refilling of the storage ring. The electrons circulate in bunches of 20 *ps* to150 *ps* long, on structures based on the main RF frequency [72, 73]. The bunches are spaced according to different operating modes, such as single or several bunch mode (only one or few bunches with well distanced orbits) or multibunch filling mode (one or more trains of bunches circulating at the same time). Hybrid filling modes are also possible, which combine the partial multibunch filling with isolating single or several bunch modes, in order to accommodate timing and non-timing experiments simultaneously.

In the 3rd generation SR sources, the stored electron beam emits synchrotron radiation at bending magnets and especially at insertion devices (undulators or wigglers) [77]. The emitted radiation spectrum of the bending magnets and wigglers are continuous, while the synchrotron radiation from undulators shows a line spectrum as a result of interference effects which lead to high

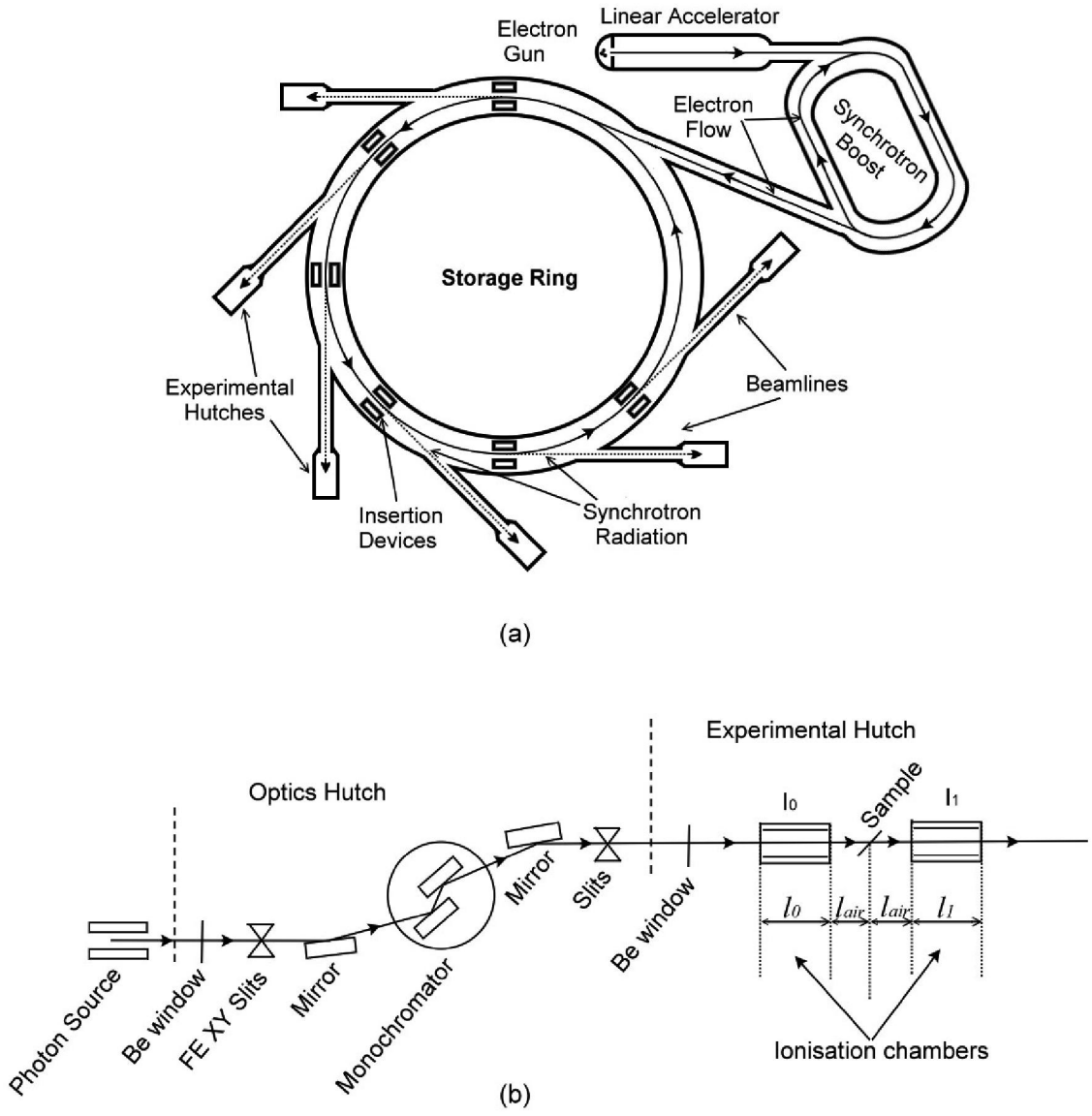

Figure 3.7. (a) Synchrotron radiation facility – general view
(b) Beamline prepared for XAFS measurement with ionization chambers

brilliance. The SR spectrum ranges from infrared light to soft and hard X-rays. The emitted radiation is guided tangentially away from the storage ring through beamlines to different experimental hutches and used for experiments. The main beamline optics consists of slits and collimating mirrors interpolating a fixed-exit double-crystal monochromator (DCM) [74, 75, 76] (figure 3.7 (b)). The mirrors are also useful for rejection of higher harmonics from the emergent X-ray beam. The final slit restricts, as desired, the dimensions of the beam entering the experimental hutch. Usual values ranges from few tenth to few mm^2.

This work made use of monochromatic radiation provided by the BL01B1 [74] and BL09XU [75] beamlines of the SPring-8 facility in Japan and by the X04SA-MS beamline [76] of the SLS facility in Switzerland. The light source was a bending magnet with Si(311) DCM, an in-vacuum undulator with Si(111) DCM, and a hybrid wiggler with Si(111) DCM, respectively. Photon fluxes in the range 10^9 - 10^{13} *photons/s/cm*^{2} at 10 *keV* with the energy resolution ($\Delta E/E$) in the range of 10^{-4} were available at the sample surface. Further monochromatization using high resolution optics can increase the energy resolution in the range of 10^{-6}. The nuclear resonant scattering beamline, BL09XU, is optimized for high resolution tuning of high photon fluxes [75]. This work made use of a second Si(620) DCM located down stream of the first Si(111) DCM of the BL09XU beamline shown in figure 3.7(b), in order to tune X-ray beams as intense as 2.0 x 10^{12} *photons* cm^{-2} s^{-1} in steps of 0.0877 *eV* at energies between 9 and 10 *keV*. The above mentioned beamlines were prepared for transmission mode measurements, similarly with a standard XAFS measurement, using two gas-flow type ionization chambers, as shown in figure 3.7(b). This permits both the monitoring of the X-ray beam flux incident on the sample and also the positioning of the sample in the front of the beam. The absorption spectra of the sample can be obtained by simultaneously recording of the output of the ionization chambers versus the tuned energy of the SR beam.

3.2 X-Ray and Gamma-Ray Spectroscopy. Experimental Methods

The field of x- and γ- ray radiations detection is an old, well studied and developed domain which has improved continuously in the course of time. Different types of detection systems have been created for different spectral ranges and for different applications. They are all based on the same principle: the total or partial radiative energy transfer to the detectors mass, where it is converted in other forms, mostly in electric signals which are much easier to process, analyze and acquire. An usual X- or γ-ray spectroscopy system comprise the detector itself, the associated pulse processing electronics or back-end electronics and the data acquisition system.

3.2.1 Radiation Detectors. Ionization Chambers. Semiconductor Detectors

In SR experiments, the ionization chambers are extensively used for monitoring X-ray beam intensities and because of their controlled transparency to incident radiation they are also used as suitable detectors for measurements in transmission mode. They normally operate in the ion saturation mode of the I-V characteristics [71], where the collection of all the charges created by ionizing radiation within the gas when a sufficiently high voltage is applied between electrodes, suppressing the recombination processes to a negligible level. The ionization chambers are filled with different mixtures of gases for different ranges of the incident radiation energy (E_{beam}) in order to maintain their efficiency into acceptable limits. Usually, a mixture of N_2 and Ar is used at atmospheric pressure. The electric current of the ionization chamber is amplified by a high-gain current amplifier and the voltage is converted to the frequency of standard logic pulses, which then are counted. The total gain ($G_{A\rightarrow F}$)

obtained is usually in the range of 10^2 to 10^4 *counts/nA*. If N_0 is the number of counts per unit time counted by the first ionization chamber of the experimental arrangement depicted in figure 3.7(b), the X-ray flux incident on sample may be expressed as:

$$\Phi_0(E_{beam}) = \frac{N_0 w_{gas}}{eE_{beam}G_{A\to F}S_{beam}(1-e^{-\mu_{gas}d_{IC}^{(0)}})} e^{-(\mu_{gas}d_{IC}^{(0)}+\mu_{air}d_{air}^{(0)})} \qquad (3.1)$$

where $d_{IC}^{(0)}$ is the length of the first ionization chamber filled with a mixture of gases, having the total absorption coefficient μ_{gas}. The gas mixture requires a mean energy w_{gas} expenditure per each electron-ion pair produced by an incident radiation beam, having a spot area S_{beam}. There is a distance $d_{air}^{(0)}$ of air to be traversed by the beam before hitting the sample. An analog formula - excepting the last factor of equation (3.1) which should be replaced by the exponential loss of photons from the beam before entering the chamber ($e^{\mu_{air}d_{air}^{(1)}}$) - may be used to describe the flux of X-ray photons transmitted through the sample (Φ_1) from the number of counts recorded by the second ionization chamber. The absorption of the sample, $\ln(\Phi_0/\Phi_1)$, can be then expressed as a function of incident radiation energy. The absorption spectra of a high purity sample with increased transparency of a known element recorded in transmission mode measurement may be used for calibration of the energy of the monochromatic SR beam provided by monochromator. While the principle of monochromatization is the diffraction of the wide-band radiation on atomic planes of a crystal lattice, the calibration formula is based on the Bragg's diffraction law.

Usually a single calibration parameter, θ_0, is required as a correction term of the glancing angle, θ supplied by the feedback components which monitor the monochromator crystal position:

$$E_{beam}(\theta)[eV] = 6.1992\times10^3 \frac{n}{d_{hk^a}\sin(\theta-\theta_0)} \qquad (3.2)$$

where *n* is the order of diffraction on the *(hkℓ)* plane of the crystal, such as Si(311) plane. The lattice plane spacing, $d_{hk\ell}$, is expressed in *Å* and θ in radians. Exemplified in figure 3.8 is the absorption spectrum of a Cu-foil near the K-edge photoionization threshold. The characteristic near-edge peak at 8978.72 *eV* [78, 79] was used for energy calibration of SR deducting the correction term to the value of glancing angle.

The very low signal output for the ionization chamber makes this detector difficult to use for detecting individual gamma-rays. That is why they are commonly used only as integrating detectors to measure beam flux rather than to detect individual photons. A solid state detector should be used for the energy- and time-resolving of single photons, and from this class, the semiconductor detectors offer the best energy and time resolution achievable today as compared to any other class of detectors. That is because of the larger number of carriers (electron-hole pairs) created in the active volume of the detector for a given incident radiation, as a result of reduced ionization energy. This is about 3.6 *eV* for silicon and 2.9 *eV* for germanium, which are the most widely-used semiconductor detector material. They are basically large, reverse-biased n–i–p diodes, the intrinsic (i) region - depleted of charge carriers - is the interaction medium of incident photons with the detector, the place where the carrier-pairs are produced. In the presence of the electric field these pairs separate and rapidly drift to the detector contacts. Because germanium has a relatively low band gap, these detectors must be cooled in order to reduce the thermal generation of charge carriers (thus reverse leakage current) to an acceptable level.

The charge collection time, which defines the pulse rise time, associated with any ionizing event is a complex function of the detector parameters, the dominant factor is the thickness (W) of the depletion region, which equals the thickness of the detector element. Empirically, $T[s] \sim W[mm] \times 10^{-8}$ [80] for germanium at LN_2 temperature and about one order of magnitude larger

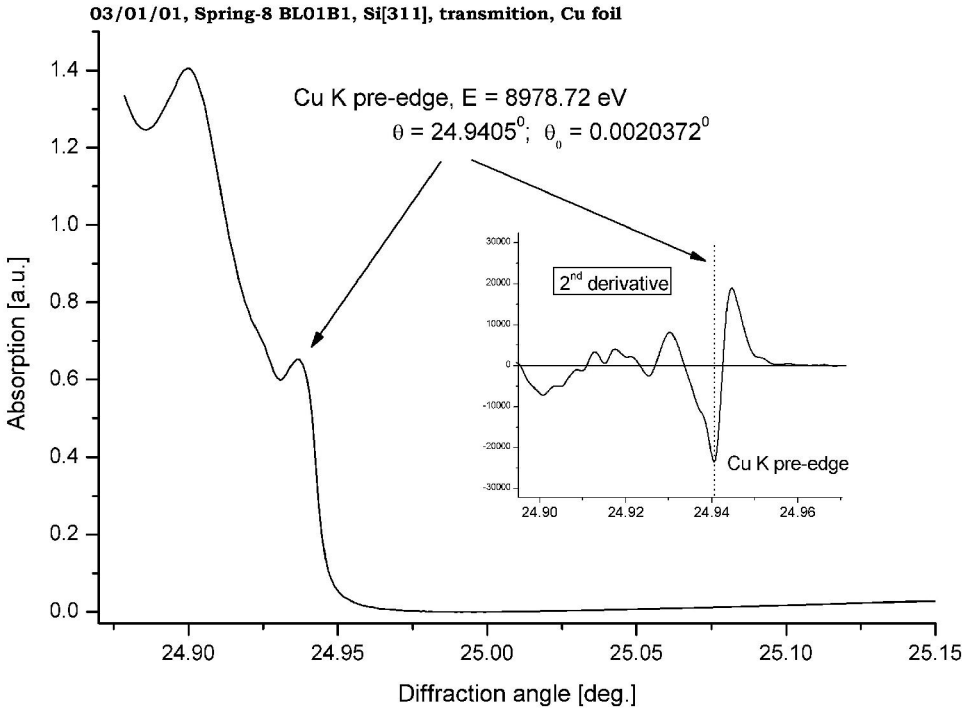

Figure 3.8. Absorption spectrum of Cu-foil at K-edge photoionization threshold. The pre-edge peak at $\theta = 24.9405^0$ is used for calibration of the monochromatic SR beam.

for silicon. It results that a compromise will always be between the "speed" of detector and its efficiency, while the volume of active area is the determinant factor, which establish the relative efficiency of the detector, $Eff_{rel}(\%) \sim Vol_{det}$ [80]. The high purity Ge (HPGe) detector element is preferred for energies above 20 *keV*. In this work, an Ortec GLP type detector was used for monitoring and characterization of bremsstrahlung radiation with energy below 100 *keV*. This is a planar, small area (~ Φ 6 *mm* × 5 *mm*) HPGe photon spectrometer having a maximum efficiency at about 40 *keV*. The natural and stimulated γ-emission of $^{178}Hf^{m2}$ nuclei was investigated using Ortec GMX coaxial detectors (~ Φ *50 mm* × ~ 45 *mm*) with 10% relative efficiency. The detector element is placed at about 3 *mm* from the Be entrance window (0.5 *mm* thick) having maximum efficiency at 300 *keV* that decreases to about 10% at 80 *keV* and 1 *MeV*.

In order to avoid overloading of the large HPGe detectors with low energy X-ray photons and also to minimize the influence of electromagnetic noises, they have been fitted with multilayer graded-Z shielding. This was the front-shielding and consisted of W (50 μm), Cd (0.5 *mm*), and Cu (3 *mm*). The side-shielding, consisted of thick layers of Cu and Pb that absorbed all high energy X-ray and γ-ray photons. In fact, the Cu shielding was a grounded cylinder covering entirely the detector capsule, having also properties of an electromagnetic shielding.

For photon energies lower than 20 *keV* the Si based detector is recommended, because the escape phenomena are less prominent than in Ge [81]. Due to their design, which assures an extremely small value of the anode capacitance, the Si drift detectors (SDD) offer the best performances (timing and energy resolution) in the range of 1 *keV* to 20 *keV*. The leakage current level is so low that the drift detector can be operated with good energy resolution at room temperature or with moderate cooling by a single stage Peltier element.

Much faster detectors, such as the Si-based avalanche photodiodes (APDs) have been used for the detection of visible light for many years. The usage of the APDs for the detection of X-rays is a new application [82, 83, 84]. These are compact devices so that internal electric field can reach values high enough to allow electron multiplication by impact ionization (avalanche multiplication of photocurrent), when a high enough reversed bias voltage is applied across the p-n junction. The charge gain is, in general, in the range of few tens to few hundreds, depending exponentially on the applied voltage. This makes possible that the APD to output very short pulses in the nanosecond and sub-nanosecond region with large enough amplitude.

The short wavelength type series of Si APD manufactured by Hamamatsu Photonics have already demonstrated to be able to provide excellent time resolution of about 0.08 *ns* and single-photon counting rates in the order of 10^8 *photons/s* [87]. These characteristics have made possible using the APD detector as the bunch-purity monitor of synchrotron rings [85-88]. These detectors have been used also in nuclear resonance scattering experiments with synchrotron radiation [61].

In order to monitor the pulsed time structure of synchrotron radiation, in this work, a Hamamatsu S9073 Si-based APD detector was used. It had an effective active volume of 0.03 $mm^2 \times 10\ \mu m$, with maximum sensitivity at 620 *nm* wavelength and a maximum cut-off frequency of 900 *MHz*. An internal gain of 50 could be reached, when it was operated closed to its breakdown voltage of 150 *V*. In order to maintain a fast response of the APD device, and minimize the electrical noises, its signal was capacitively coupled immediately into a fast pulse preamplifier (Phillips Scientific PS6954) with a fixed gain of 100 and a broad bandwidth from 100 *KHz* to 1.8 *GHz*.

In all the cases where HPGe, SDD or APD detectors were used, the preamplifier output was a long-tail pulse type with fast front edge and floating DC level. Each pulse was riding on the tail of the

previous pulse. The tail could range from hundreds of *ps* in APD to few μs in HPGe. The energy information of the detected event was carried in the amplitude of the pulse (few mV - $1V$), which was proportional with the charge created in the detector mass by the incident photon, while the timing information was carried in the front edge of the pulses. The pulse tail contained no useful information. The energy and timing information could be extracted by further processing techniques, which are discussed in the next subchapter.

3.2.2 Back-End Electronics. Pulse Processing Technique

Because of its small amplitude and long tail type pulsed signal with floating base line, the processing stage of differentiation is first needed to restore the baseline reference level for each pulse. It is followed by amplification and proper shaping as shown in figure 3.9. These functions are included in the amplification devices, such as spectroscopy amplifiers and timing filter amplifiers (TFA).

The spectroscopy amplifier recovers the energy information by shaping the differentiator output into an integration stage (low pass filter) with a fixed time constant (TC) which must be chosen accordingly with the detector type and the photon acquisition rate. To fully process a pulse from the preamplifier, the TC needs to be about ten times the rising time of the input pulse or higher, otherwise the processing of the pulse stops before it has risen to its maximum amplitude, thus loosing the height proportionality with the energy released by the incident photon in the detector mass ("ballistic deficit" effect). A semi-gaussian pulse suffering from this effect contains the energy information in its area instead of its height. The gated integrator (GI) circuit recovers the energy information at small TC by integrating the area under the unipolar pulse, which leads to increased

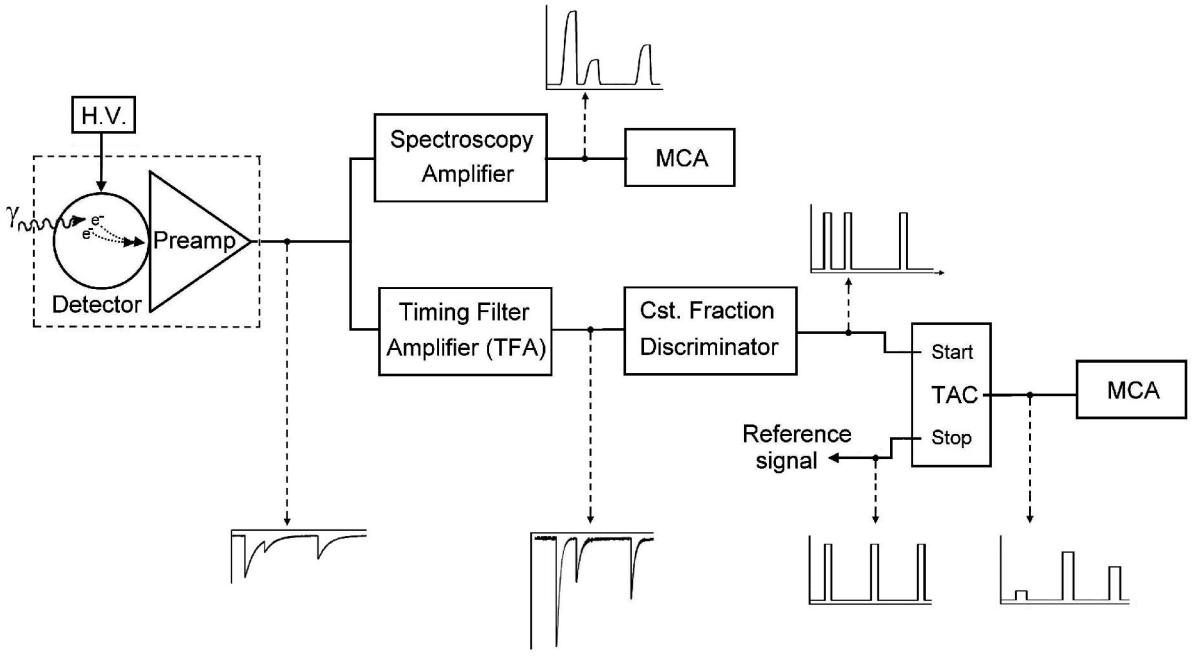

Figure 3.9. Pulse height spectroscopy and time interval measurement between the moment of detection of a gamma photon and a reference.

throughput and better energy resolution over almost the entire range of shaping TC as compared to the unipolar shaping [80]. The better definition of the height of the GI shape makes this shaping suitable with the data acquisition system used in this work, as it is discussed in subchapter 3.3. Ortec's 673 spectroscopy amplifiers have been used in combination with HPGe detectors, for X- and γ-ray spectroscopy in this work.

Different from linear spectroscopy amplifiers, the timing filter amplifiers (TFA) used as the first stage of timing pulse processing deliver amplified low noise and fast rise times output pulses as seen in figure 3.9. This improves the timing accuracy, where the amplification linearity is not so important. The best timing resolution is usually achieved when the amplifier rise time is comparable or less then the detector preamplifier rise time [80].

Once the preamplifier output is correctly amplified and filtered, it is passed to a discriminator stage in order to identify and signal the arrival time of each pulse. In the simplest case of leading-edge discriminator, this task is realized by a voltage comparator which generates a standard logic pulse each time the leading edge of the analog pulse crosses a predefined voltage threshold. The rising edge of the logic pulse marks the arriving time of the analog input pulse. Because of this principle of operation, the timing definition is very sensitive to electric noises. A noisy input causes an uncertainty (jitter) of the time at which the analog pulse crosses the discriminator threshold. Another source of jitter is the statistical fluctuation of the slope of the pulses as a result of the statistical fluctuation of the interaction location of incident photons in the detector mass. In order to minimize the jitter, the discriminating threshold must be set at the point of the maximum slope of the analog input. The slope of pulses at the output of the detector preamplifier is also a function of the pulse amplitude for the same rising time; pulses with the same rising time, but different amplitudes will reach the threshold level at different times. This is the "walk" effect. It produces systematic inaccuracies to timing

resolution, which is the dominant limitation on the resolution of leading-edge discriminators. The constant fraction discriminating (CFD) technique [80] should be used in order to minimize the walk effect.

The best timing resolution is achieved when the proper preamplifier, amplifier and discriminator chain are chosen accordingly with the detector type. This work made use of Ortec 579 TFA for reshaping and amplifying of the output of 10% HPGe coaxial detectors, supplying as low as 5 *ns* rise-time pulses to the CF800 CFD. After discrimination, in order to measure the time interval between a specific event and the photon detection time, the output of the discriminator that is signaling the detection of the photon must be inputted to a time-to-amplitude converter. Such devices use an analogue technique to convert small time intervals to pulse amplitude. Their working principle is based on the charging of a converting capacitor from an internal constant current source in the time interval between a logic timing signal arrived at the START input and the first logic timing signal arrived at the STOP input (figure 3.9). The voltage developed across the capacitor is proportional with the time interval between the logic pulses at the inputs of the TAC device, and it is reflected at the output of the TAC as the amplitude of an analog rectangular pulse. The ramp voltage of Ortec 567 TAC is calibrated to develop a maximum of 10 *V* on each selectable full time scale.

The time-to-amplitude converter is only able to process one pair of start and stop pulses in each conversion. Once a start pulse has been accepted all further pulses at the start input are ignored until the conversion and reset processes are finished. Starts with no stops will cause excessive dead time in the TAC. In order to minimize the dead time of the TAC, it is always necessary to choose between the two input signals, the one with the lowest counting rate to be the one who starts the time-to-amplitude conversion. This may require as the other signal, which becomes the stop signal, to be additionally delayed relative to the first one. The length of this delay should be approximately

90% of the time range selected on the TAC. Intermediate delaying modules can be required on the one of the TAC inputs in order to align the input signal.

The reference signal can be the irradiation periodic signal or the result of a logical operation between different other signals. That is the situation of multi-detector coincidence measurements, when an coincidence (logic AND operator) circuit should be used in order to develop an "event" signal that pulses each time a number of inputs greater or equal with the coincidence level pulses in an definite temporal window. Additional delay modules are usually required on each CFD output in order to align the signals. It is also necessary that the TAC output to be delayed in order to synchronize it with the spectroscopy amplifier output of the same detector as shown in figure 3.10.

For monitoring the synchrotron radiation temporal structure, the time of detection of the X-ray photons of the SR beam should be measured relative to a periodic signal synchronic with the movement of electron bunches in the storing ring. The clock cycle period of the synchrotron storage ring was used as the reference signal for stopping the time-to-amplitude conversion of the TAC associated with the APD detector as illustrated in figure 3.11. Because conventional CFD does not have adequate bandwidth to properly process sub-nanosecond pulses delivered by the 1.8 *GHz* PS6954 charge preamplifier of the S9073 APD detector, the Ortec 9327 - *1 GHz Amplifier and Pico-Timing Discriminator* was used in this work to discriminate the *sub-ns* rise-time pulses.

In conclusion, by using analog pulse processing techniques, both the energy of detected photons and the detection times relative to a reference signal can be extracted from the output signal of the detector and expressed as the height of other analog signals. In both situations the pulse height ranges from 0 *V* to 10 *V*, proportional with the measured event. Further, a multichannel scaler (MCS) has to be used in order to record the counting rate of events as a function of time or a multichannel analyzer (MCA) for a pulse height distribution analysis.

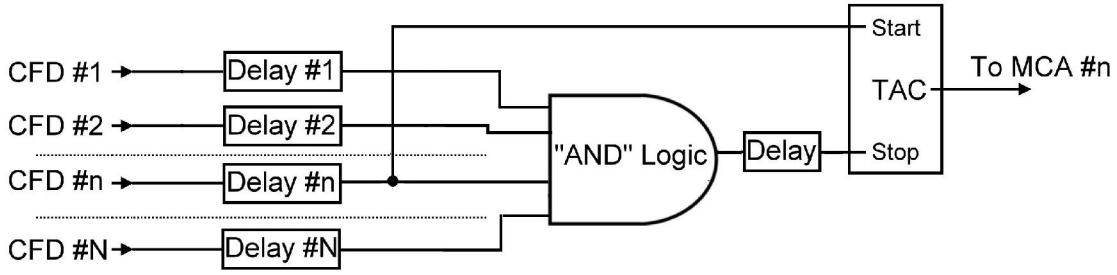

Figure 3.10. The reference signal for stopping the time-to-amplitude conversion in multidetector coincidence experiments is delivered by an “AND” logic unit, with coincidence level ≥ 2

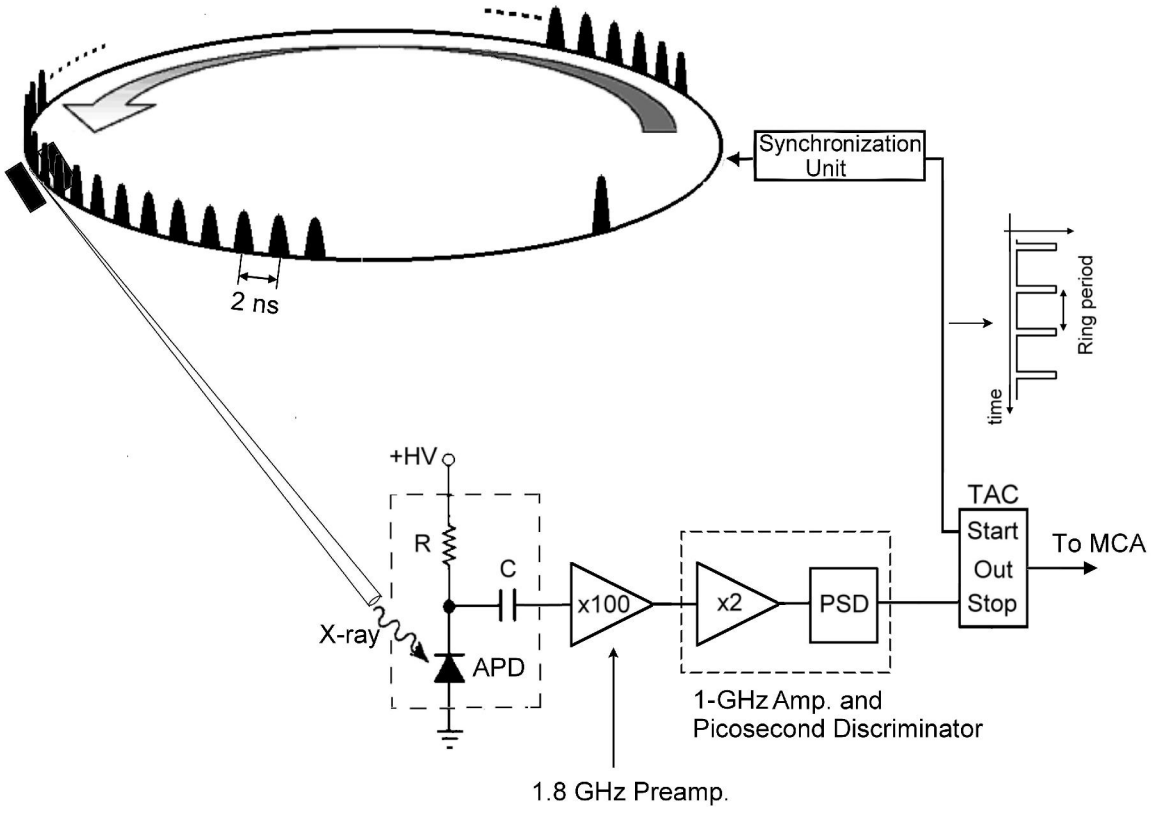

Figure 3.11. Monitoring the temporal structure of the SR beam with APD detector

3.2.3 Multichannel Analyzer. Data Logging.

A pulse height distribution analysis (PHA) of spectroscopy amplifier or TAC outputs can be obtained from a dedicated instrument, the multichannel analyzer (MCA). It accomplishes this task by dividing the pulse-height space in a number of equally spaced intervals, usually referred to as channels or channel-array, and expressing the height of the sequentially arriving pulses in terms of channels (the index of the channel-array cell which includes between its limits the value of the height of the pulse). These values can be stored into a list (List-mode MCA) or can be used to directly perform a pulse-height distribution analysis (PHA-mode MCA) yielding a histogram (spectrum) representing the frequency of occurrence versus pulse height. Energy or time spectrum is thus obtained if the input pulses come from a spectroscopy amplifier or from a time-to-amplitude converter, respectively. The number of the channels the system is capable to differentiate represents its resolution.

The most important component of MCA is the analog-to-digital converter (ADC) because it is the one which divides the amplitude space into channels (binary values). Thus, the performance characteristics of MCAs such as resolution, linearity and dead-time, are normally dependent on the specifications of the ADC. Only two type of ADC are used in the traditional nuclear spectroscopy instrumentation. The Wilkinson-type ADCs have an excellent linearity, but long conversion time (dead-time of 20 - 165 μs) which is dependent on the amplitude of the pulse analyzed. The successive-approximation ADCs are much faster having fixed dead-time, but have poorer linearity [80, 89].

Flash-type ADCs provide a much faster conversion. Recently, they started to be used in nuclear spectroscopy as the basic components of the Digital Signal Processing (DSP) systems [90, 91].

In these systems, the detector preamplifier output is directly digitized at high sampling rate, usually at 100 *MS/s* with resolution of 11–12 *bits*, after some preconditioning and amplification. The digitized data is then filtered and optimized using digital processing algorithms, which entirely replace the classical analog pulse processing techniques.

In this work, flash-type ADCs have been used to continuously digitize the outputs of the back-end electronics (spectroscopy amplifier and TACs) at high enough sampling rate in order to accurately describe the waveform of those outputs. The work of MCA/MCS is thus replaced by the PC-based ADC and data processing.

3.3 PC-based List-Mode Multiparameter Data Acquisition System (DAQ)

The data acquisition of a PIGE experiment must be compatible with the induced radiation emitted, in order to be able to detect it, and also must be compatible with the temporal structure of the irradiation source. More exactly, for a pulsed irradiation source, working in burst mode, the DAQ should be able to trigger with the irradiation pulses and to separately detect and record inbeam data during the period of each irradiation pulse. Accumulation of baseline data immediately after irradiation and of a cold-baseline data between the consecutive irradiation bursts is required in order to detect any relaxation of long lived exited nuclear states implied in the deexcitation path (if this is unknown). Irradiation with monochromatic SR requires synchronization with the monochromator, accumulation and recording the data at each stepped of the monochromatic energy, with target held inbeam and outbeam. If fast-timing or investigations by coincidence method are required, then a list-mode acquisition DAQ is mandatory.

In this work a special multi-parameter list-mode DAQ has been developed, based on virtual instruments concept. The main scheme consists in the continuous, simultaneous and fast digitization at constant rate of all the final back-end electronics outputs. With only PC-based facilities data is analyzed to obtain and log the parameters of the pulses such as height, width and time of detection detected in outputs.

In this work, National Instruments PCI-6110 plug-and-play, multifunction device for PCI bus computers was used. This device is able to simultaneously sample four bipolar analog inputs (A/I) at a maximum of 5 *MS/s* with 12 bit (4096 channels) resolution. Each A/I channel is owning its ADC, driven by a common 20 *MHz* time-base clock (the primary frequency source of the device). Ten Programmable Function Inputs (PFIs) can be used to input or output any timing signal, enabling the NI PCI-6110 to control and to be controlled by other external devices and circuits. Two 24-bit counter/timers are also available to be used for counting and/or timing needs.

The simultaneous sampling is an important feature of these devices because it maintains the phase relationships of the incoming signals on the all four A/I channels. This feature can be extended between the A/I channels of multiple PCI-6110 devices present in the system by using the internal Real-Time System Integration (RTSI) bus [92] - a specialized timing bus used for synchronization of multiple devices and able to drive any timing signals, the time-base inclusive.

That permits comparisons to be performed between digitized data of different acquisition channels in order to validate the simultaneous occurrences of different signals. That is the case, for example, when energy and timing information are collected simultaneously from the same detector. Each timing signal must have a corresponding signal on the energy channel in order to be validated. This will strongly improve the timing spectrum especially in a noisy environment when high frequency electromagnetic interferences (EMI) on the detector output may become trigger sources for

discriminator. The procedure can be extended to the validation of a multi-detector γ-γ coincidence event. That must imply the detection at the same time of at least two photons by two different detectors producing the timing and energy pair signals on the corresponding acquisition channels. Their simultaneous occurrences must be satisfied as shown in figure 3.12. In the same way, in timing experiments with SR, when the fast-detection time of each γ-photon has to be measured relative to the periodic passage of an electron bunch in the storage ring, each detected photon should have a timing signal associated with and their simultaneous occurrences must be satisfied.

The successive digitized data is temporary stored into an on-board buffer memory until they can be transferred into PC-system memory. The same number of samples of each channel builds a data block that is transferred to the PC memory at once, to further preserve the synchronization of sampled data. Having the advantage of direct-memory-access (DMA) technology [92], implemented in both the digitization board and the host PC, blocks of the continuous stream of digitized data are directly transferred at high-speed from the on-board memory buffer to the preliminary reserved buffer of PC memory, without involving the central processing unit (CPU) and so keeping it free to perform other tasks. The availability of DMA transfer together with the requirement that the data analyzing and storing speed to be higher than that of digitized data flow, are the main principle of a continuous acquisition, without duty cycles.

The procedure for analyses requires at least identification of incoming pulses in the digitized data stream, validation of the shape of the pulses, and computation of the pulse parameters such as height, width and detection time. Other parameters and validations specific to each experimental detail may be also necessary to be established. That may imply comparison between the acquisition

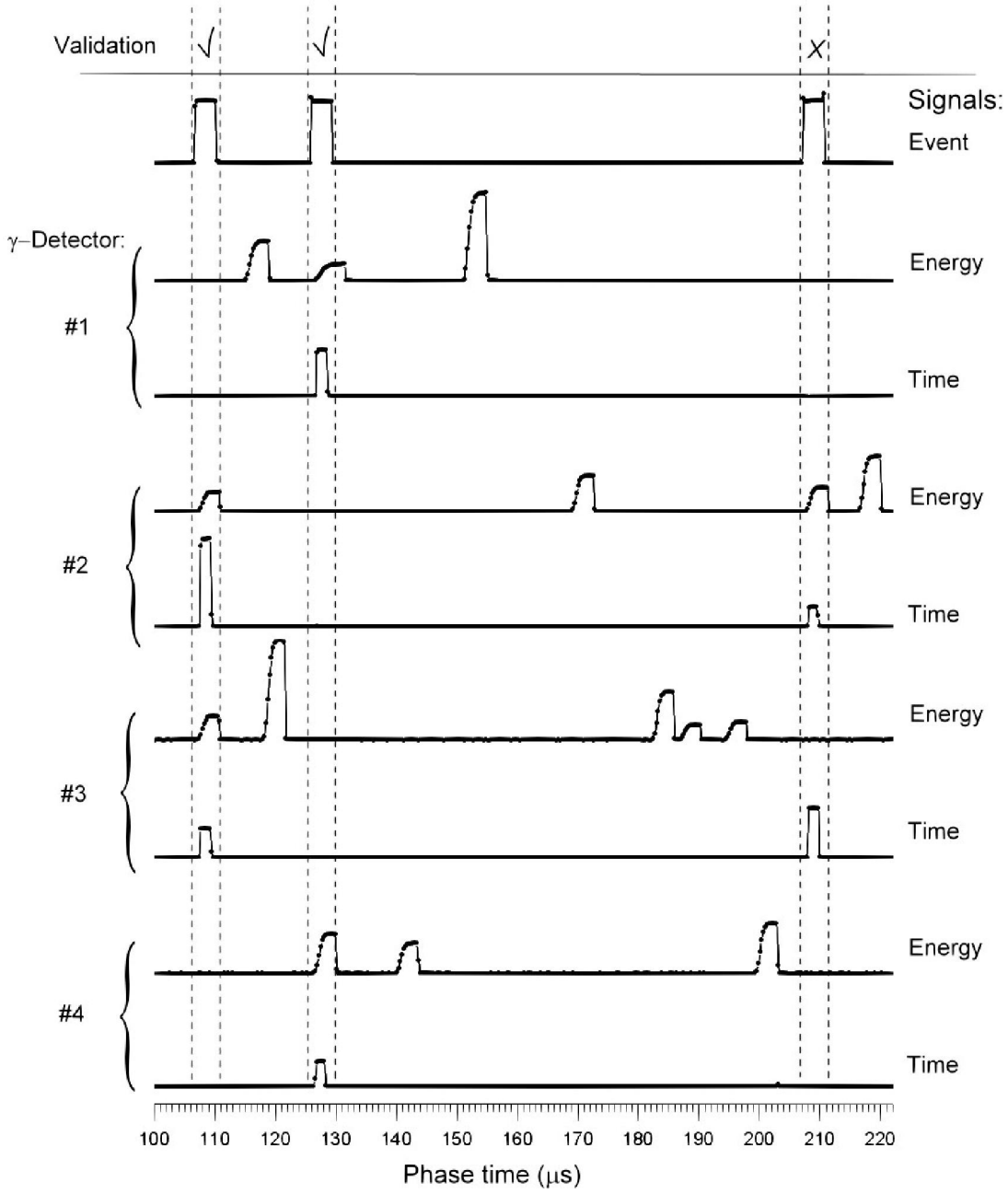

Figure 3.12. Coincidence event validation as a result of simultaneous digitization of corresponding channels

channels or interpretation of other information that the acquisition system should receive. Examples may include identifying if the pulse was detected in inbeam or outbeam condition, and its association with the stepped energy of the monochromator.

The pulse identification procedure requires a predefined number of consecutive digitized samples with values larger than a threshold value, which is usually chosen to equal 20 channels as indicated in figure 3.13. The index of the first sample of a pulse which meets this criterion can be defined as a time stamp of that event. The pulse width will represent the number of consecutive digitized samples that will still have a value higher than the threshold. Depending on the characteristics of the expected pulse shape, the maximum amplitude should be fund in a definite location of the pulse. A generalized method, adopted in this work sorts the constituent samples of the pulses in the ascending order of their digital value and then averaging the first 3 or 5 samples with top values, as shown in figure 3.13. While the baseline is not always constant and can slightly oscillate in time, a measure of the signal baseline is always necessary. The average value of a few samples, right before the time stamp of the corresponding pulse, with the precaution not being the components of a previous pulse, can be subtracted from the average of top values to obtain a more accurate value of the pulse amplitude.

While the outputs of the back-end electronics are pulses of well-defined shape (rectangular, unipolar, or GI) with fixed width, the most simple pulse shape validation procedure should be based on this property. The pulse width distribution analysis shows that one can make distinction between spikes (shape-unfinished signals), well-shaped pulses and pile-up effects. The figure 3.14 is an exemplification of a width distribution analysis of the detected signals from a spectroscopy amplifier, showing in the insets typical pulse shapes corresponding to different regions of the distribution. The spectroscopy amplifier time-constant was TC = 2 μs at an acquisition rate of $2x10^3$ *photons/s* and

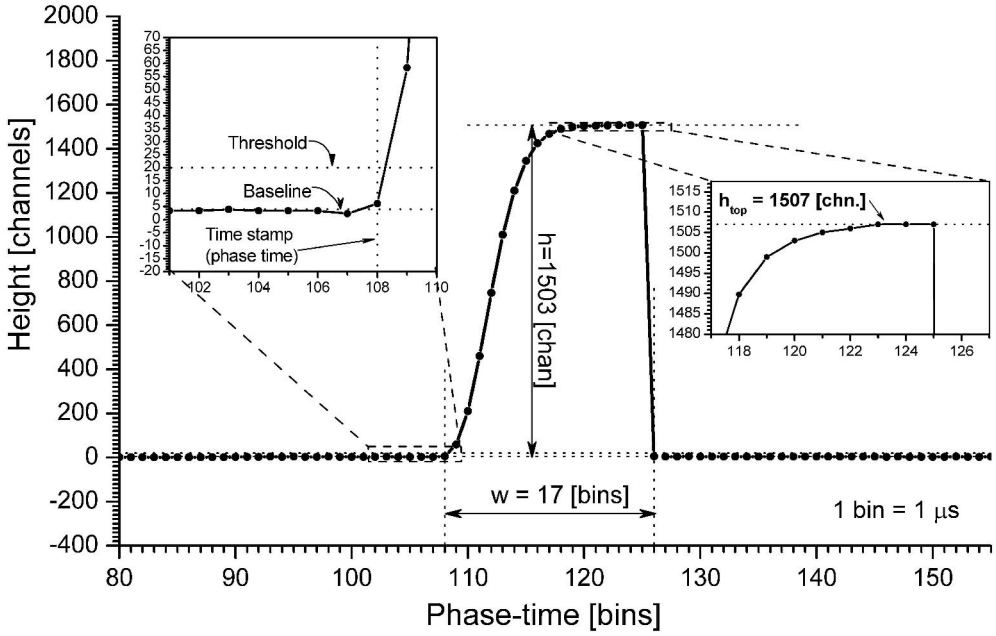

Figure 3.13. Pulse height analysis of a GI-shaped pulse from the spectroscopy amplifier

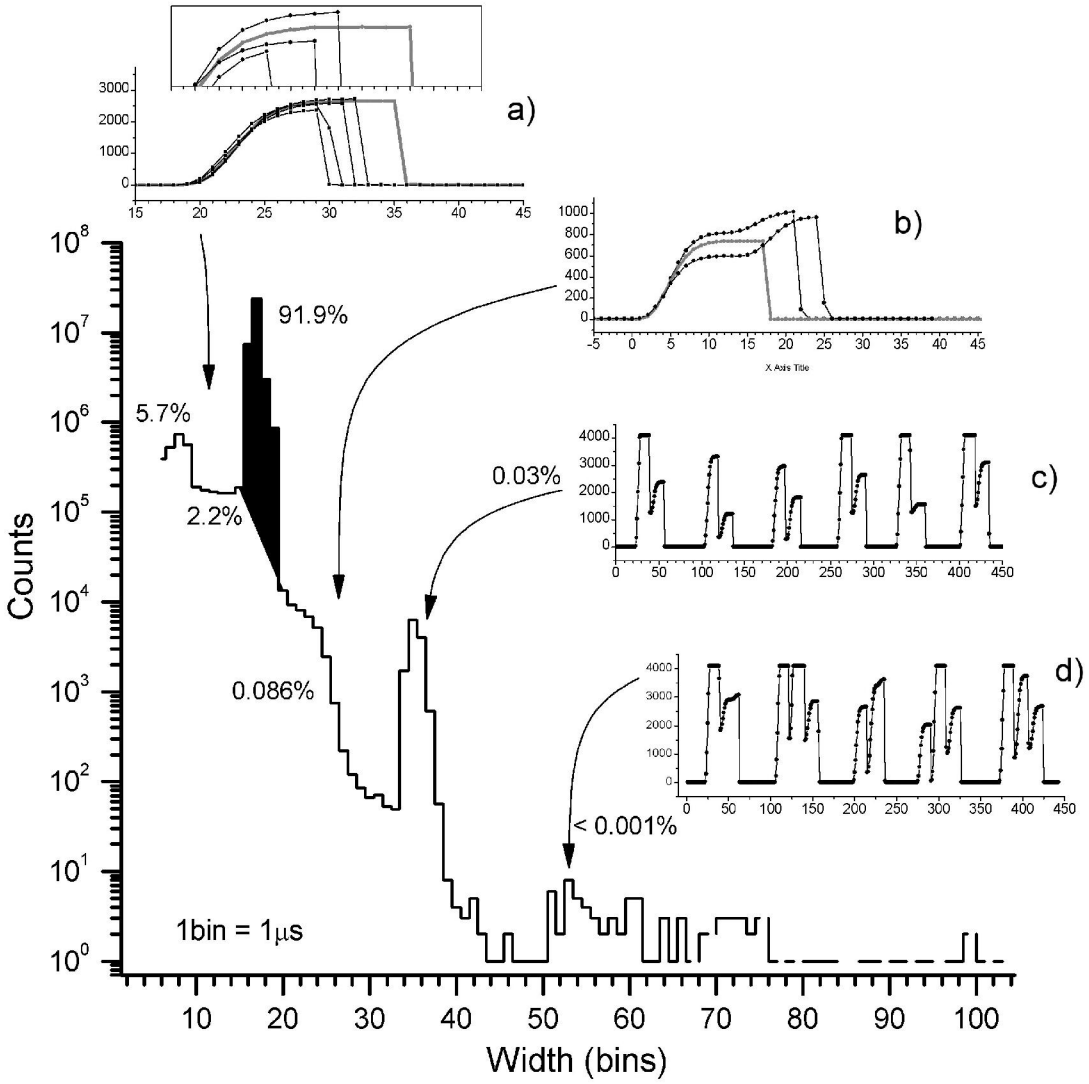

Figure 3.14. Pulse width distribution analysis of the pulses identified at the spectroscopy amplifier analog output as a result of its digitization. Marked in black is the main peak of the distribution, comprising well-shaped signals. The insets show typical pulses corresponding to different ranges of the distribution. In the insets a) and b) in accentuate gray are for comparison the "normal" shapes of signals from the main peak. The b), c) and d) regions are pile-up effects, while the region a) are unfinished pulses.

1 *MS/s* sampling rate. The main peak of the distribution, marked in black, corresponds to the correct shaping of output signals, and in this example it comprises about 92% of all the data considered in that distribution. While it is obvious that the pile-up signals have to be rejected, the part of the distribution containing unfinished-shape signals requires further analyses. The spectra of different ranges of the width distribution show that the width channels(w) $w < 9$ comprise photons with the energy under the spectroscopy amplifier threshold (figure 3.15 (c)) and they does not present any interest.

The inset (a) of the figure 3.15 shows the contribution to the 325 *keV* γ-line of $^{178}Hf^{m2}$ gamma spectrum of the 1% of the data of the main peak of the distribution ($15 \leq w \leq 20$) in comparison with the contributions to the γ-spectrum of the adjacent width channels. It can be seen that the out of the main width distribution peak data contribute to the left tail of the spectral line. Most pronounced effects are from $w = 10$ and $w = 11$ data, but their contribution to the γ-spectrum is less than 0.8 %.

It may be concluded that each detected-signal (photon) can be always characterized by at least three parameters: pulse-height, pulse-width and phase-time (relative to the beginning moment of digitization). The combination of height (energy) and *sub-μs* phase-time information makes possible the system to be more flexible than any combination of conventional multi-input MCA/MCS. It must be mentioned that there is no dead-time associated with the data acquisition because of the *sub-μs* sampling of the analog signals. The classical nuclear spectroscopy instrumentation uses ADCs which at each A/D conversion insert dead periods that are not negligible.

Maintaining the acquisition continuously, without duty-cycle, is dependent on the concrete experimental details. Mainly it requires faster analysis and data logging than the rate of digitization. These are strongly related to some interdependent parameters, such as characteristics of the host PC, the sampling rate, the number of acquisition channels, the counting rate on each channel and finally also on the complexity of the required online analysis.

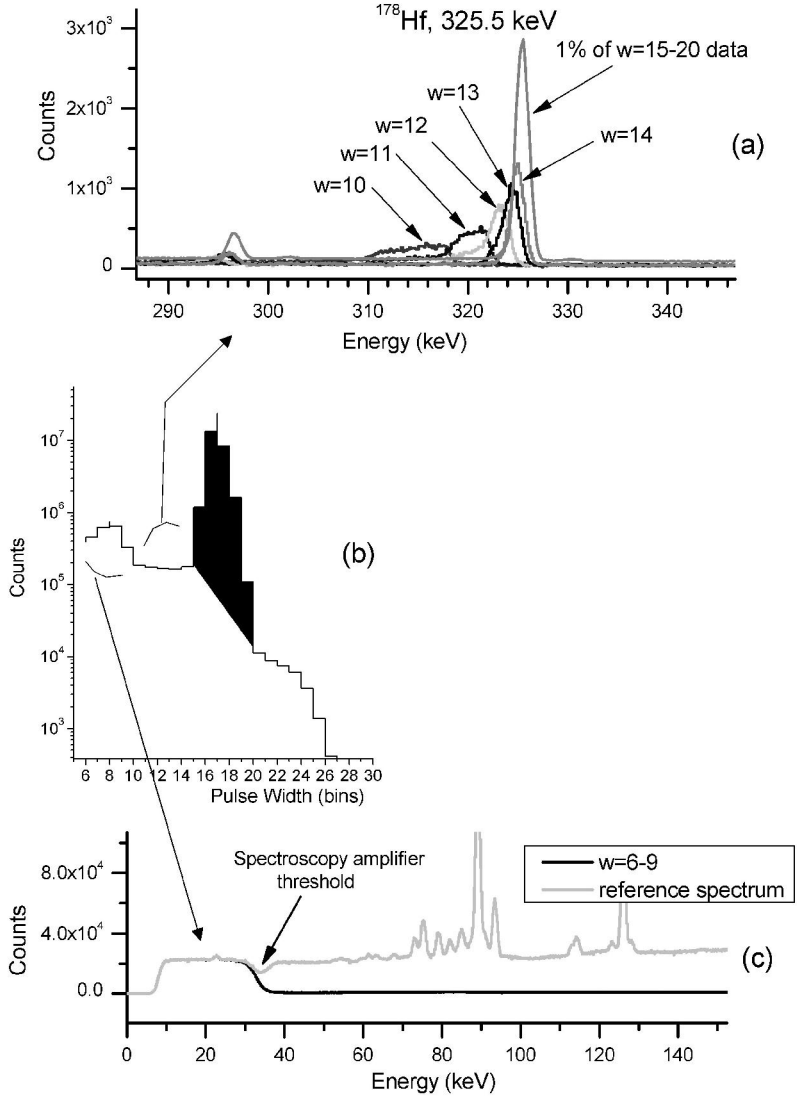

Figure 3.15. Contributions of different regions of the pulse with distribution to the γ-spectrum. Exemplified in inset (a) are the contributions of the unfinished shapes to the 325 *keV* line. The width channel is denoted by "w". The main peak of the distribution shown in inset (b), $15 \leq w \leq 20$, comprises the main and the sharpest contributions to the γ-spectrum. Smaller widths ($w \leq 14$) contribute to the left tail of the spectral line. However their total contribution is not larger than 1.5 %. Inset (c) shows that the peak at $w = 7$ is generated by pulses with height under the spectroscopy amplifier threshold.

3.3.1 Experimental Setup and Data Acquisition for PIGE Investigation in $^{178}Hf^{m2}$ with Bremsstrahlung Radiation

The bremsstrahlung X-ray generator described in the paragraph 3.1.1 was used to stimulate the induced decay of $^{178}Hf^{m2}$ during a series of experiments conducted at the Center for Quantum Electronics of the University of Texas at Dallas. The experimental setup was prepared for single spectra and coincidence data acquisition using four 10% HPGe detectors, as shown in the general diagram of the experimental setup, the figure 3.16. The back-end electronics supplied to the DAQ system four energy and four timing acquisition channels. A supplementary event channel from the coincidence logic unit (AND logic circuit), that was signaling each time when at least two detectors had detected events in a 200 *ns* interval, was delayed and reshaped in order to be synchronized with the outputs of the spectroscopy amplifiers. One more energy channel from a small-area, planar HPGe detector, that was used for monitoring the irradiation, together with a voltage signal proportional with the electronic current passing through the Röentgen X-ray tube were also digitized. The latest signal was used as a phase-time reference in order to correlate the data acquisition with the irradiation. It resulted a total of eleven acquisition channels that were sampled with a 333 *ns* mesh by three synchronized PCI-6110 devices; creating 66.6 *Mb/s* of data and about $4 \cdot 10^4$ *photons/s* from all the detectors. These values made impossible to sustain a continuous acquisition, even with the fastest PC available at that time (P3-PC 733 *MHz* CPU, 133 *MHz* Front Serial Bus (FSB) speed). The solution was a duty-cycled acquisition; the continuous stream of data was accumulated in the PC memory during the first 2 seconds from the beginning of the each X-ray burst, period which was longer than the duration of a burst (1.7 *s*).

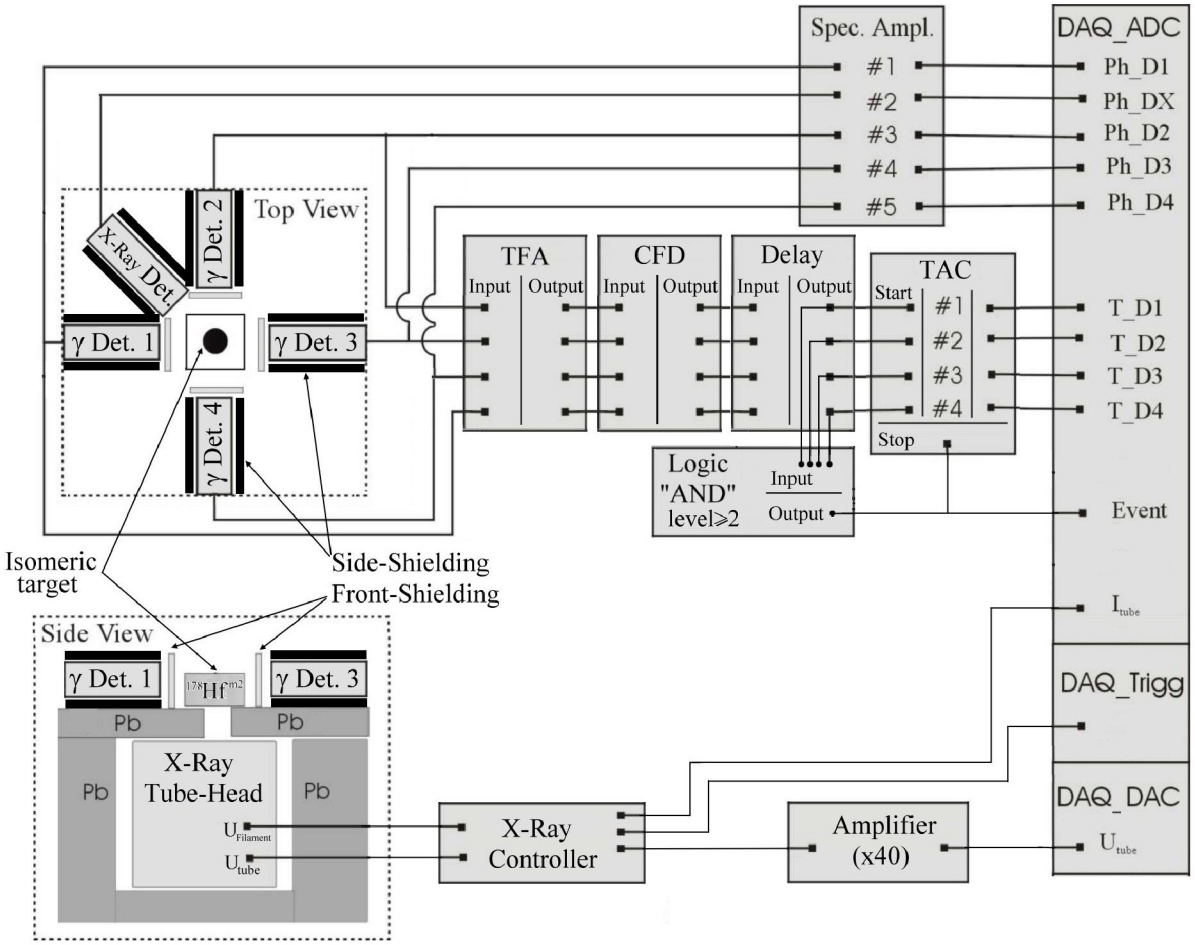

Figure 3.16. Experimental setup for PIGE study of Hf-178 with bremsstrahlung photons

The rising edge of the first X-ray pulse of each burst of irradiation was used as the main trigger to start the acquisition in two modes: “Burst” (as described above) and “cold baseline” (CBL) mode. The latest one was delayed by 30 *s* relative to the beginning of the burst and started right in the middle of the gap between two consecutive irradiation bursts for another 2 seconds.

The data analysis procedure started with the identification of the X-ray pulses in the time-reference acquired channel and divided accordingly the rest of the data-channels in periods of X-ray irradiation (16.66 *ms*). The index of each detected X-ray pulse is retained, and this was a number between 1 and 100 (there were 100 X-ray pulses in each X-ray burst). The data was divided so that the first 2.5 *ms* corresponded to irradiation during an X-ray pulse (inbeam data) and the rest of data, corresponded to the gap between the two consecutive pulses of 14.16 *ms* (outbeam data). The energy- and event-signals were then identified on each channel of divided data. A list of detected photons was created for each detector. This means that there were 5 lists which recorded the values of the five parameters characterizing each energy-signal: X-Ray burst ID, X-Ray pulse ID, photon energy (pulse height), pulse width and the phase-time. Separately, a list of coincidence events was built, which recorded for each detected event signal the energy- and time- pulse height for each detector. If a signal was not identified in the 4 μs window around the event-signal, the value was declared “0”. The validation procedures explained in the previous subchapter were also applied.

After preliminary standard data-checking procedures consisting in analyzing the energy calibration parameters and energy resolution of gamma spectra accumulated about each hour as validation criteria of instrumentation stability, data was sorted in matrices for further analysis. Two types of matrices for each detector in each acquisition mode (“burst” and CBL mode) were created: gamma-energy versus phase-time (γ-t) matrices and (γ-γ) matrices, respectively. The analysis of the (γ-γ) matrices is not the subject of this thesis. The analysis of (γ-t) matrix - corresponding to the

X-ray detector - is presented in the subchapter 3.1.1, as the characterization of the X-ray device emission, while the analysis of the (γ-t) matrixes - corresponding to the gamma detectors - is the subject of chapter 4. It should be mentioned at this point, that the inbeam data used in the chapter 4 was discarded of data collected during transient periods of the high voltage applied on the X-ray tube. During those periods, the transient electromagnetic fields were strong enough to be picked-up by the germanium crystal of the detectors, and amplified by the fast preamplifiers. Unfortunately, by the nature of the experiment, the detector end-caps had to be placed in the close proximity of the head-tube, and so of the HV transformer as seen in figure 3.16. The electromagnetic interferences were strong and fast enough to be separately detected by the spectroscopy amplifiers, which having a slow timing response, become overloaded and then blocked. Even after efforts have been done for EMI shielding of the detectors, of the head-tube and of the rest of the X-ray source, the spectroscopy amplifiers were still blocked on that short periods of time. The figure 3.17 shows the number of γ-photons from the spontaneous decay emitted by the isomeric target versus phase-time. What can be seen is that the effect of residual EMI suppressed the counting rate of the spontaneous emission by overloading the acquisition system. The insets are magnified views around those periods. They show that those periods of interference were limited to about 30 μs intervals at the beginning and at the end of the current pulses to the X-ray head.

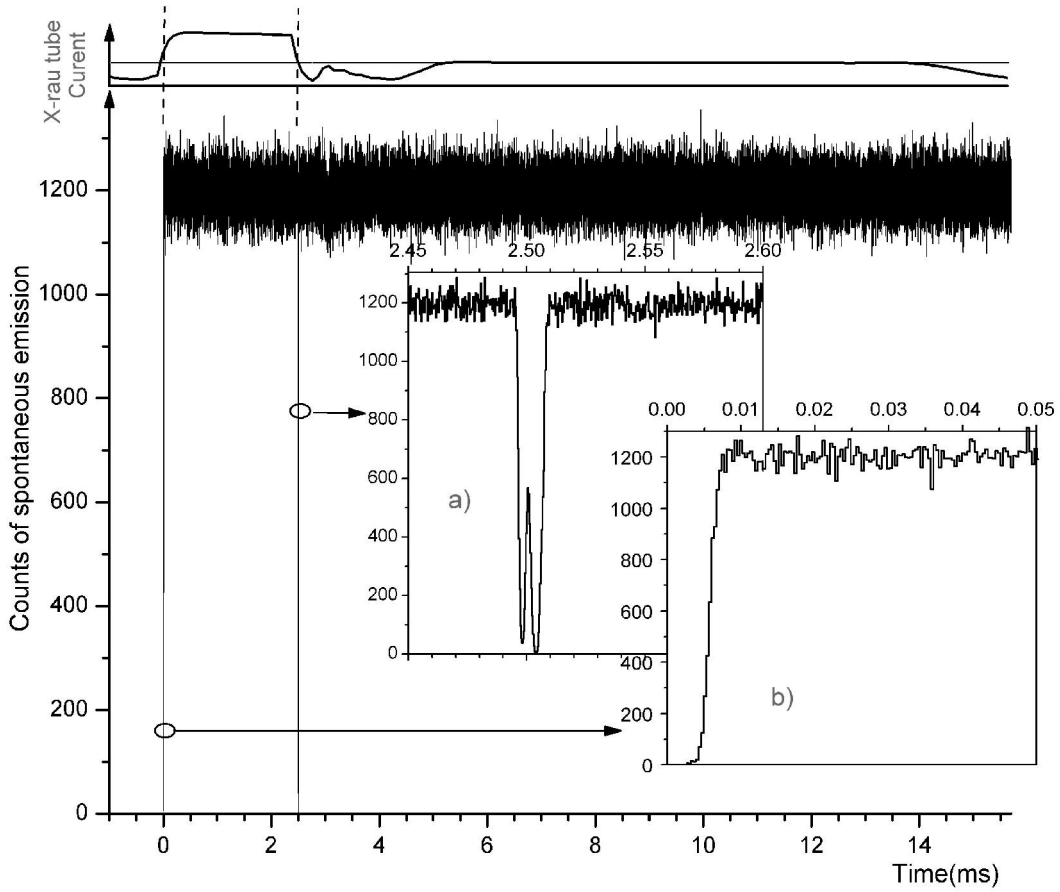

Figure 3.17. Phase-time distribution analysis of gamma photons from the natural decay of $^{178}Hf^{m2}$ during one period of irradiation (16.6 *ms*). During the first 2.5 *ms* the high voltage (HV) is applied on the X-ray tube. The spectroscopy amplifiers are blocked by EMI during the fast transients of the applied HV. These periods are seen in the insets as sharp dead-time periods of gamma acquisition

3.3.2 Experimental Setup and Data Acquisition for PIGE Investigation of $^{178}Hf^{m2}$ with Synchrotron Radiation

In a different manner, the data acquisition in experiments with monochromatic synchrotron radiation had continuous characteristics, meaning that the data digitization and logging worked concomitantly. That was required because the periods of irradiation, at constant energy of incident SR beam where in the range of hundreds of seconds, making impossible hosting the data by PC and logging it at an ulterior time. Also, the decision was made to record the continuous raw stream of digitized data of the back-end electronics. This was done in order to be able to replay them at any ulterior time. Enhanced performances of the computer system were necessary and updated PCs were used in different synchrotron irradiation experiments.

In general, the energy and timing information, corresponding to two 10% HPGe detectors, together with one more timing channel associated to the APD detector were continuously acquired (figure 3.18). The timing channels corresponded to the interval of time measured between the each detected gamma-photon and the clock cycle period of the synchrotron storage ring.

In order to synchronize the acquisition system with the beamline system that controlled the advancing of the monochromator and monitored the incident flux on sample, the digital signal used for gating the counters of the ionization chambers was passed to the DAQ system and used for triggering. The gating signals were generated for equal periods of time at each stepped energy of the SR beam, immediately after changing the monochromator energy, as shown in figure 3.19. The inbeam data was acquired on each period of the gate signals, same as for the ionization chambers. At the end of each inbeam data accumulation period the DAQ system commanded a motorized absorber

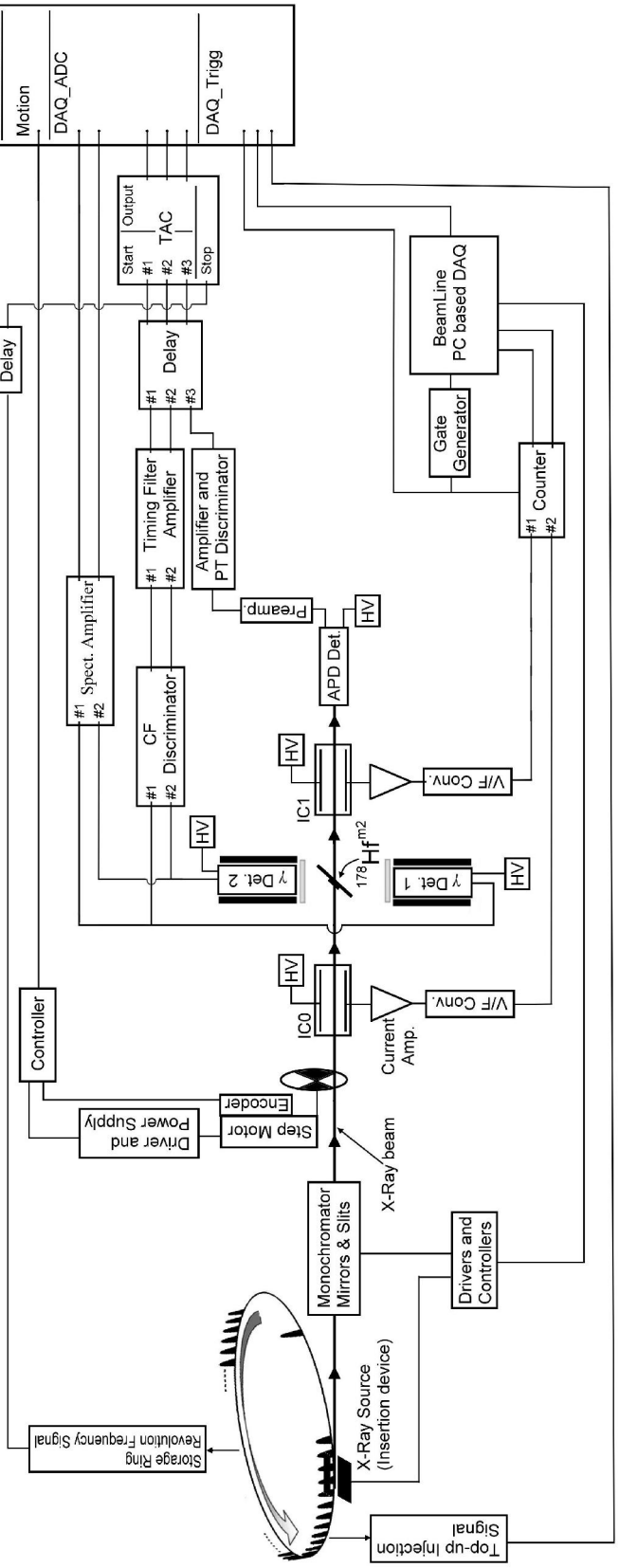

Figure 3.18.Experimental setup for PIGE study of Hf-178m2 with monochromatic synchrotron radiation

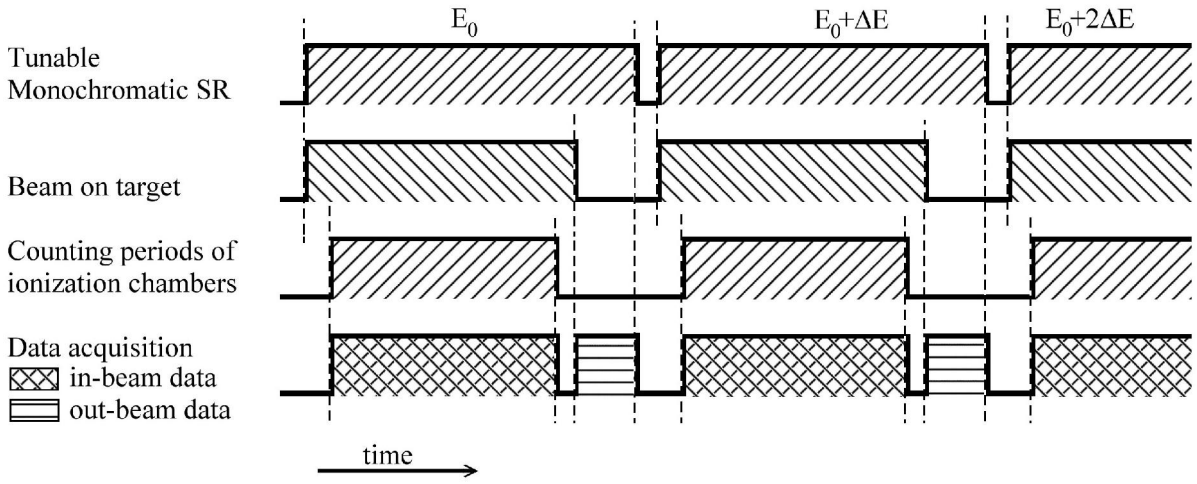

Figure 3.19. Irradiation and data acquisition schedule in experiments conducted at SR facilities

to move in the front of the beam in order to impede it from hitting the isomeric target. This permitted us to collect the outbeam data for a period of time usually chosen to be a quarter of the time for inbeam data accumulation. The monochromator was commanded to change the energy only after the outbeam data acquisition was finished.

The absorber consisted of a 1.5 *cm* thickness stainless-steel disk having a chopping design with alternate large open windows (100% transparency). It was mounted in the front of the target, perpendicular to the beam direction as shown in the figure 3.18, so that by its rotation it was obstructing the incident beam or was leaving it free to hit the isomeric sample. Its movement was under the control of an NI PCI-7334 Stepper Motion Controller with rotary encoder feed-back.

In the acquisition time, inbeam or outbeam, consecutive blocks of digitized data from the all input channels corresponding to each consecutive second of fast digitization were read from the DMA buffer memory location fast enough to prevent the overloading of the buffer memory and thus maintaining the continuous characteristic of acquisition, without dead-times. Each block of data was analyzed in real time just enough to supply enough information for monitoring of the acquisition, while a considerable amount of time was required for raw data compressing and logging. Each compressed data file was named in a coded way, so that to uniquely identify each second of digitization corresponding to inbeam or outbeam conditions at each stepped energy of the SR beam set it by the monochromator.

The complete analysis of the raw digitized data was performed at the end of the experiment. It involved building lists of photons at the first stage of analysis, in the same manner as presented in subchapter 3.3.1. This made distinction between photons acquired at different energy of SR beam. The standard validation procedures were also applied. Two or three-dimensional matrices, γ-x (γ -energy versus X-ray beam energy) or γ-t-x (γ -energy versus fast-time versus X-ray beam energy)

were created for inbeam and outbeam data, respectively and for each run of acquisition. Standard rebinning procedures were applied on the data matrices if the calibration parameters showed significant changes. Different representations of data were extracted from matrices and were used for analysis. The results of data analysis are presented in the chapter 5, 6 and 7.

CHAPTER 4

GAMMA-RAY TRANSITIONS INDUCED IN NUCLEAR SPIN ISOMER BY BREMSSTRAHLUNG X-RAYS

4.1 Preface

Chapter 4 contains the original text of the manuscript *Gamma-ray transitions induced in nuclear spin isomers by X-rays* by C. B. Collins, N. C. Zoita, A. C. Rusu, M. C. losif, D. T. Camase, F. Davanloo, J. M. Pouvesle, R. Dussart, V. I. Kirischuk, N. V. Strilchuk, C. A. Ur, I. I. Popescu and F. J. Agee. It was originally published in Journal de Physique IV 11**,** Pr2-437 in 2001 and is reprinted here by permission of the Edition Diffusion Press (EDP) Sciences. The paper appears in this dissertation unaltered from its J. de Phys. IV form except for the numbering of figures. It presents parts of the 2000 experimental efforts conducted at the Center for Quantum Electronics of the University of Texas at Dallas for studying the accelerated decay process of $^{178}Hf^{m2}$ by X-rays.

As a senior graduate student, N. C. Zoita had the responsibility of redesigning the X-ray device and of the data acquisition and logging system. While the experimental setup has been designed for multi-detector single-spectra and γ-coincidence measurements, N. C. Zoita had also the responsibility of single-spectra data reduction and shared the data analysis with C. B. Collins, J. M. Pouvesle and R. Dussart. Original text was written by C. B. Collins in collaboration with the authors.

4.2 Gamma-Ray Transitions Induced in Nuclear Spin Isomer by X-Rays

4.2.1 Abstract

Because of the high density of energy storage and the large cross section for its release there is considerable significance of the triggering of induced gamma emission from nuclear spin isomers to efforts to develop intense sources of short-wavelength radiation. The work reported here describes the current experimental focus and results recently obtained.

4.2.2 Introduction

At low energies there are similarities between structures of the excited states of atoms and nuclei that encourage studies of the analog for nuclei to the phenomenon of resonance fluorescence in atoms. Both systems involve the storage of energy in the quantized movement of the constituent charges. In atoms electrons populate excited states which can be conveniently described in terms of single-particle orbitals such as 1s and 2p. In nuclei the neutrons appear as relatively negative concentrations in the overall positive fluid of the nucleus; so there is the possibility to store energy by raising either protons or neutrons, or both, up distinctly separate "ladders" of excited single-particle states. Because many of the interesting cases occur in nuclei deformed from the idealized spherical shape, for nuclei the nomenclature appears more complex. An excited state such as $1h_{11/2}$ $9/2[514]_n$ (or simply, $9/2[514]_n$) would describe the population by a neutron of a 1h orbital with total angular momentum, *J*, of 9/2 with the [514] describing fine points of the orientations of the nodes in the wavefunctions on the various coordinates of the aspherical nucleus. An oddity is that the structural requirement for atoms that quantum numbers, $n \geq (\ell+1)$ does not apply to nuclei because the fundamental potentials are different.

In either the case of atoms or nuclei the energy stored in the population of excited states is often released by the spontaneous emission of electromagnetic radiation. Atoms emit photons of light and x-rays while nuclei emit gamma photons, but the principles and selection rules remain the same. When spin of the constituent particles is introduced into the models, the possibility for long-lived metastability is clear in both systems. Figure 4.1a shows a schematic comparison of the single particle states important in the formation of a typical metastable He atom and two nuclear analogs for long-lived excited states of ^{178}Hf termed "isomeric". In each system spontaneous emission is "forbidden" for simple dipole transitions because there is no lower energy state to which the excited particle could "fall" without overturning its spin, a step particularly forbidden by selection rules. In addition to illustrating the analog of metastability in nuclei, figure 4.1 is also useful for introducing another concept unique to the nuclear systems, the formation of "mixed states" which have been found to be important for the triggering of the release of the metastability. In this example because there is the accidental occurrence of open states for both neutrons and protons that have the same *J* and same energies of excitation, quantum interference produces the more realistic situation shown in figure 4.1b in which the resulting metastable, or isomeric, state is composed of a superposition of excited neutron and proton structures and so is not the result of promoting in energy a single constituent particle. An unusual example, it nevertheless typifies one distinction between atomic and nuclear structure in that in the latter case it is likely that constituent entities being promoted in energy have more complex structure than implied by schematics such as figure 4.la. Accepted terminology would designate the state actually realized as a 2-quasiparticle (2qp) isomeric state as shown in figure 4.1b, the digit, 2- indicating that two entities populate states with total spins not canceled by "pairing" of angular momenta in antiparallel arrangements. Besides the mixing of charge identities there are possibilities for mixings of other types, such as those introducing

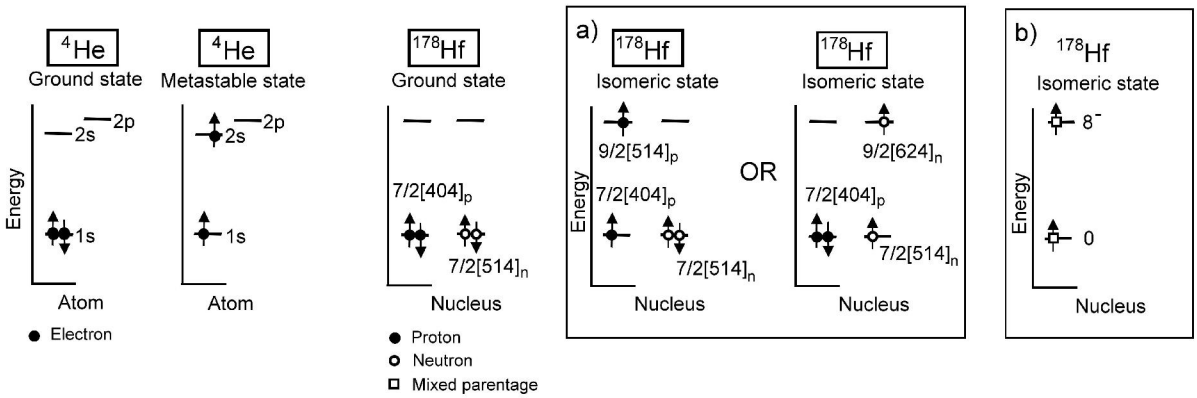

Figure 4.1. Schematic diagram illustrating the similarities between metastable states of atoms and spin-isomers. States, if any, at lower energies than shown are assumed to be filled with pairs of particles with antiparallel *J*.

properties resulting from the quantized rotation of the aspherical nucleus as a whole, or even from oscillation between prolate and oblate asymmetries [93, 94]. By introducing additional degrees of freedom from such mixings, more transitions may become allowed to facilitate spontaneous decay.

The most interesting of the nuclear metastables may be the 16^+ 4-qp isomer of ^{178}Hf in which one member of a pair of both protons and neutrons is raised in energy to the next open excited state and "flipped" in spin so that spontaneous emission of electromagnetic radiation is doubly "forbidden" by selection rules applying both to the protons and to the neutrons. These states store 2.445 *MeV* for a half-life of 31 years meaning that as a material, such isomeric ^{178}Hf would store 1.3 *GJ/g*. Small samples exist for experimentation and the stored energy has been released by exciting the isomeric state to a higher level of mixed composition from which spontaneous decay was no longer forbidden [22, 23]. The trigger excitation was provided by the resonant absorption in the nucleus of a photon of less than 20 *keV* energy and the energy gain per event exceeds 100-fold. Neither the quantum structure of the mixed state excited by the incident x-rays nor the precise energy of excitation has been determined. Nevertheless, because of the high density of energy storage and the large cross section for its release there is considerable significance of this triggering of induced gamma emission from nuclear isomers to efforts to develop intense sources of short-wavelength radiation. The work reported here describes the current experimental focus and results recently obtained.

4.2.3 Experiment and Results.

The original experimental system described previously [70, 94] has been recently rebuilt to provide better stability and control of the apparatus. The sample of isomeric ^{178}Hf is still irradiated in proximity of 5.5 *cm* to the x-ray anode within a sealed head normally used in dental medicine. However, the power

supplied to the tube has been replaced with a waveform synthesizer used to provide a stepped pulse of current which could be programmed to values as great as 80 *mA* for a duration of 2.5 *ms* to excite line and Bremsstrahlung x-rays with an end point of 63 *keV*. The x-rays are emitted in a vertical beam into the isomeric target and the fluorescent gamma rays are collected by 4 Ge detectors equally spaced radially in the perpendicular plane containing the target. The x-ray source is operated in bursts producing 100 pulses at a 60 *Hz* rate, one burst made each minute. During the burst, the analog signals from the detectors are continuously digitized on a 333 *ns* mesh and the results stored for analysis between bursts. With only PC-based facilities, that data is analyzed to obtain and log the energy and time of arrival of each gamma photon collected. The intrinsic activity of the isomeric target and its proximity of about 20 *cm* to the detectors yields about 10^6 events per detector per hour to be logged. A processor speed of 750 *MHz* with 512 *MB* RAM has been found adequate to support the data acquisition. Since the data log contains both time and energy for every photon detected, the effect of the x-ray irradiation in accelerating the decay of the isomeric population can be found by comparing photon counting rates logged within a burst during the time the x-rays were present and absent for some of the energies of the fluorescent gamma photons.

Figure 4.2 shows a small part of the energy level diagram for the ^{178}Hf nucleus. Only the relatively few levels through which transitions pass during the spontaneous decay of the isomer have been shown. Since the nucleus has prolate deformation the scheme superficially resembles that for a diatomic molecule with "rotational bands" being built upon intrinsic states of single-particle excitation. Besides the 4-qp isomer, 16^+ only the two intrinsic states used above as examples are important in the spontaneous decay of the ^{178}Hf isomers. Transitions between members of the rotational bands built upon those two contribute most of the lines seen in the spectrum. The two bands are the ground state band, GSB and the 8^- band and they are connected by the interband transition at 88.86 *keV*

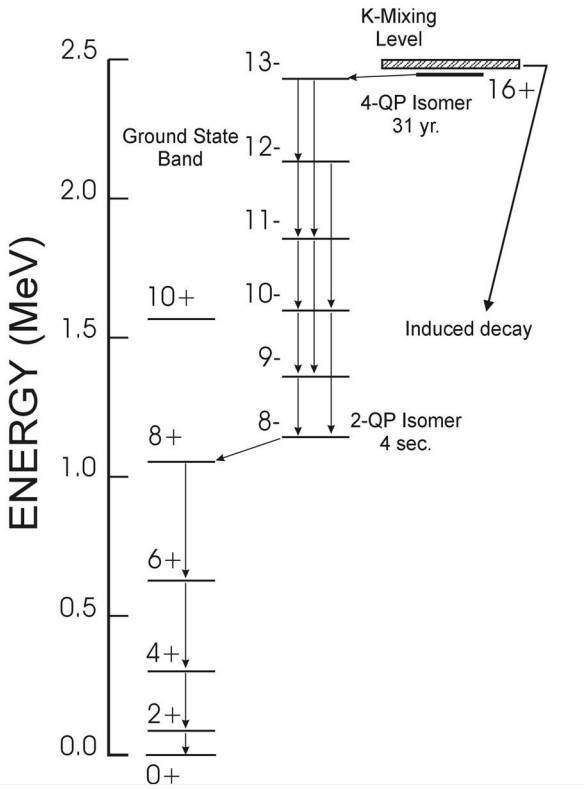

Figure 4.2. Schematic diagram of the nuclear energy levels important in the spontaneous decay of the spin isomer ^{178}Hf

which is delayed by the 4 *sec* half-lifetime of the 8^- bandhead. However, in the actual target used in these experiments, lines from daughter nuclei from the decay of Hf impurities complicate the data collection. Only about 5.7% of the events logged arise from transitions in the GSB of ^{178}Hf and those contribute the most prominent parts of the spectrum.

Figure 4.3 shows the part of the spectrum of the gamma rays for which emission was induced by absorption of low energy x-rays. It was obtained by subtracting the spectrum of spontaneous emission from the photons logged when the x-ray irradiation was turned off from the spectrum of spontaneous plus the extra induced emission logged at times when the x-ray irradiation was active. Since the gammas from the impurities is not affected by x-ray irradiation, the absence of any effect in the 181.56 *keV* line from ^{172}Lu is an ideal test to verify that the two data sets being subtracted to show the extra induced emission were properly scaled to reflect same times for the collection of data. Results shown in figure 4.3 for each of the two different levels of pulsed current through the x-ray source required the logging of data for about 100 *hrs* of operation.

4.2.4 Conclusions

The work reported here continues to confirm that the irradiation of samples of 4-qp isomers such as ^{l78}Hf with x-rays at power levels of mW/cm^2 containing component lines and continua with end points greater than 20 *keV* [70] can materially increase the rate of decay of long-lived nuclear populations. In this case of ^{178}Hf the half-life for the storage of energy is 31-yr and the energy gain per triggering event exceeds 100-fold, making this a very interesting system. From figure 4.3 it can be appreciated that the released energy most readily detected is the result of transitions between members of the GSB excited in the course of the normal spontaneous decay. However the distribution of intensities differs. In the

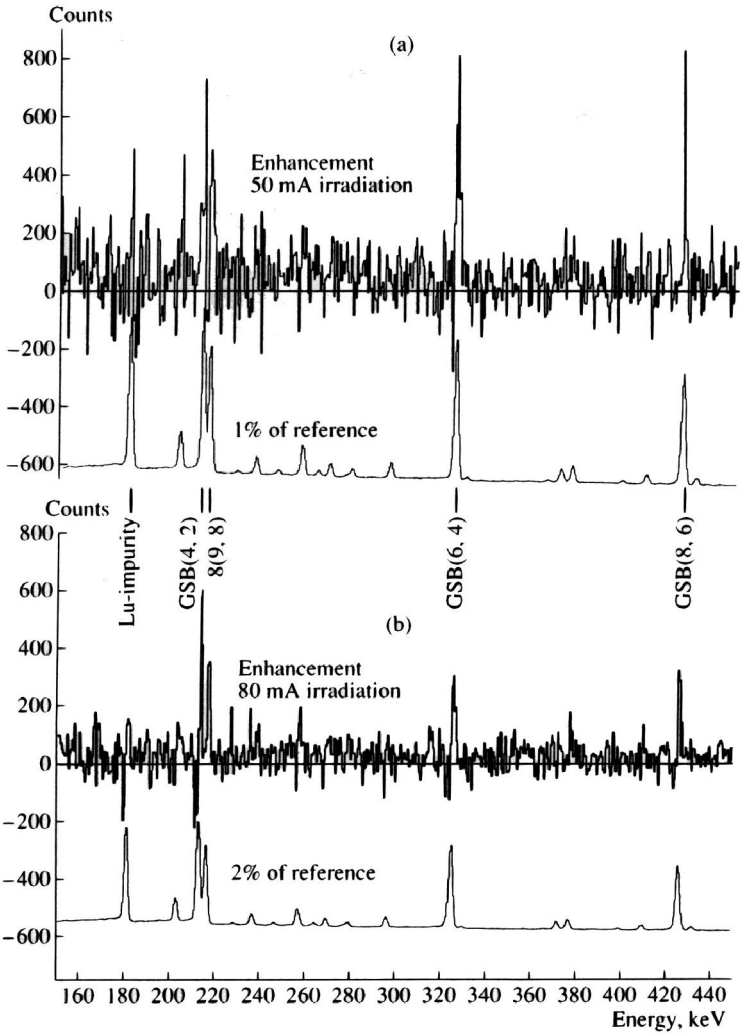

Figure 4.3. Data showing the enhanced gamma emission from the 16^{+} spin isomer of ^{178}Hf induced by pulses of x-rays. For comparison and identification, spectra are shown that were obtained without irradiation and that were scaled by the amounts shown. a) Irradiation with 50 *mA* current in the x-ray tube, b) with 80 *mA* in the x-ray tube

spontaneous decay the 8^+ level of the GSB is populated by the interband transition and the subsequent transitions occur in steps passing through each lower level in sequence. As a result all members of the GSB have about the same intensity in spectra of spontaneous emission. In contrast, the induced emission can be seen to be stronger in lines from transitions connecting lower members of the GSB. The x-rays excite the isomer to the mixing level from which electromagnetic transitions are no longer forbidden, but then by some path not yet identified, cascades of transitions convey the excited state population into lower members of the GSB without dropping them down in energy through the higher members. It has been indicated [70] that some newly observed lines have arisen from transitions through these induced cascades, but intensities in any one of the lines has been insufficient to fully explain the scheme of induced decay. It has been proposed that once induced, the decay from the mixing level proceeds through many parallel cascades, no one of them concentrating enough emission into a single spectral line for unequivocal detection. Current research objectives focus upon the collection of more data from which the additional decay cascades may be deduced.

Acknowledgments

The authors gratefully acknowledge the USAF Air Force Office of Scientific Research through AFOSR Contract No. F49620-99-1-0082 for support of this experiment.

CHAPTER 5

INDUCED γ–EMISSION FROM $^{178}HF^{m2}$ BY SYNCHROTRON RADIATION

5.1 Preface

The text of chapter 5 contains the original manuscript *Tunable synchrotron radiation used to induce γ-emission from the 31 year isomer of 178Hf* published in Europhysics Letters 57 (5), 667 on March 2002 and is reprinted here by permission of the Edition Diffusion Press (EDP) Sciences. It was authored by C. B. Collins, N. C. Zoita, A.C. Rusu, M. C. Iosif, D. T. Camase, F. Davanloo, S. Emura, T. Uruga, R. Dussart, J. M. Pouvesle, C. A. Ur, I. I. Popescu, V. I. Kirischuk, N. V. Strilchuk and F. J. Agee.

As the title implies, the paper presents the first experimental investigations of induced deexcitation of $^{178}Hf^{m2}$ isomer with tunable synchrotron radiation, as a result of previous experimental efforts with bremsstrahlung radiation which established unusually high values of the interaction cross section and also that only photons with energy lower than 20 *keV* can stimulate the deexcitation of the isomer. The implication of the electronic shell was assumed as mediating the nuclear excitation process, starting from the *m2* isomeric level. Therefore, irradiation with high flux of tunable synchrotron radiation was required for testing this presumption and also for identification of the energy of photons which contribute to the acceleration of the isomeric decay. For these, two separate experimental series were conducted in March and June 2001 at the BL01B1 beamline of the third generation synchrotron radiation source SPring-8, in Japan, which are the subject of this chapter.

The author of this thesis had the responsibility for the design and implementation of the data acquisition in experiments with synchrotron radiation, for data reduction, and shared a major part of the responsibility for the analysis of the data. The original paper was written by Carl B. Collins in collaboration with the authors. The paper appears in this dissertation unaltered from its Europhys. Lett. form except for the numbering of figures and references.

5.2 Tunable Synchrotron Radiation Used to Induce γ-Emission from 31-Year Isomer of ^{178}Hf

5.2.1 Abstract

A process for transferring energy from electron shells into nuclear excitation, NEET, has offered the promise for modulating nuclear properties at accessible levels of power. It had been proven recently by exciting a nuclear level of ^{197}Au with synchrotron radiation, but measured couplings were far below theoretical objectives. Reported here is an extension of that approach for excitation to ^{178}Hf^{m2} isomeric nuclei. Isomeric targets were irradiated with X-rays in the beamline BL01B1 at the synchrotron radiation source SPring-8. Energies were tuned from 9 to 13 *keV*. In this range an excitation branch attributed to NEET was found to have a probability of 2×10^{-3} relative to *L*-shell photoionization. The resulting emission of exoergic γ-photons was observed from the target at a rate approaching the theoretical maximum.

5.2.2 Introduction

In 1993, Ho *et al.* [39] described how higher-order processes for non-resonant excitation (NEET) could couple energy into nuclei from the surrounding electronic shells. “Satellites” on absorption transitions between nuclear levels were predicted. Kishimoto *et al.* [61] have recently proven such NEET phenomenology by exciting the ground state of ^{197}Au with synchrotron radiation (SR). They observed the excitation and decay of the ($1/2^+ \rightarrow 3/2^+$) (Mössbauer) transition of ^{197}Au at 77.351 *keV* by resonant absorption of SR at 80.989 *keV*. Although the absorption satellite for exciting the nuclear transition was not explored by tuning the SR energy to other “off-resonant”

values, it was reasonably concluded that excitation through *K*-shell photoionization was responsible with a branching probability for NEET of $5.0 \pm 0.6 \times 10^{-8}$.

As a vehicle for the further demonstration of NEET spectroscopy, the 16^{+} state of $^{178}Hf^{m2}$ is particularly attractive. It is a 4-quasiparticle state having 2.446 *MeV* of excitation and a half-life of 31 years. If NEET were excited by SR there would be the possibility for exoergic emission of γ photons with energies exceeding those of the irradiation. Then, the experimental arrangement could be facilitated by the use of layered absorbers to selectively remove X-rays scattered from the SR source. Reports of the use of X-rays with energies below 20 *keV* to accelerate the decay of $^{178}Hf^{m2}$ spin isomers [22, 70] further encouraged planning for the use of that isomer in a NEET experiment.

Reported here are the first successful examples of the irradiation of samples of $^{178}Hf^{m2}$ isomeric nuclei with synchrotron radiation. Moreover, in this work the SR was tuned over the range of energies 9–13 *keV*, selected because it contains much of the transition strength for photoionization of the *L*-shell electrons of Hf. A branching ratio of 2×10^{-3} was found for the excitation of nuclear transitions from absorption of SR by the *L*-shell electrons. Those events led to the emission of exoergic γ-photons.

5.2.3 Experiment and Results

Two targets were used in these experiments. Both were fabricated from material in which the isomeric fraction was about 10^{-3} of the total Hf content. One was composed of two separately encapsulated samples of 5.8×10^{12} $^{178}Hf^{m2}$ isomeric nuclei each. The other target contained three sealed samples of 1.3×10^{13} each. They were irradiated with the tunable output from a bending magnet in the BL01B1 beamline at the synchrotron radiation source SPring-8 in two separate

experimental series separated by weeks. Passed through a monochromator the output beam reaching the target was 2 *mm* × 5 *mm* in size in the first survey experiment. The flux was $3.0 \pm 0.6 \times 10^{10}$ *photons* cm^{-2} s^{-1} with a nominal spectral bandwidth of 0.5 *eV*. It was tuned from 9.0 to 13.0 *keV* in steps of about 5 *eV*, remaining 10 *s* at each energy. The basic scan was repeated four times. Of particular importance was that the first target was optically thin to SR between 9 and 13 *keV* when mounted at 45°. The target constructed for the second experimental series was designed to give higher signal rates. It was mounted in grazing incidence inclined 12° with respect to the line of the SR beam which was adjusted to have cross-sectional dimensions of 1 *mm* × 5 *mm*. Tuning range intervals found to be interesting in the first experiment were re-examined with 0.5 *eV* steps in SR energy. Data were collected for 50 *s* at each X-ray energy and each scan was repeated 3 or 4 times, depending upon limitations imposed by the periodic reinjection of the synchrotron current.

The performance of the target is of critical importance in such experiments. Spontaneous decay of the population of isomers produces energetic γ's able to escape from millimeter thicknesses of target structure and mounting. However, if not optically thin to the SR at the X-ray energies used, the spontaneous emission from the entire target can readily "drown" any component of NEET contributed by the outer micron thickness of sample exposed to the SR. Several attempts at demonstrating NEET with isomeric targets have recently failed for lack of optical transparency at the resonant energies for NEET [95]. In the work reported here particular attention was given to the properties of the target structure. In the second series of experiments the SR intensities were continuously measured in-line with ionization chambers placed before and after the isomeric target. Figure 5.1 shows the SR flux (corrected for attenuation caused by passage through the first ionization chamber) that was incident upon the target assembly for each of the several intervals of SR energy examined. Also shown in figure 5.1 is the resulting attenuation coefficient of the target obtained from

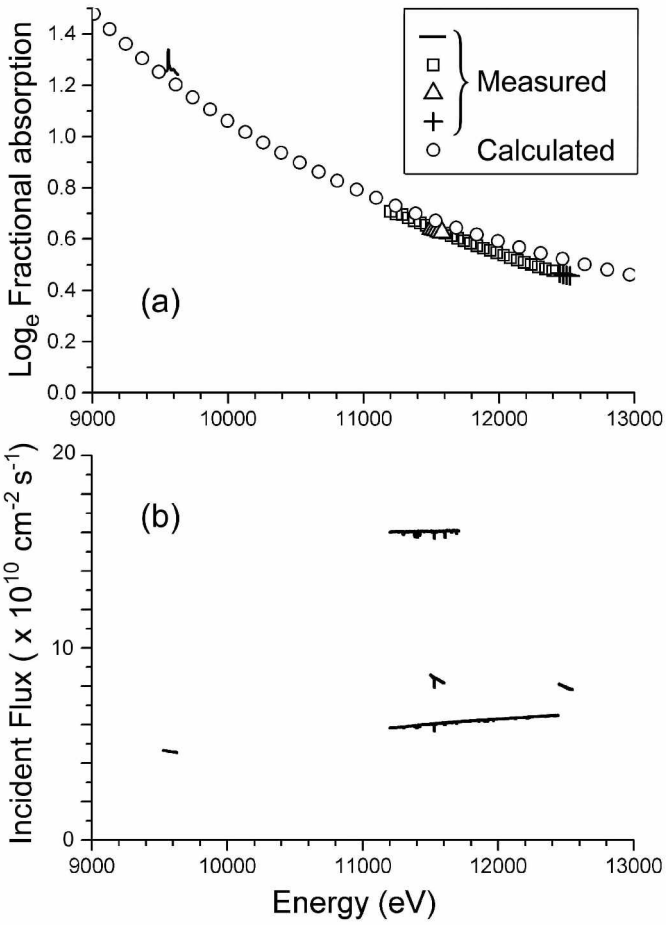

Figure 5.1. Irradiation environment. (a) Absorption coefficient of the target measured in-line as a function of SR energy during the different irradiations. (b) Measured values of SR flux.

both ionization chambers. Despite the considerable changes in SR flux set during the experiment, agreement can be seen between the absorption coefficients extracted for the target for the different conditions, and with the attenuation calculated for the geometry and measured density of the plastic encapsulations of the samples stacked into the target. No fitted parameters were used in preparing figure 5.1.

A Si drift detector (SDD) was used both to confirm the location of the target activity in the SR beam and to survey the level of scattered SR in the detector environment. Figure 5.2 shows the level of elastic scattering to be sufficiently low to facilitate gating upon photons selected to record the intensity of L_α fluorescence from the Hf component of the target. Figure 5.3 shows the technique used to locate the activity of the target in the SR beam. The data were obtained by moving the target vertically with a stepping motor while the absorption coefficient was measured with the ionization chambers and the intensity of L_α fluorescence from the Hf component was monitored by the SDD. The slit limiting the vertical dimension of the SR beam was narrowed to 0.1 *mm* during this adjustment. After the activity was located, the slit was set as shown in figure 5.3. The process was repeated in the horizontal direction and showed the activity to extend 4.6 *mm* in that direction. The activity had the form of an elliptical annulus in each sample and the samples had been assembled into the target slightly out of register to prevent the Hf components from shadowing each other and that accounts for the morphology seen in figure 5.3.

A Ge spectrometer 10 *mm* thick ×16 *mm* dia. was placed 25 *mm* from the target at right angles to the beam and was shielded with layered foils of W, Cd, and Cu, as seen by the beam. It was connected to an EG&G 673 spectroscopy amplifier from which the output was continuously digitized and recorded to permit subsequent re-examination of the electrical pulses describing the detected photons. The spectrum of the target has been described previously [22, 70] and was composed of

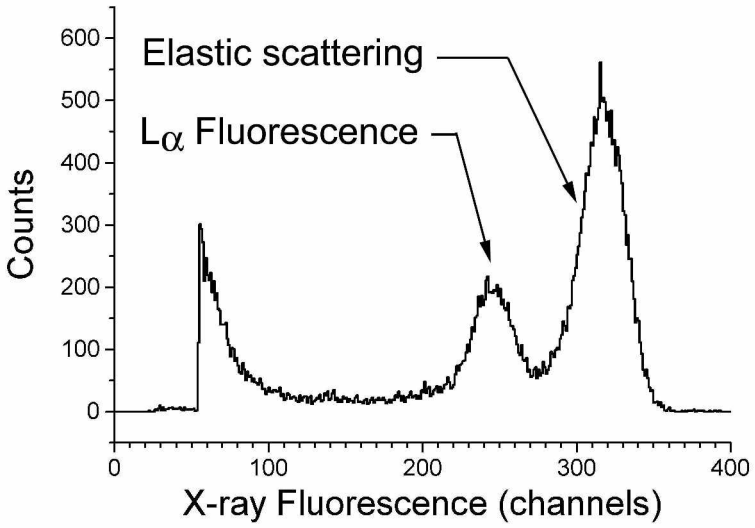

Figure 5.2. Spectrum of the low-energy X-rays scattered by the target from the SR beam.

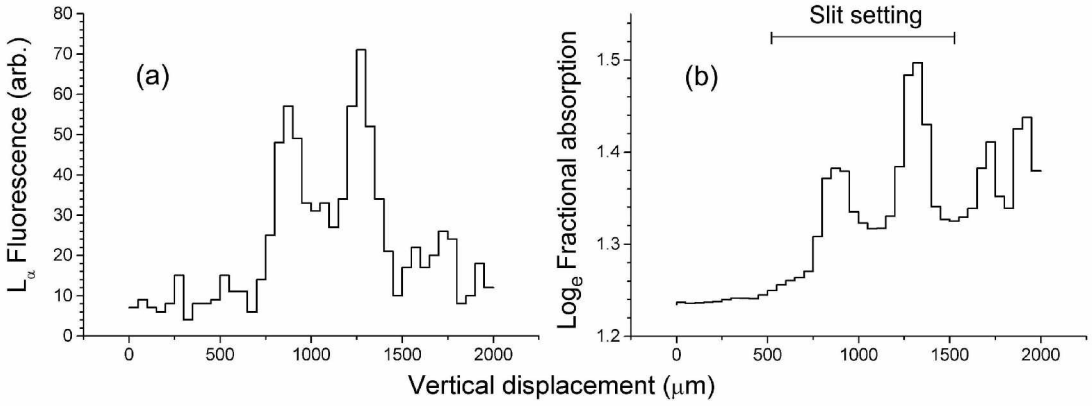

Figure 5.3. Target alignment. (a) Hf(L_α) fluorescence from the target as a function of vertical displacement. (b) Absorption coefficient of the target measured in-line with the SR beam narrowed to 0.1 *mm* vertical height.

only the well-known decays [96] of $^{178}Hf^{m2}$ and of the ^{172}Hf impurity and its daughters. Of the former, only the (4, 2), (6, 4), and (8, 6) members of the ground state band, GSB at 213.4, 325.6, and 426.4 *keV*, respectively, and the lowest member of the 8^- band at 216.7 *keV* were recorded at significant counting rates because of declining efficiency of the Ge-detector for higher energy γ's. Of the lines from the impurities, only two, 125.8 and 181.5 *keV*, could be recorded with significance. Data were analyzed with a mesh of 8.8 γ channels per *keV*. When the monochromator changed energies, a digital signal was sent to a second channel of the data logging system to correlate the signals from γ-photons with the energies of the irradiation. Regions of interest (ROIs) associated with each of the spectral features were identified in the 4096 channel histograms of the numbers of γ-photons detected during each period of irradiation with SR. For simplicity, in most cases the sums for the ROIs for 213.4 and 216.7 *keV* were used to study the excitation functions of the $^{178}Hf^{m2}$ sample. The ROI for the 181.5 *keV* impurity line provided a convenient indication for the null effect.

The most pronounced evidence for NEET is shown in figure 5.4. Raw data are shown in the form of counts collected in ROI(216.7) during 60 *s* periods of irradiation. The energy of the SR X-rays was incremented in 3 steps of 0.5 *eV* each during those periods. The intervals over which total counts were collected for entry into table 5.1 are indicated. The corresponding feature at the L_3 edge for photoionization was examined in 0.5 *eV* steps with 50 *s* duration repeated 4 times. Figure 5.5 shows the results in terms of fractional increases over the average counting rates observed at the lower X-ray energies just below the L_3 edge. Numerical values of the counts are reported in table 5.1.

From the data of table 5.1 the cross-sections, σ_c, for excitation can be readily expressed as $\sigma_c = fA/F$, where f is the fractional enhancement over spontaneous emission, A is the rate coefficient for spontaneous emission ($A = 7.09 \times 10^{-10}\ s^{-1}$), and F is the irradiating photon flux. Values of flux were taken from figure 5.1(b) and were corrected for the absorption from the encapsulation. For the 3

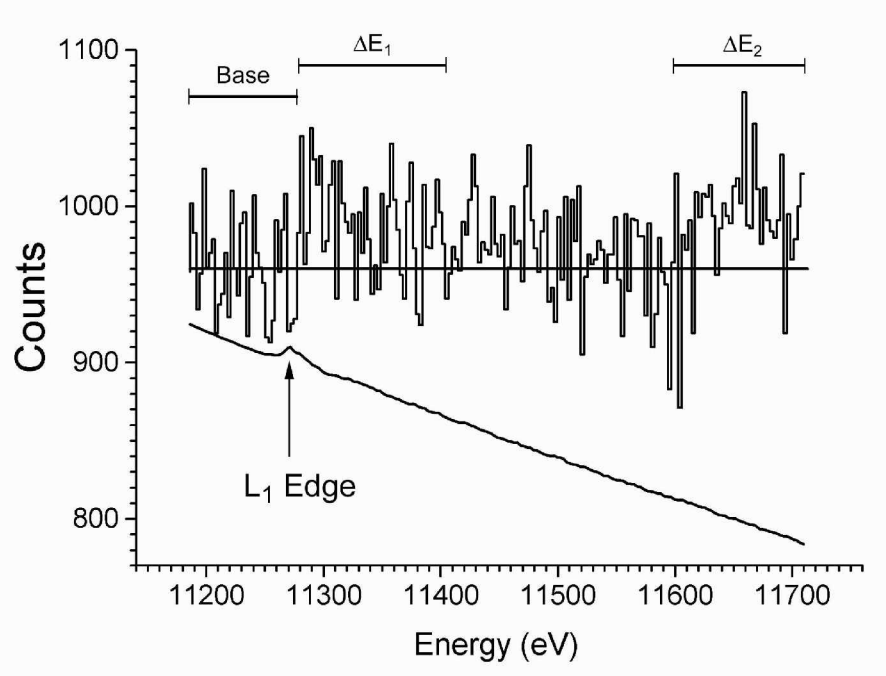

Figure 5.4. Photon counts collected in the ROI(217), together with the fractional absorption showing the Hf(L_1) edge. Intervals of SR energy used in analysis are shown.

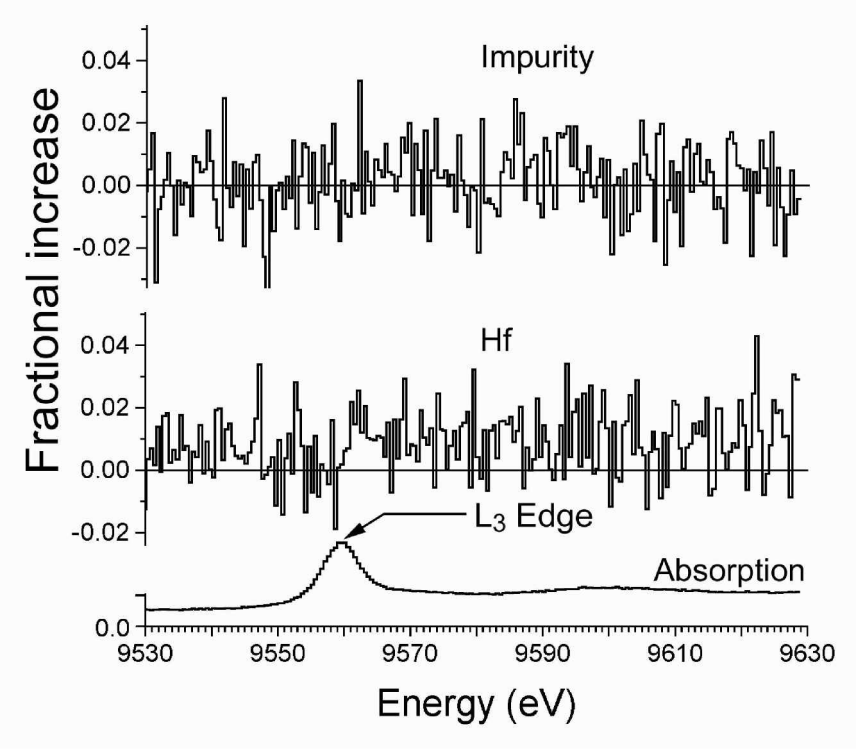

Figure 5.5. Photon counts collected in the ROI(181+126) for the impurities and ROI(213+217) for Hf, together with the fractional absorption showing the Hf(L_3) edge.

Table 5.1. Comparison of the gamma-emission from isomeric Hf nuclei and from impurities in the target. Data are presented as counts collected when irradiated with X-rays having energies in the structure studied in comparison with results when irradiated with "Baseline" energies proximate to those in the structure.

Feature	ROI	In structure Counts	Adjacent baseline		Excess (counts)
			Counts	Norm.[a] Counts	
Fig. 5.4 - ΔE1	ROI(181)	66175(257)	50681(225)	66609(296)	-434(392)
	ROI(217)	45476(213)	33597(183)	44156(241)	1320(322)[b]
Fig. 5.4 - ΔE2	ROI(181)	55737(236)	50681(225)	56473(251)	-736(344)
	ROI(217)	38662(197)	33597(183)	37437(204)	1225(284)[c]
Fig. 5.5	Area (126+181)	276333(526)	112399(374)	274753(914)	1580(1054)
	ROI (213+217)	433703(659)	175385(419)	428719(1023)	4984(1217)[d]

[a] Multiplied by ratio of durations for counting.
[b] Estimation of the effect: (3.0 ± 0.73)%.
[c] Estimation of the effect: (3.3 ± 0.76)%.
[d] Estimation of the effect: (1.2 ± 0.28)%.

sample target at 12° inclination, the effective average fluxes over the activity for the SR energies shown in figure 5.4 and figure 5.5, respectively, were reduced from figure 5.1 with multiplication by 0.72 and 0.58. Resulting fluxes and cross-sections are summarized in table 5.2. As can be seen, the confidence factors exceed 4σ for all the 3 measurements reported in this work.

The photoionization cross-section at the L_1 edge is $7.5 \times 10^{-20}\ cm^2$ [97], so these excitation bands represent about 2×10^{-3} of the photoionization probability. Though large, such a value still conforms to the upper limits for NEET of a few $\times 10^{-3}$ calculated [39] for neighboring nuclei. The work reported here appears to extend the first proof of the NEET process for nuclear excitation [61] to the isomeric nucleus $^{178}Hf^{m2}$. Particularly notable is that in this case of isomer excitation, probabilities approach the theoretical maxima of a few $\times 10^{-3}$ for *L*-shell photoionization.

Table 5.2. Integrated cross-sections obtained for the three structures for excitation of the $^{178}Hf^{m2}$ isomeric population by NEET.

Feature	Eff. photon flux ($cm^{-2}s^{-1}$)	Enhancement *f*	Cross-section (cm^2)
Fig. 5.4 - ΔE1	$1.2x10^{11}$	66175(257)	-434(392)
Fig. 5.4 - ΔE2	$1.2x10^{11}$	55737(236)	-736(344)
Fig. 5.5	$2.7x10^{10}$	276333(526)	1580(1054)

Acknowledgements

The authors gratefully acknowledge support of this experiment from the USAF Air Force Office of Scientific Research, through AFOSR contract No. F49620-99-1-0082. The synchrotron radiation experiments were performed at SPring-8 in cooperation with the Japan Synchrotron Radiation Research Institute (JASRI) through Proposal No. 2001A0082-NX-np and Proposal No. 2001A0570-UX-np. The isomeric targets were loaned by courtesy of General Coherent Technology, Inc.

CHAPTER 6

NEET/EBM MECHANISM FOR INDUCING THE γ-EMISSION FROM $^{178}Hf^{m2}$ ISOMER

6.1 Preface

Chapter 6 contains the original text of the manuscript *Accelerated Decay of the 31-yr Isomer of Hf-178 Induced by Low Energy Photons and Electrons* by C. B. Collins, N. C. Zoita, F. Davanloo, S. Emura, Y Yoda, T. Uruga, B. Patterson, B. Schmitt, J. M. Pouvesle, I. I. Popescu, V. I. Kirischuk, and N. V. Strilchuk It was originally published in Laser Physics, Vol. 14, No. 2, page 154 in 2004 and is reprinted here by permission of the International Academic Publishing Company (IAPC) *Nauka/lnterperiodica*. The paper appears in this dissertation unaltered from its Laser Phys. form except for the numbering of figures.

As a senior graduate student, N. C. Zoita had the responsibility for the designing and implementation of the data acquisition and data analysis for single spectra and timing measurements in experiments with synchrotron radiation. He had also contributions to the planning of the experiments, seconding the leader of the group, Carl B. Collins. As always in experiments conducted at synchrotron facilities valuable contributions to the designing and planning of the experiments were received from the beamline scientists, as well as from all other members of the team. The final data analysis was performed by N. C. Zoita and Carl B. Collins. The original paper was written by Carl B. Collins in collaboration with the authors.

6.2 Accelerated Decay of 31-yr Isomer of Hf-178 Induced by Low Energy Photons and Electrons

6.2.1 Abstract

A process for transferring energy from electron shells into nuclear excitation (NEET) was first proposed by Masato Morita in 1973. It was generalized to a broader class of electron bridging mechanisms (EBM) by Matinyan. These proposals offered an exciting promise for modulating nuclear properties with X-ray photons at accessible levels of power. The development of 3rd generation synchrotron radiation (SR) sources made it possible to conclusively demonstrate NEET/EBM in two recent experiments by exciting nuclear levels of ground state ^{197}Au and isomeric ^{178}Hf^{m2}, respectively, with SR X-rays from SPring-8. X-ray energies incident upon the isomeric target were tuned from 9 to 13 *keV*, and an excitation branch attributed to NEET/EBM was found to have a probability of 1.6×10^{-3} relative to L-shell photoionization of the surrounding electrons. The rate for the resulting emission of exoergic γ photons approached the theoretical maximum for such processes. These landmark results were reconfirmed and extended in a series of experiments at SPring-8 conducted in May 2002. Increases in the rates of spontaneous decay of the isomeric nuclei, ^{178}Hf^{m2}, were studied when targets were irradiated with monochromatic SR X-rays tuned over hundreds of *eV* with spectral widths of both 1.0 and 0.1 *eV*. A close correlation of accelerated gamma emission with rates of ionization of the L-shell electrons in the target was observed. The frequent appearance of a triplet structure in the excitation spectrum for induced gamma emission resembled the additional structure seen in XAFS studies of the inner-shell electrons at energies near the ionization edges. In addition to the accelerated emission of some gamma lines present in spectra of spontaneous decay, new lines were also observed. Features in the excitation functions for such lines suggested that electrons as well

as X-ray photons could initiate the accelerated decay of isomeric nuclei. In 2003, measurements of the temporal correlations between the pulses of SR stimulation and the fast response of the resulting gamma emission were studied successfully at the SR sources (SLS) at the Paul Scherrer Institute and at SPring-8. Results encourage prospects for applications depending on the control of nuclear properties with X-rays.

6.2.2 Introduction

The need to compensate the spontaneous power density radiated at threshold continues to impede the development of ultra-short wavelength lasers. Plans for both hard X-ray and γ-ray lasers demand insertion into the working medium of power densities far beyond our present means at the instant threshold is to be reached. The inability to focus most of the pump sources being considered for such devices further exacerbates the problem. Quite early, it was recognized [10] that storing the requisite energy density *in situ* could be a solution if (1) a material for storing high energy densities could be found and (2) the stored energy could be promptly released upon application of a triggering pulse of much lower energy. Focus immediately fell upon the nuclear spin isomers.

At low energies, there are similarities between structures of the excited states of atoms and nuclei that help to explain the importance of nuclear spin isomers. Both systems involve the storage of energy in the quantized movement of the constituent charges. In atoms, electrons populate excited states, which can be conveniently described in terms of single-particle orbitals. In nuclei, the neutrons appear as relatively negative concentrations in the overall positive fluid of the nucleus; so there is the possibility to store energy by raising either protons or neutrons, or both, up distinctly separate “ladders” of excited single-particle states. Many interesting cases occur in nuclei deformed from the

idealized spherical shape and the possibility for long-lived metastability is clear, just as it is in the atomic analogs. Both spins and projections of spins can be aligned to create particularly stable states of excitation. However, while difficulties in arranging suitable lifetimes for populations of metastable states at the atomic level have limited the development of practical applications, at the nuclear level, spin isomers store excitation at densities of *GJ/g* for decades.

In either the case of atoms or nuclei, the energy stored in the population of excited states is often released by the spontaneous emission of electromagnetic radiation. Atoms emit photons of light and X-rays while nuclei emit gamma photons, but the principles and selection rules remain the same. In each system, spontaneous emission can be "forbidden" for simple dipole transitions because there is no lower energy state to which the excited particle could "fall" without overturning its total spin, *J*, or a projection onto the figure axis of *J* (termed *K*). Either would be a step particularly forbidden by selection rules. More characteristic of just the nuclear systems is the formation of "mixed states," which have been considered as important for the triggering of the release of the metastability. Besides a mixing of charge identities that has no analogy at the atomic level, there are possibilities for mixings of other types, such as those introducing properties resulting from the quantized rotation of the spherical nucleus as a whole or even from oscillation between prolate and oblate asymmetries. By introducing additional degrees of freedom from such mixings, more transitions may become allowed that would facilitate subsequent decay. With the demonstration that induced gamma emission is possible by scattering X-rays from such materials, considerable interest has been developed in the study of these processes because it seemed that the intermediate excitation of mixed states could be involved.

The types of *K*-mixing states needed in such schemes to induce the decay of nuclear isomers were first reported [13] in ^{180}Ta and subsequently described in ^{174}Hf and other isomers [98]. In the

case of Ta, the resonant absorption of X-rays excited the 2-quasiparticle isomer of $^{180}Ta^{m}$ to a *K*-mixing level at 2.8 *MeV*, which then spontaneously decayed in part to the ground state through a gamma cascade. The integrated cross section for the resulting de-excitation of the isomer was 1.2×10^{-25} cm^2 *keV*. After 11 years of substantial controversy, independent confirmation was reported [99] that X-rays could accelerate (or "trigger") the prompt decay of a nuclear spin isomer in the case of $^{180}Ta^{m}$. However, since trigger photons of *MeV* energy were required, this success had little direct application to the γ-ray laser problem.

Extensive searches for other attractive isomers have suggested as many as 32 possibilities [8]. However, the application of scaling studies [69] of the excitation energies of potential *K*-mixing states, together with actual measurements [100], and the need for reasonable shelf life of a practical material have reduced the list to one isomer, $^{178}Hf^{m2}$. As a vehicle for the further study, the 16^{+} state of $^{178}Hf^{m2}$ is particularly attractive. It is a 4-quasiparticle state having 2.446 *MeV* of excitation and a half-life of 31 years, meaning that as a material it would store 1.3 *GJ/g*. This is an energy density of considerable significance to the development of ultrashort wavelength lasers.

In 1997, scaling studies [69] of the isomers of Hf presented "further evidence for a *K*-mixing level in $^{178}Hf^{m2}$ lying no more than about 300 *keV* above the isomer." Since the cross section for exciting a level depends upon ΔE^{-2}, where ΔE is the transition energy, the value measured for $^{180}Ta^{m}$ could be scaled upward by four decades if the excitation energy required were 28 *keV* instead of 2.8 *MeV*, provided the width of the triggering process remained the same. However, as energies of nuclear transitions scale downward, lifetimes for spontaneous emission increase and widths reduce, unless the inner-shell electrons become involved. In actual cases, the rates for γ transitions between levels separated by small energies are usually accelerated further by internal conversion in which inner-shell electrons are coupled into the process and significantly increase the widths. For example,

the spontaneous decay of the $^{178}Hf^{m2}$ isomer begins with a radiative transition for which the rate (and width) is increased by some few $\times 10^4$ because of internal conversion to the surrounding electrons in the L_3 inner shell; in this case, the coupling between nucleons and the electrons in the L_3 shell that surround them is particularly effective. Such couplings between nucleons and the inner-shell electrons might act to prevent the width of isomer triggering from decreasing so much as transition energies were reduced and then initial and final states could be reversed so that energy was transferred into the nucleus.

A process for transferring energy from electron shells into nuclear excitation was first proposed by Masato Morita in 1973 [14]. Called NEET (Nuclear Excitation by Electron Transition), it was developed further by Ho [39] and generalized to a broader class of electron bridging mechanisms (EBM) by Matinyan [16]. Those proposals offered an exciting promise for modulating nuclear properties with X-ray photons at accessible levels of power and even for facilitating the triggering of the decay of nuclear isomers.

In 1998, samples of the 31-yr isomer of $^{178}Hf^{m2}$ were exposed to Bremsstrahlung X-rays from a small source normally used in dental examinations and acceleration of the spontaneous decay was reported [22]. Operating parameters had been selected to provide maximum flux at the energies corresponding to transitions from L-shell electrons of Hf without allowing the end point of the Bremsstrahlung to reach the energy of the *K* edge. Filtering of the X-rays with Al foils showed that pulsed irradiation by the parts of the Bremsstrahlung with E < 20 *keV* increased the rate of spontaneous emission of γ photons corresponding to some of the characteristic transitions found in spontaneous decay of $^{178}Hf^{m2}$ by a few percent. Integrated cross sections of the order of 2.2×10^{-22} $cm^2\,keV$ were reported [70, 101]. The enhancement was found to scale linearly [102] with flux at 20 *keV* around 10^{10} photons $cm^{-2}\,keV^{-1}\,s^{-1}$. An intense round of Comments [103–105] and

Reply [106] concerning those results established that scaling of the integrated cross section with E^{-2} while holding the width constant did not produce cross sections violating any fundamental upper limits (RULs) if the electrons were involved [105].

The quantitative model used by Ho [39] for the use of inner-shell electrons to enhance the acceleration of the decay of isomeric nuclei was limited by his assumption that the initial state of the process was a stationary state even though it included an inner-shell vacancy. He described the event as occurring in sequential steps, which is not a realistic view for solid media under laboratory conditions. Inner-shell ionization is a scattering process in which interferences between indistinguishable options for the trajectories of the incident projectile produce the rich phenomenology found in the X-ray absorption fine structure (XAFS) literature [107]. Excitation functions for higher order effects, such as visible or X-ray fluorescence, typically show [108] complex structure from resonances at energies displaced from the simple ionization edge by as much as tens of *eV*. These result from the scattering interferences in the projectile state and so reflect the geometry of the local potentials in the medium. As a result, sample preparation and thickness are key physical quantities affecting the excitation functions for higher order effects of photoionization [109]. Although neglecting the structure arising in the incident channel for the process, Ho's estimations for the output branch coupling the excitation into the nucleus should have been unaffected by his approximations. He reported that the branch into nuclear excitation could be as great as 0.4% of the number of inner-shell vacancies produced in the intermediate steps of the scattering [39]. Simply adding Ho's exposition of the branch for nuclear excitation to the XAFS perspective makes it reasonable to expect nuclear excitation to result from photoionization by X-rays. The excitation function for the nuclear branch would be expected to display the same complex structure typical of other higher order effects arising from photoionization.

Working at SPring-8 and KEK in 2000, Kishimoto *et al.* [61] demonstrated that synchrotron radiation (SR) scattered by inner-shell electrons did lead to γ fluorescence from ^{197}Au, but the yield was only 5×10^{-8} at the single X-ray energy used. At SPring-8 in 2001 and 2002, our group extended the successful results of Kishimoto *et al.* to the 31-yr isomer of $^{178}Hf^{m2}$ and reported [63] a yield for several X-ray energies of 0.2%, a value approaching the theoretical maximum. These landmark results were reconfirmed and extended in a series of experiments at SPring-8 conducted in May 2002. Increases in the rates of spontaneous decay of the isomeric nuclei, $^{178}Hf^{m2}$, were studied when targets were irradiated with monochromatic SR X-rays tuned over ranges of hundreds of *eV* and tens of *eV* with spectral widths of 1.0 and 0.1 *eV,* respectively. A close correlation of accelerated gamma emission with rates of ionization of the L-shell electrons in the target was observed. The frequent appearance of a triplet structure in the excitation spectrum for induced gamma emission resembled the additional structure seen in XAFS studies of the inner-shell electrons at energies near the ionization edges. In addition to the accelerated emission of some gamma lines present in spectra of spontaneous decay, new lines were also observed. Features in the excitation functions for such lines suggested that electrons as well as X-ray photons could initiate the accelerated decay of isomeric nuclei. In 2003, measurements of the temporal correlations between the pulses of SR stimulation and the fast response of the resulting gamma emission were studied successfully at the SLS at the Paul Scherrer Institute and at SPring-8. Results encourage prospects for applications depending on the control of nuclear properties with X-rays.

In 2001, concurrently with our successful experiments at Spring-8, an attempt was made to excite the same isomer at the APS SR source at Argonne, which failed [95] to produce any evidence for an acceleration of the spontaneous decay. Despite the availability of published work [70] reporting that the X-ray energies important for exciting the accelerated decay of the isomer were $E < 20$ *keV*,

the design of the first failed experiment at APS included a target in which the isomeric activity was buried in a thick layer of Al that effectively excluded X-rays with $E < 20$ *KeV*. In 2002, the target was redesigned, but the experiment failed again at APS [110]. The authors attempted to interpret the negative results as "proving" an upper limit on the cross section for accelerated decay of the isomeric $^{178}Hf^{m2}$ that was considerably smaller than the established value [110] of 1.6 to 2.0×10^{-3} of the photoionization cross section for L_3 electrons. However, from the published data [110], it can be seen that the instrumentation used to search for γ photons from accelerated decay was totally blind at the energy of the "new" line reported [101] to be a unique result of triggered decay. Moreover, the γ spectra shown [110] were collected with a gate set to open seconds after the irradiating SR X-rays were moved off the target. Since the triggered decay is prompt, they were looking too late to collect any γ fluorescence that had been triggered several seconds previously. Nevertheless, the impression has remained that such persistent failures [95, 110] from attempts to accelerate the decay of isomers at APS somehow place further burdens of proof upon the successful works.

The purpose of the work reported here was to collect and extend our past measurements with a focus on the observations on which the highest confidence can be placed. As reported here, the confidence that an XAFS branch materially affects the decay of the 31-yr isomer of ^{178}Hf reaches 12σ when X-ray energies lie close to the L_3 edge for photoionization. The effect most readily observed is the emission of a new γ line near 130 *keV* and a prompt increase in the emission of γ photons belonging to transitions in the ground state band (GSB) of 178Hf. Such results encourage prospects for a γ-ray lasers, as well as set fiducial points with which to calibrate future experiments on isomer triggering.

6.2.3 Experiment

The design of an experiment to quantitatively measure the acceleration of the decay of isomeric nuclei is immediately confounded by the complexity of the bands of excited states. Figure 6.1 shows an energy level diagram of the excited states involved in the spontaneous decay. In that case, only two bands are involved, the GSB and the 8^- band built upon the 4 *s* isomeric state. The corresponding spectrum of spontaneous decay from the targets used in our work has been described previously [22, 70] and was composed of only the well-known decays shown in figure 6.1 and of a ^{172}Hf impurity and its daughters. Of the former, only the (4,2), (6,4), and (8,6) members of the GSB at 213.4, 325.6, and 426.4 *keV*, respectively, and the lowest member of the 8^- band at 216.7 *keV* are recorded at significant counting rates. Of the lines from the impurities, only two, 125.8 and 181.5 *keV*, can be recorded with significance.

However, at least 17 other bands are known to have energy levels lying below that of the 16^+ isomeric level. There has been no reported cascading of spontaneous decay into those bands aside from the path shown in figure 6.1. However, when decay is induced by *K*-mixing, then "new" γ lines should be expected in the spectrum as larger changes of *K* are "mixed in" by the coupling to the electron transitions. One such line has been reported [101] by our group near 130 *keV* to arise from both triggering with Bremsstrahlung X-rays and with monochromatic X-rays from SR sources. Moreover, since the moment of inertia of the Hf nucleus is large and only little affected by quasiparticle excitation, the spacing of levels within bands often repeats. For example, within the 1^- band with origin at 1310.1 *keV*, there are transitions at 129.4 and 216.4 *keV* that start at the same 4^- level and which decay promptly with other transitions feeding the GSB starting with the (4,2) member

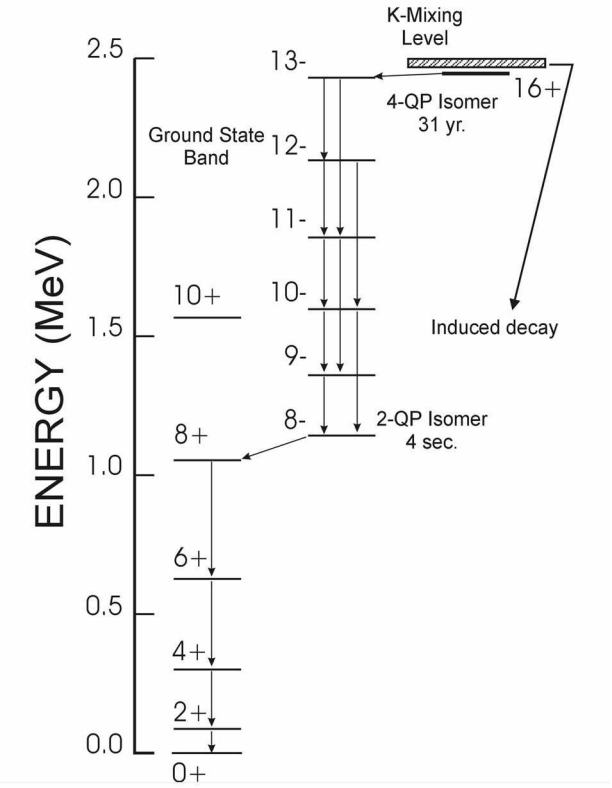

Figure 6.1. Energy level diagram illustrating the spontaneous and induced decay of the 31-yr isomer of $^{178}Hf^{m2}$.

at 213.4 *keV*. Another example is found in the 2^- band originating at 1566.7 *keV*, with transitions from the 4^- level being emitted at 180.4 *keV* in coincidence with other transitions too energetic to be detected with our Ge detectors, but which also feed the (4,2) member of the GSB. The two examples do not even approximately span the scope of complexity but already suggest that the observation of "prompt" triggering through 216 *keV* (not 9^-, 8^- but 4^-, 3^-) in coincidence with the 213.4 *keV* component of the GSB would be possible, as would be the observation of triggering through ~181 *keV* (not the impurity but the 4^-, 2^- of ^{178}Hf) in coincidence with the same 213.4 *keV* GSB reference line. The pair of lines at 494.6 and 495.0 *keV* from quite different bands and the pair 574.2 and 575.0 *keV* from different bands add the potentials for considerable uncertainty when the pattern of enhancements of spectral lines is not what is expected.

The design of an experiment to develop the highest possible confidence in the accelerated decay of the ^{178}Hf^{m2} isomeric nucleus by X-rays should simply avoid, to the extent possible, any dependence upon γ transitions for which contributions to spontaneous decay could be enhanced by photons from transitions at nearly the same energies but arising from very different bands not normally observed. From this perspective, the (4,2) member of the GSB is satisfactorily isolated at 213.4 *keV* while the next (6,4) at 325.6 *keV* could be troubled by another transition at 324.9 *keV*.

The specific objectives of the experiments reported here were to demonstrate the following: (1) that the excitation function for observed enhancement of γ photons from ^{178}Hf^{m2} isomeric nuclei contained XAFS-type structures that reproduced with high confidence, (2) that the enhancements observed included the excitation of at least one γ line not found in the spectrum of spontaneous decay, and (3) that the enhancement effect had a reproducible time-dependent relationship with the cause arising from the passage of electron bunches that generated X-rays within some insertion device in the SR source. The schematic design shown in figure 6.2 was intended to support those objectives.

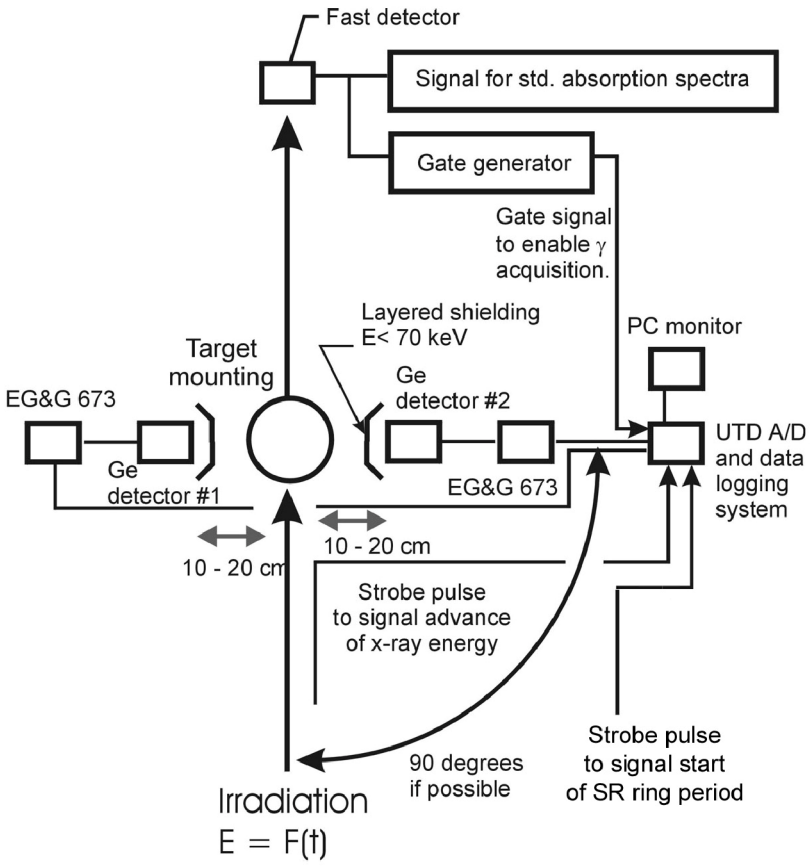

Figure 6.2. Schematic drawing of the experimental arrangement.

It was used in all of the SR experiments to date, with small adaptations being made to conform to lessons learned and to physical constraints encountered at different facilities.

As a vehicle for the demonstration of NEET or EBM spectroscopy, the 31-yr 16^{+} state of $^{178}Hf^{m2}$ has been particularly attractive. When used with SR excitation through photoionization of the L shell, NEET and EBM offer the possibility for exoergic emission of γ photons with energies exceeding those of the irradiation. Consequently, experimental arrangements are facilitated by the use of layered absorbers to selectively remove X-rays scattered from the SR source [63]. That first report of the spectroscopy for the NEET or EBM excitation of $^{178}Hf^{m2}$ suggested the existence of resonances in addition to those arising simply from the photoionization edges in the L shell. Reexamined in subsequent work reported here, the additional resonances were confirmed by tuning the incident monochromatic X-rays with high resolution and long dwell times through the L_3 photoionization edge.

Four targets were used in these experiments. All were fabricated from the same material used in our previous work [63] and each contained about 1.8×10^{13} $^{178}Hf^{m2}$ isomeric nuclei. The isomeric fraction was about 10^{-3} of the total Hf content. Two of the targets were fabricated in both 2002 and 2003 according to the same plan. In each target, the activity was deposited in a rectangular area nominally 1.3×5 *mm* and the sample was encapsulated. In use, a target was mounted on a digitally controlled goniometer and inclined 7° to 15° above the plane of propagation of the incident X-rays. In this way, the normal area presented by the target to the SR flux was smaller than the cross section of the SR beam.

In 2002 two beamlines at SPring-8 were used for irradiation, BL01B1 and BL09XU, in which the SR was generated by a bending magnet and by an undulator, respectively. Fluxes were $9.5 \pm 0.5 \times 10^{10}$ and $5.0 \pm 1.0 \times 10^{11}$ *photons* cm^{-2} s^{-1} with nominal spectral bandwidths of 1 *eV* and

100 *meV*, respectively, after being passed through monochromatic filtration. In the first case, spectra were examined by advancing the energy of the X-rays in steps of about 1 *eV* with data being collected for 100 *s* at each step. Movement through a range of energies was repeated three times, and the results were summed. In the second case, the energies were advanced in steps of about 80 *meV* and remained at each for 200 *s* while data were collected and then for an additional 35 *s* during which the SR was blocked by a thick absorber. For comparison, the data were summed over five adjacent steps to improve statistics.

The performance of the target is of critical importance in such experiments. The first attempts elsewhere to excite isomeric targets with SR seem to have failed for lack of optical transparency at the resonant energies for NEET and EBM and because of ill-conditioning of the targets [95]. In the work reported here, the same attention was paid to the properties and mountings of the target structures as had been detailed previously [63]. The SR intensities and sample absorption coefficients were continuously measured in line with ionization chambers placed before and after the isomeric target. Overall absorption of the targets in these experiments was not significantly different from our previous experiments, except that uniformity of the distribution of the activity was improved. Values of flux and absorption coefficients are shown in figure 6.3 for a typical arrangement at the BL01B1 beamline. Also as before, a Si drift detector (SDD) was used both to confirm the location of the target activity in the SR beam and to survey the level of scattered SR in the detector environment by observing the L_α fluorescence from Hf in the target. An example is shown in figure 6.4. The data were obtained by moving the target vertically with a stepping motor while the intensity of L_α fluorescence from the Hf component was monitored by the SDD [63]. Because of the glancing angle of incidence, the contour seen is the near-Gaussian intensity distribution of the SR beam being “scanned” by the thinner projected dimension of the Hf content of the target. In vertical dimension, the beam can be

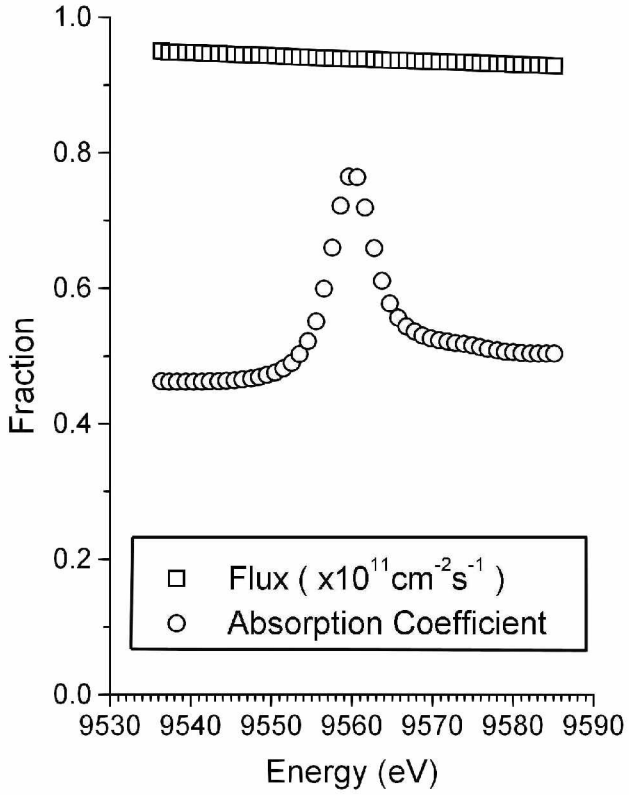

Figure 6.3. Irradiation environment showing the absorption coefficient of the target measured in line as a function of SR energy during a typical irradiation at SPring-8 in 2002 together with measured values of SR flux.

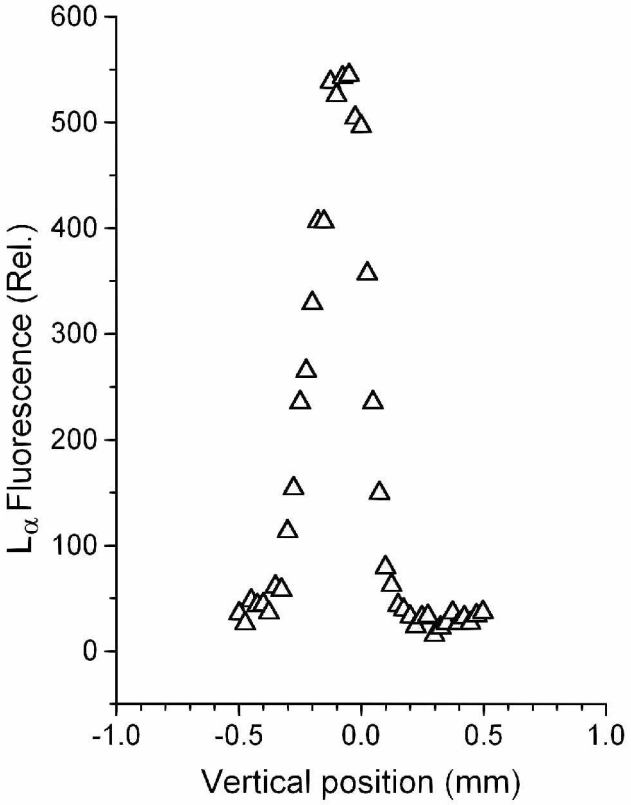

Figure 6.4. Profile of the SR X-ray beam scanned by the smaller dimension of the target as displayed by the counting rate L_α fluorescence.

seen to have been about 0.25 *mm* in the *z*-direction, and mechanical slits were set to trim the horizontal dimension to 7.0 *mm*. From the position seen in the figure, a final adjustment would have been made to center the peak at 0 *mm*.

Two opposed Ge detectors 47 *mm* thick and 45 *mm* in diameter and 43 *mm* thick and 50 *mm* in diameter, respectively, were placed 22 *mm* from the target at right angles to the beam with the target between them. Each was shielded with layered foils of W, Cd, and Cu, as seen by the beam. They were connected to EG&G 673 spectroscopy amplifiers, from which the output was continuously digitized and recorded to permit subsequent re-examination of the electrical pulses describing the detected photons. Data were analyzed with a mesh of 6.8 γ channels per *keV*. When the SR monochromator changed energies, a digital signal was sent to a third channel of the data logging system to correlate the signals from γ photons with the energies of the irradiation. Regions of interest (ROIs) associated with each of the spectral features were identified in the 4096 channel histograms of the numbers of γ photons detected during each period of irradiation with SR.

An illuminating comparison of the measurements systems used in the recently contradictory works is summarized in figure 6.5. Histograms of counts of γ photons detected during periods reported to be “typical” measurement series [110] are directly compared. Even though we collected only about 10% of the total number of photons, our histogram spectrum displays much better S/N, better energy resolution, and three-times better peak-to-Compton ratios. Most significant are the comparative sensitivities to lower energy photons. The three lines so marked arise from the decay of the impurity ^{172}Hf and its daughters, so the relative strengths of the lines are fixed. The relative heights of the three lines in measurement histograms are proportional to the sensitivities of the detection system at those three photon energies. It can be seen that the APS (Argonne) system had no

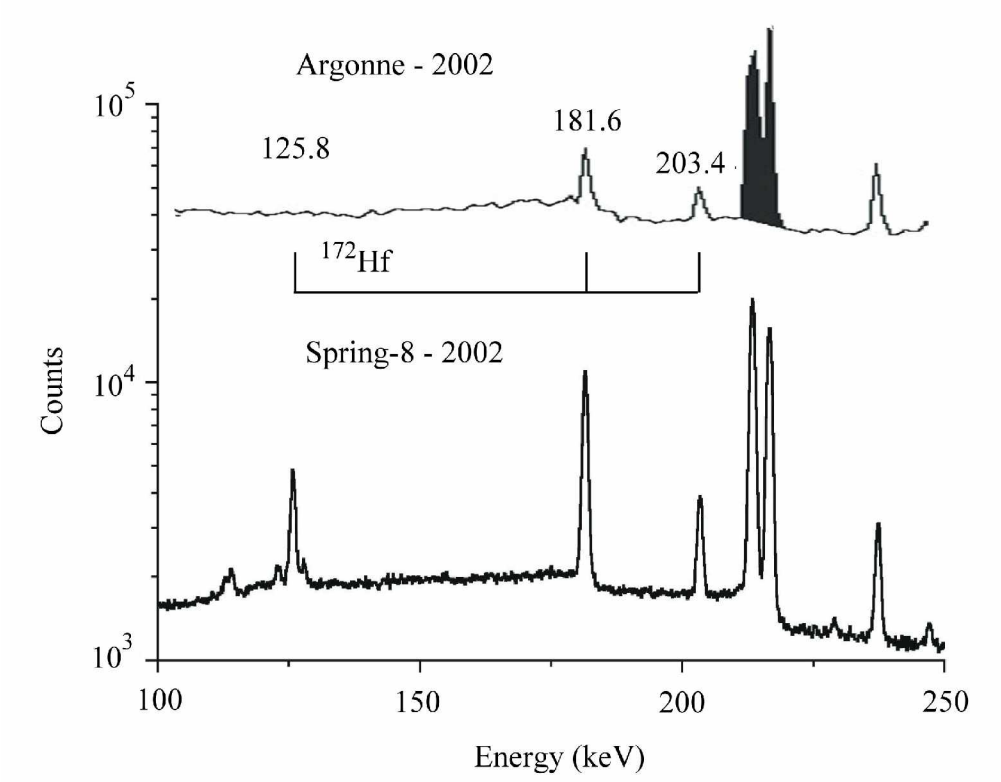

Figure 6.5. Comparison of the energy resolution and amount of spectroscopic data reported by different groups for experiments performed in 2002 at the SR facilities shown.

sensitivity at 125.8 *keV* and so they could not have detected any photons from the important γ line near 130 *keV* that is only emitted by the accelerated decay of the isomers. In general, the performance of the measurement system used in the APS work was not functioning at modern norms.

For simplicity, in most cases in the work reported here, the sums of counts for the ROIs for the accessible members of the GSB at 213.4, 325.6, and 426.4 *keV* were used to study the excitation functions of the $^{178}Hf^{m2}$ sample. The ROI for the 181.5 *keV* impurity line provided a convenient indication for the null effect, provided it was not contaminated by contributions from one of the accidentally coincident lines of triggered isomeric nuclei.

6.2.4 Results

The most remarkable evidence for excitation of the isomeric nuclei is shown in figure 6.6 in terms of fractional increases over the average counting rates observed at the lower X-ray energies below the L_3 edge. Data identified in the legend box to the left were taken at SPring-8 in 2002. Plotted on the same figure are data identified in the right legend that were taken in 2003 at the SLS SR source of the Paul Scherrer Institute with essentially the same instrumentation, but while using the two targets fabricated in 2003. Because incident flux was somewhat greater, data have been reduced by a factor of 1.5 for comparison.

Figure 6.6 confirms the suggestions of additional structure seen in figure 5.6 in our previous work [63] and corresponds to the general morphology of X-ray absorption fine structure (XAFS) measurements [107] made at the purely atomic level. Spectra for the excitation functions for higher order effects resulting from photoabsorption, such as visible or X-ray fluorescence [108], typically show additional resonances at energies above and below the simple ionization edge seen in spectra of

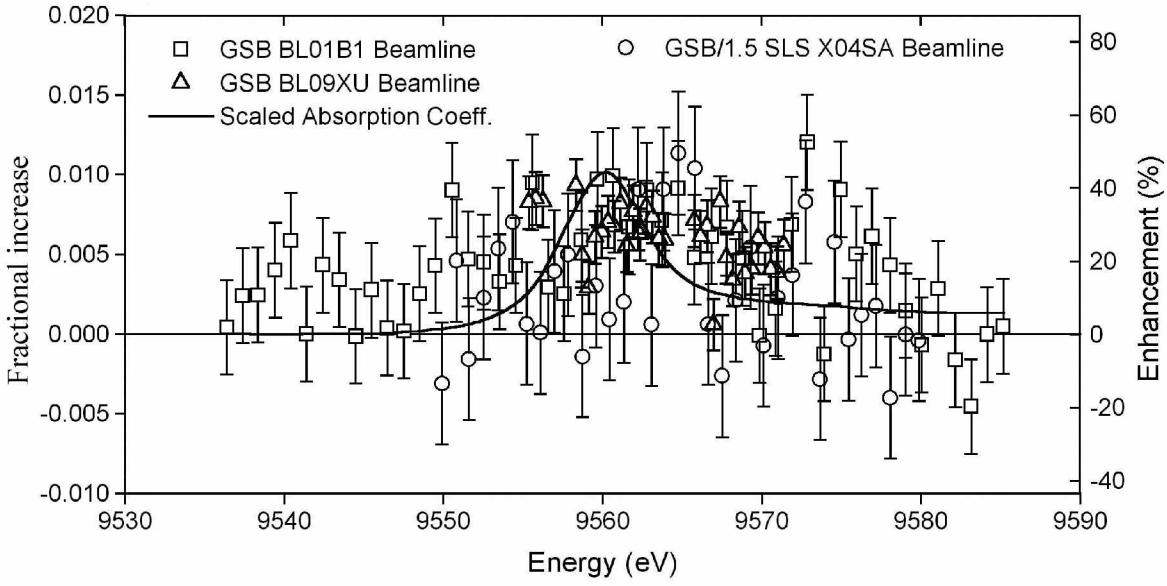

Figure 6.6. Fractional increases in the number of γ photons collected in the ROI for the GSB of ^{178}Hf together with the relative absorption coefficient scaled to fit the vertical range to show the Hf(L_3) edge. Data from three beamlines are shown as marked. The scale to the right has been corrected for the duty cycle of the SR excitation.

X-ray absorption; in those techniques, the sample preparation and thickness are the key physical quantities [109]. Main causes include transitions of inner-shell electrons to nonlocalized final states, such as the valence and conduction bands at X-ray energies below the edge. The involvement of two electrons can add structure above the edge. It seems reasonable to conclude that such behavior has been found in these additional higher order effects of photoionization when the excitation is transferred into fluorescence from the nucleus.

The difficulty in extracting quantitative information from data such as that shown in figure 6.6 lies in determining the baseline above which the enhancement occurs without having data from a broader range of X-ray energies. For the first analyses, the baseline was selected to be a constant number shown by the line at zero in figure 6.6. It is not unique, but is one which is possibly consistent with the assumption that the effect of the SR irradiation is not to suppress the spontaneous decay of the isomeric nuclear state. Then, over the range of X-ray energies 9555.6 to 9568.9 *eV* corresponding to the main peak in photoionization at the L_3 edge, the average enhancement in figure 6.6 for the 2002 data is 0.0068, corresponding to 10756 counts in excess of the 1587214 counts from spontaneous decay. The cross sections σ for excitation can be readily expressed as $\sigma = fA/F$, where f is the fractional enhancement over spontaneous emission (0.0068), A is the rate coefficient for spontaneous emission ($A = 7.09 \times 10^{-10}\ s^{-1}$), and F is the irradiating photon flux [63]. Values of flux were taken from figure 6.3 and were corrected for the mean of the absorption shown, giving for the resulting flux and cross section, $6.5 \times 10^{10}\ cm^{-2}\ s^{-1}$ and $7.4 \times 10^{-23}\ cm^2$, respectively. The photoionization cross section at the L_3 edge is $4.6 \times 10^{-20}\ cm^2$; so this excitation in these targets represents about 1.6×10^{-3} of the photoionization probability. Though somewhat less than the value of 0.2% previously reported [63], this seems to be reasonable agreement, confirming again that this is a major effect.

During both experiments in 2002, SPring-8 was operating in the multibunch mode, meaning there were 11 repetitions of a "bunch" of 160 current pulses lasting 50 *ps*, with each pulse being followed by a spacing gap of 2 *ns*. Between bunches, there were a few extra spaces, and for stability a 12th bunch was left unfilled. Neither a bending magnet nor undulator has significant Q; so the SR follows the same duty cycle. Thus the γ emission from the GSB must originate from a source with a duty cycle of (11/12) × (50/2000) = 1/43. When the duty cycle is considered, the acceleration of decay of the $^{178}Hf^{m2}$ isomeric population caused by the creation of $2p_{3/2}$ holes in the electron shells of the atoms approaches 50% near the maxima seen at 9561 and 9573 *eV* in figure 6.6.

Also significant among the results obtained in 2002 were the importance of "new" γ lines from transitions not seen in spontaneous decay. The number of counts from γ photons collected during the period the beam was blocked was multiplied by the ratio (200/35) and then was subtracted from the total number of counts collected during irradiation. Figure 6.7 shows an interval from the resulting difference spectrum without any further scaling. The Gaussian curve fitted to the data of figure 6.7 gave an energy for the line of 130.23(14) *keV*. However, the uncertainty expressed in the centroid of the line is only statistical and does not reflect possible small shifts arising from the location of the line on the far wing of the larger impurity line at 125.8 *keV*. The value for the energy of the new line obtained as 130.23 *keV* is not significantly different from the value of 129.5 *keV* reported earlier [101]. The area under the curve in figure 6.7 was 405(118) counts. Coincidence measurements [101] had shown that this line was emitted only during the period of irradiation and was not present in delayed measurements [95, 110], such as those that had failed to show any enhanced decay.

Measurement of the excitation function of the new γ line at 130.2 *keV* provided a significant supplement to the measurements of enhancements of members of the GSB previously reported. The upper panel of figure 6.8 shows the numbers of counts collected in the best measurements made in

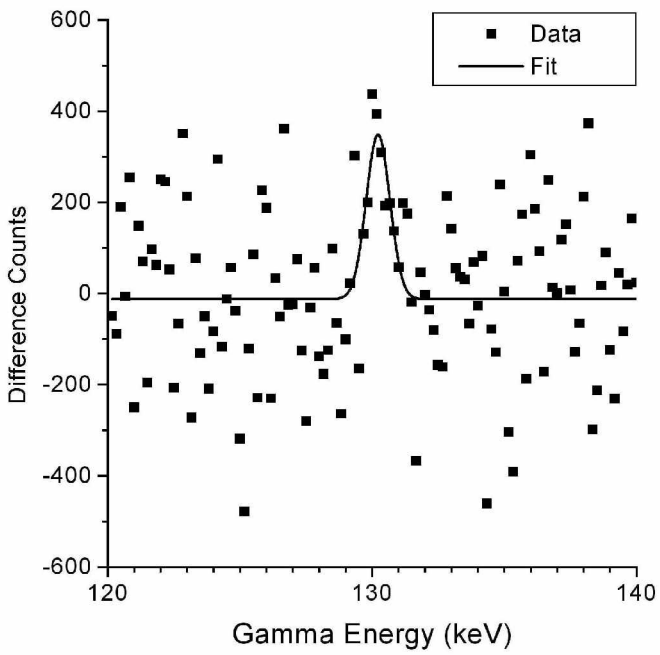

Figure 6.7. Differences in the number of counts from γ photons collected with SR incident and blocked.

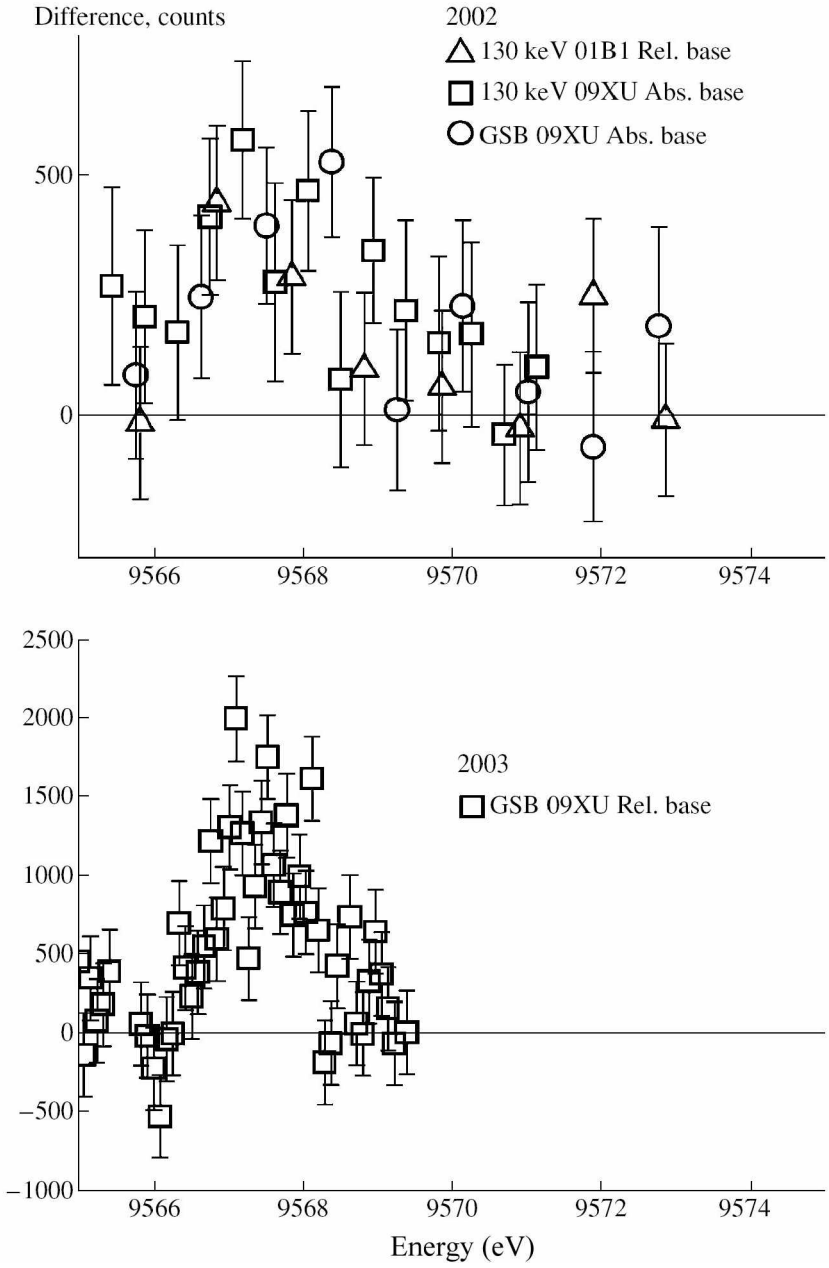

Figure 6.8. Differences in the counts collected in the γ lines indicated. “Abs” indicates that the baselines were obtained with the X-ray beam blocked as described in the text.

2002. In the case of data for the 130 *keV* line made on the 09XU beamline, the scanning through the SR X-ray energies was made with a step of 0.1 *eV* and σ was calculated from the variance when ten successive measurements were combined into one with a width $E = 1.0$ *eV*. The GSB data were taken as described above. Summing the counts and combining σ's in accordance with statistical rules for the data between 9566 and 9572 *eV* gave a total accumulation of 6123 (970) extra photons over the course of our SR experiments in 2002. This indicates a confidence of 6.3σ, including all causes of variation, not just counting statistics as described above.

The lower panel of figure 6.8 shows the improvement realized by remeasuring the pronounced feature for triggering near 9567 *eV* with monochromatic X-rays at the 09XU beamline at the SPring-8 source in 2003. Longer measurement times were used over reduced tuning ranges to obtain better statistics. A range of 7 *eV* was scanned with SR X-rays having a width of 100 *meV*. Data were accumulated for 500 *s* at each X-ray energy. The total number of counts within the structure above the base shown in figure 6.8 is 11954. Combining the σ's for each corresponding point according to usual statistical practice gives an uncertainty for the total of 997. In summary, the number of extra counts induced in the GSB within the XAFS-like peak shown in figure 6.8 is 11954 (997), giving a confidence of 12σ that the number of γ counts is increased by the X-ray irradiation. The combination of the confidence of 6.3σ established by measurements in 2002 and 12σ achieved independently in 2003 appears to be a reproducible and compelling demonstration that monochromatic SR X-rays at energies of 6 *eV* above the L_3 edge in Hf will accelerate decay of $^{178}Hf^{m2}$ isomeric nuclei.

6.2.5 Timing

An additional aim of the research on which this report is focused has been to measure the induced decay of the 31-yr isomer of Hf-178 while correlating the detection of the resulting gammas with the passage of an electron bunch. The most immediate objective was to confirm the efficacy of the measurement technique and to determine if the primary cascades of gamma transitions induced by the SR X-rays occurred promptly. Such knowledge would further illustrate the means through which reproducible measurements of isomer triggering could be made with high confidence by removing another possibly free parameter of experimentation.

An avalanche photodiode (APD) 0.2×0.2 *mm* was inserted at the position labeled “fast detector” in figure 6.2. It produced signal pulses that were conditioned with 1 *GHz* electronics. Standard nuclear instrumentation modules were used to develop a ramp voltage which increased until stopped by the arrival of a pulse supplied by SLS that was synchronized with the cycle period of the storage ring. Digitizing the final voltage reached by the ramp provided a measure of the “Phase time” at which the APD signal was detected with respect to the fiducial pulse available on each ring period and defined to be phase zero for reference. Also shown in figure 6.2 is that signals logged from detection of the gamma fluorescence by the Ge detectors were of two types. One was a standard semi-Gaussian analog pulse, the amplitude of which was proportional to the energy of the original gamma photon used to obtain the spectroscopy data reviewed above. The other was a standard NIM fast pulse containing the timing information obtained in the same way as was done with the APD signal. Both the energy and arrival (phase) time of each gamma photon were logged into a PC-based data acquisition system developed by us earlier.

Figure 6.9 shows the APD response measured as a function of the phase of the cycle of transit of the electron bunches around the storage ring at an average flux on the target of 2.2×10^{12} *photons* cm^{-2} s^{-1}. A vacancy was introduced into the pattern in order to isolate a single bunch to facilitate determination of the degree of rapidity with which the effect followed cause. With a combination of digital delay generators and software, the zero for the phase times was set as a point just before the onset of the vacancy in the pattern of bunches. Figure 6.10 shows a magnification of a part of the measured bunch pattern near the end of the vacancy. The actual duration of the passage of a current pulse is believed to be about 50 *ps*; so the temporal width seen in the figure is a measure of the limitation of the amplifier bandwidth to 1 *GHz*.

Figure 6.11 shows the induced decay of the isomeric nuclei as a function of the phase tune of the electron bunches around the ring. The data for the Ge detector was arranged to develop histograms of the numbers of gamma photons detected at the different phase times for each of the gamma energies corresponding to transitions between nuclear levels for either isomers or for impurities contained in the sample. During collection of the data, a digitally controlled beam shutter alternately opened and closed the beamline for a ratio of durations of 4:1. Photons collected while the shutter was closed were considered to represent the spontaneous emission from the sample. Data shown in figure 6.11 were the differences obtained by subtracting the number of counts collected for spontaneous emission and scaled by the relative times for collection from the data collected during irradiation. As mentioned above, the principle transitions in the GSB usually considered to show the induced emission and the rotational states of the nuclei to which the transitions correspond have been426.4 *keV* (8,6), 325.6 *keV* (6,4), and 213.4 *keV* (4,2), respectively. In this work, we added the remaining member at 93.2 *keV* (2,0), respectively, so that the data marked GSB in figure 6.11 represents the entire GSB.

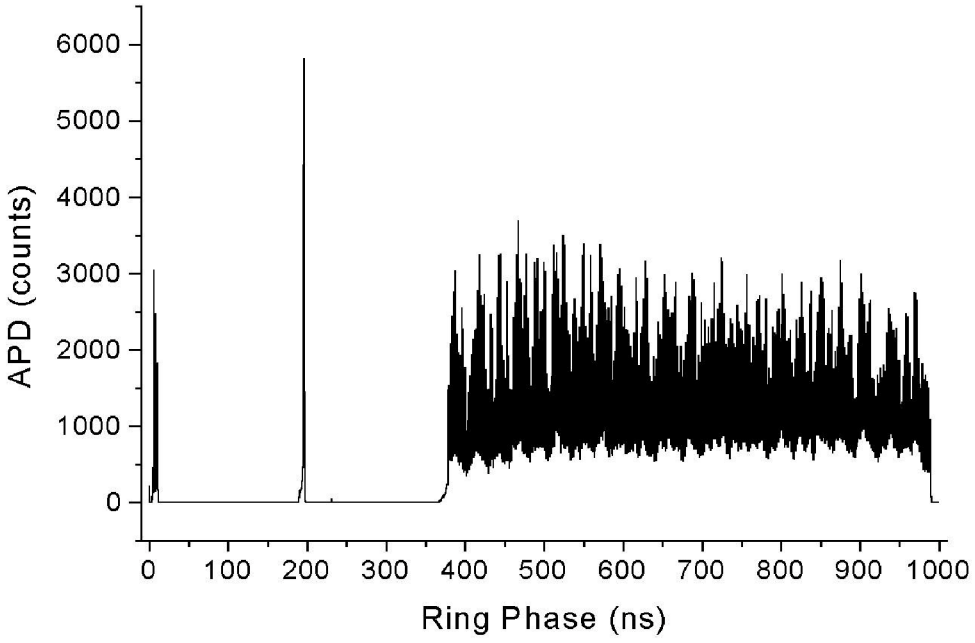

Figure 6.9. Plot of the APD response measured as a function of the phase of the cycle of transit of the electron bunches around the storage ring at an average flux on the target of 2.2×10^{12} *photons* cm^{-2} s^{-1}.

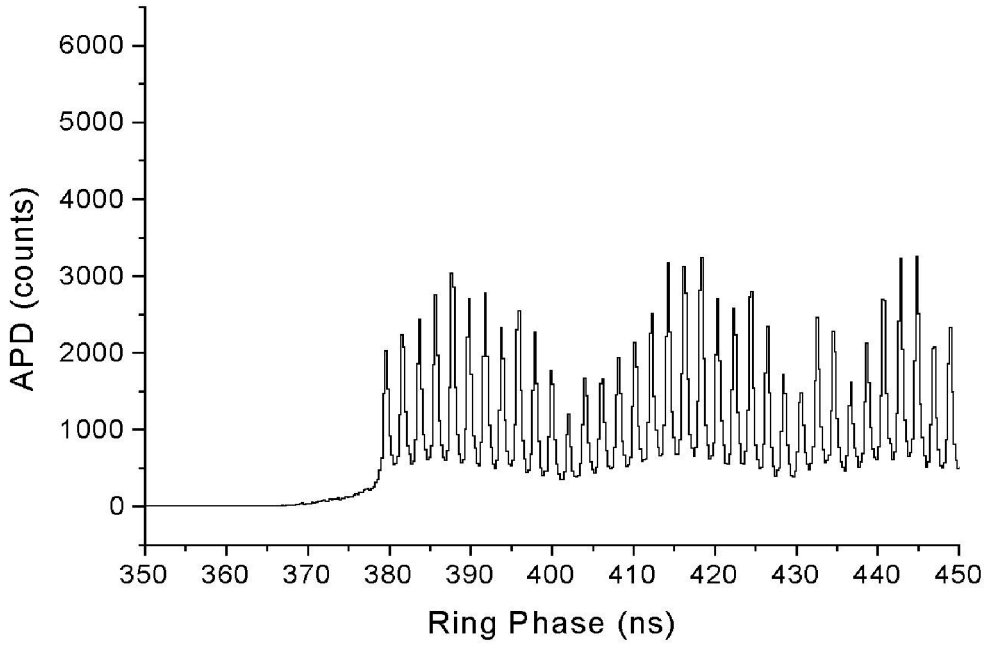

Figure 6.10. Magnification of a part of the measured bunch pattern near the end of the vacancy.

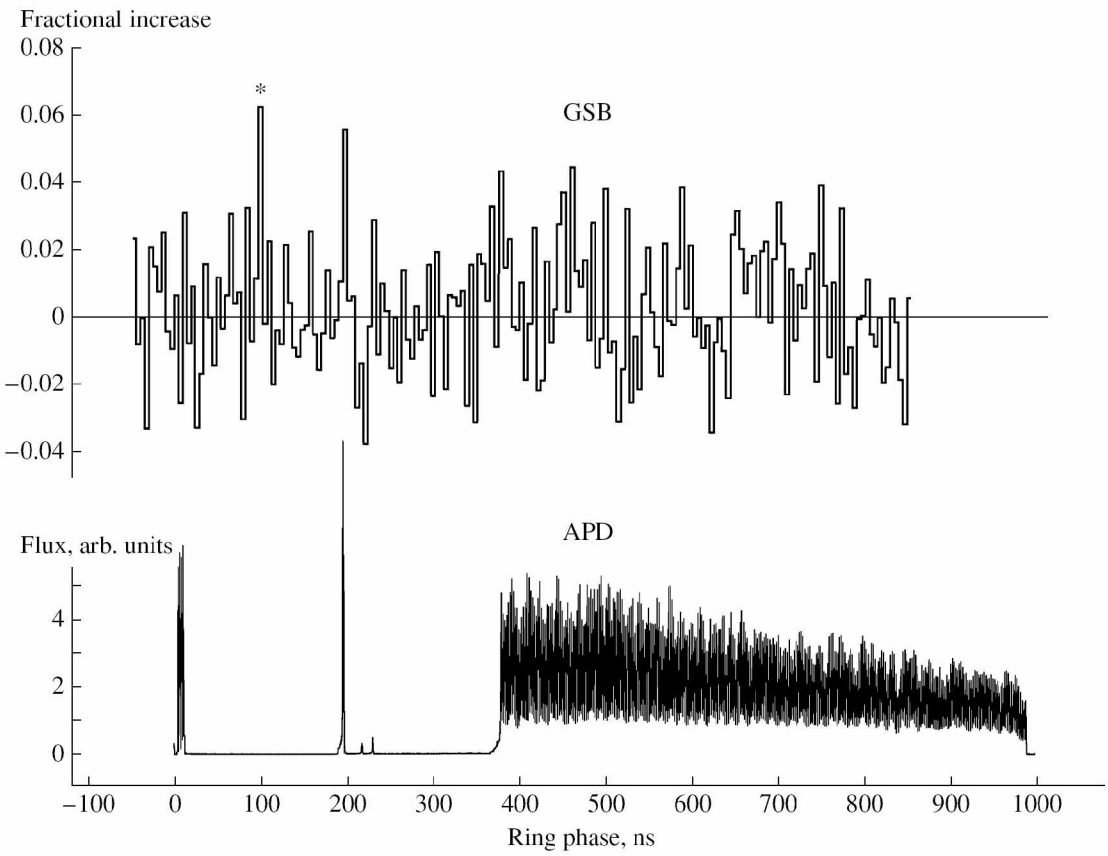

Figure 6.11. Plot showing the induced decay of the isomeric nuclei as a function of the phase time of the electron bunches around the ring. The upper panel shows the fractional increase of γ photons counted in the GSB when the target was irradiated at the phase times shown over the amount of spontaneous emission collected when the SR beam was blocked with a shutter.

The most significant result from figure 6.11 is the strong confirmation of the immediacy of the GSB cascade following irradiation with SR X-rays from each electron bunch. Also shown is one of the principal challenges to further work, SR noise. The peak marked with the asterisk is such an artifact. Unlike the rest of the structures, that peak shows in data for every gamma line. Further attention to electrical shielding is indicated in future experiments. The significance of the immediate timing of the induced decay is that it explains further why some competing experiments with the same material conducted at other SR facilities report failure to induce decay. A prevailing concept in other studies has been that induced decay should generally follow the decay cascades found for spontaneous emission, meaning that gamma fluorescence of the GSB should be delayed after irradiation with a statistical time lag of 4 *s* at the 8^- level in between the isomeric state and the ground state. Because of artifacts such as those marked by the asterisk, it is an easier experiment to compare gamma counting rates being detected some seconds after the SR beam is blocked mechanically and then to look for a 4 *s* half-life for the decrease of that fluorescence. Since this current work has shown that the gamma fluorescence follows SR irradiation by an interval smaller than the few nanosecond resolution of this experiment, the negative results in the simple measurements attempted elsewhere can be understood as waiting too long before opening the gate for data collection.

Figure 6.6 shows by open circles the excitation function for stimulating fluorescence through the GSB during phase time in the interval 350–550 *ns*. In order to make a direct comparison with the earlier results for this graph, the counts recorded in the GSB excluded contributions from the (2, 0) transition.

6.2.6 Conclusions

In 2002 and 2003, four experiments conducted on three beamlines at two different monochromatic SR sources have produced a compelling set of results which affirm that the decay of the 31-yr isomeric $^{178}Hf^{m2}$ nuclei can be accelerated by irradiation with low energy X-ray photons. Confidence of 6.3σ was developed from data collected in 2002 and was increased to 12σ by remeasurements conducted in 2003.

When examined as an incident monochromatic beam tuned through X-ray energies near the L_3 photoionization edge of Hf, the excitation function measured for accelerated decay of the isomers in the sample displays structure resembling what is usually found in XAFS studies of inner-shell photoionization phenomena. Thus the induced emission of γ fluorescence can be perceived as a nuclear output channel of XAFS phenomena for which the branching ratio exciting it is 1.6×10^{-3}. The most pronounced structure in that excitation function for nuclear XAFS is a peak at 6 *eV* above the L_3 edge at 9561 *eV,* which has been found in all measurements we made with SR sources.

For X-ray energies around the peak for nuclear XAFS, the induced decay of the isomeric nuclei is prompt. Any delay is shorter than we could measure with the timing system described above, meaning a few nanoseconds. When the complexity of the nuclear band structure of ^{178}Hf is considered, it may not be surprising that the induced decay is prompt. After the *K* quantum number is mixed at the instant of triggering, there are considerably more cascades available that will avoid the statistical time lag associated with the 8^- bandhead than there are cascades that feed the 8^- level. Consistent with the observation that the γ fluorescence is promptly emitted after decay is accelerated is the observation of “new” lines in the γ spectrum of the induced decay. One such line lies near

130 *keV*. The excitation function for that line agrees with what is observed for the GSB and supports earlier published reports that the 130 *keV* line is excited in coincidence with the (4,2) member of the GSB at 213.4 *keV* [101]. A number of other new lines have been observed, but additional experimentation will be needed to establish reliability.

Confirmation of the efficiency with which monochromatic X-rays at fluxes between 10^{10} and 10^{12} photons $cm^{-2}\ eV^{-1}\ s^{-1}$ will trigger the decay of the 31-yr isomer of $^{178}Hf^{m2}$ can be obtained to a compelling degree of confidence by observing the prompt emission of γ photons in the GSB or around 130 *keV* when the X-ray energies are turned about 6 *eV* above the L_3 edge for photoionization of Hf. Further work will be focused on the channels of cascades within the nuclei through which the fluorescent γ photons are emitted and on the spectra of the structures being found in the excitation functions for nuclear XAFS. Results to date provide strong encouragement for the development of a γ-ray laser by demonstrating the prompt release *in situ* of energy stored in spin isomers that is triggered by X-ray photons with quantum efficiencies of 256x at 9567 *eV*.

Acknowledgments

The authors gratefully acknowledge the encouragement and support of this work by DARPA through AFOSR grant F49620-03-1-0196 and AFOSR through grant F49620-02-1-0141 in cooperation with Japan Synchrotron Research Institute (JASRI) through proposals 2001A0082-NX-np, 2001A0570-UX-np, 2002A0321-NX-np, and 2003A0054-ND3-np and the Swiss Light Source (SLS) of the Paul Scherrer Institute (PSI) through proposal 20020104. The isomeric targets were loaned by courtesy of General Coherent Technology, Inc.

CHAPTER 7

OTHER MECHANISMS FOR INDUCING THE γ-EMISSION FROM $^{178}Hf^{m2}$ ISOMER

In previous chapters, the accelerated decay of the 31-year isomer of the ^{178}Hf observed during irradiation with X-rays of an isomeric target brought the conclusion that it is sufficient to create L_3-shell vacancies in order to stimulate transitions from the *m2* isomeric level to an intermediate level with a probability of 0.16% [64]. It seems that the stimulated decay reached the GS band bypassing the 8^- band and its bandhead, the *m1* isomeric state, so that the stored energies of the isomeric nuclei were released immediately [65]. But irradiation with bremsstrahlung radiation [22] showed that the induced gamma rays were emitted from transitions which followed the normal cascades of spontaneous decay and an intense induced emission was found in the line at 495.0 *keV*. However, there were identified also γ-lines not observed in the spectrum of the spontaneous decay [22]. It indicates that other mechanisms for inducing the energy release of $^{178}Hf^{m2}$ isomer were involved, which evidently made use of a different trigger level than the one implied with X-ray photons near the L_3 photoionization edge of hafnium.

In 2002 and 2004 tunable monochromatic X-rays from the SPring-8 synchrotron radiation source were used to determine the most favorable X-ray energies for inducing the gamma emission of $^{178}Hf^{m2}$ isomer and also to verify the necessity of L_3 vacancies in the induced emission process already observed. The experimental methods in both cases were similar with those detailed in previous chapters. The BL01B1 and BL09XU beamlines were used to produce fluxes

of about 2×10^{11} *photons/cm^2/s* and 2×10^{12} *photons/cm^2/s* respectively, with 1 *eV* nominal spectral bandwidths.

The previous chapter concluded that it is sufficient to create L_3-shell vacancies in the electronic structure surrounding the isomeric nucleus in order to stimulate its energy release. To research weather L-shell vacancies are necessary in the triggering process, in 2004 a 13 *kBq* $^{178}Hf^{m2}$ isomeric sample was also irradiated with SR photons of enough energies to produce M-shell but not L-shell vacancies. To assure sufficient transparency of the target substrate, irradiations with photons of energies above 7 keV were used. That corresponded to a maximum of 10% absorption, as suggested by the measured transparency of the sample substrate shown in figure 3.1. Runs with 3000 *s* duration each were performed by tuning the monochromatic SR beam at 10 energies in steps of 1 *eV* around few main energies: 7, 7.5, 8, 8.5, and 9 *keV*. Because no evidences for induced gamma release were observed at photon energies below 9 *keV,* it one may conclude that L-shell vacancies were necessary and sufficient to accelerate the decay of $^{178}Hf^{m2}$ isomer.

7.1 PIGE of $^{178}Hf^{m2}$ Isomeric Nuclei by 20,825 *eV* X-Rays

During an experiment conducted in 2002 at the BL01B1 beamline, a survey mode of operation was adopted for searching for favorable X-ray energies for inducing the gamma emission of $^{178}Hf^{m2}$ isomer. It was found that monochromatic X-rays having energies near 20,825 *eV* may accelerate the decay of the 16^+ isomer, the induced decay was including almost entirely the natural decay path.

The figure 7.1 (b) and (d) shows the additional numbers of gamma photons detected in three consecutive runs, when the isomeric sample was irradiated with X-ray photons, having energies in the vicinity of 20,825 *eV*, for 100 *s* at each tuned energy. Also shown for a comparison is a calibrated fraction of the spontaneous γ-emission accumulated in the same time. In agreement with the first report [22] of an acceleration of the decay of $^{178}Hf^{m2}$ isomeric nuclei caused by incident bremsstrahlung X-ray pulses, the members of the $K^{\pi} = 8^{-}$ and GS band were enhanced. The excitation function of the induced decay of the isomeric nuclei shown in figure 7.2(a) confirms this fact. It includes the sums of the numbers of extra gamma photons of the most important members of the GS and 8^{-} band caused by the SR irradiation, plotted as functions of the incident monochromatic X-rays. As can be seen, the excitation functions of both band members are peaking at about 20,825 *eV*. The figure 7.2(b) shows the excitation function of the induced gamma emission of the 8^{-} and GS band members compiled together. The peak at 20,825 *eV* is identified with 4.8 σ confidence in this case.

Supplementary information to confirm that the peak is not an artifact and is a real enhancement of the emission of the 8^{-} and GS band members may be obtained by taking into account the 4 seconds lag between those two bands. The delay is imposed by the *m1* isomeric state, the band-head of $K^{\pi} = 8^{-}$ band. It shows that the enhancement of the transitions of the 8^{-} band must increase the population of the band-head and consequently, the excitation must be transferred to the GSB delayed by a statistical time lag of 4 seconds. As a result, during the first seconds of the irradiation periods more photons identified with the members of the 8^{-} band should be emitted, if the energy of incident X-ray photons were being stepped to values for which the probability of triggering was increased. This should have happened during the times when the X-ray energies were stepped from 20,820 *eV* to 20,825 *eV*, while the excitation function is

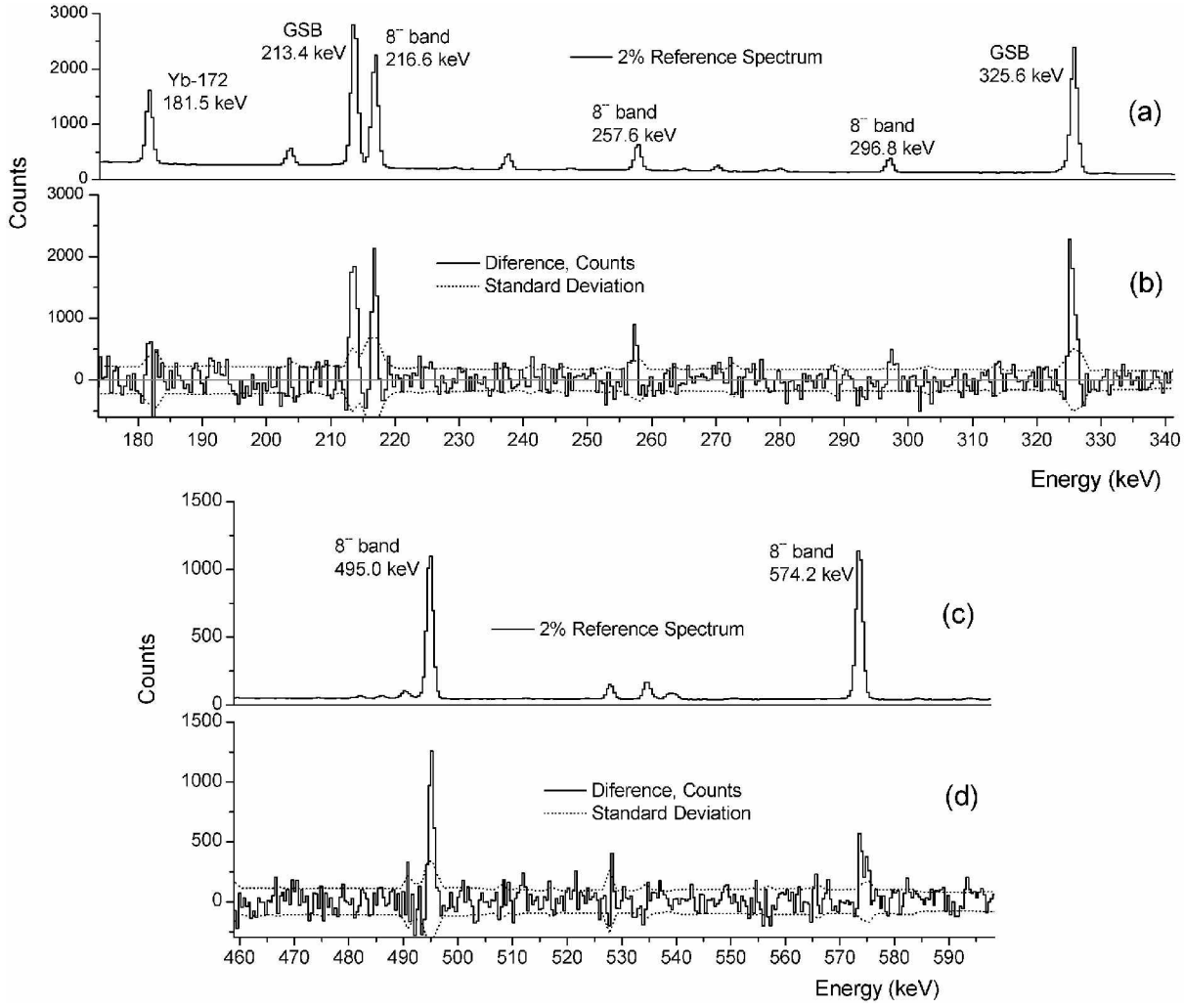

Figure 7.1. (b) and (d) Plots of the differences in counts between inbeam and baseline data obtained in the spectrum of the $^{178}Hf^{m2}$ from the isomeric target when was irradiated with X-ray photons of about 20,825 eV. The dotted lines show the computed values of the 1σ for the difference.
(a) and (c) Plots of 2% of the reference data

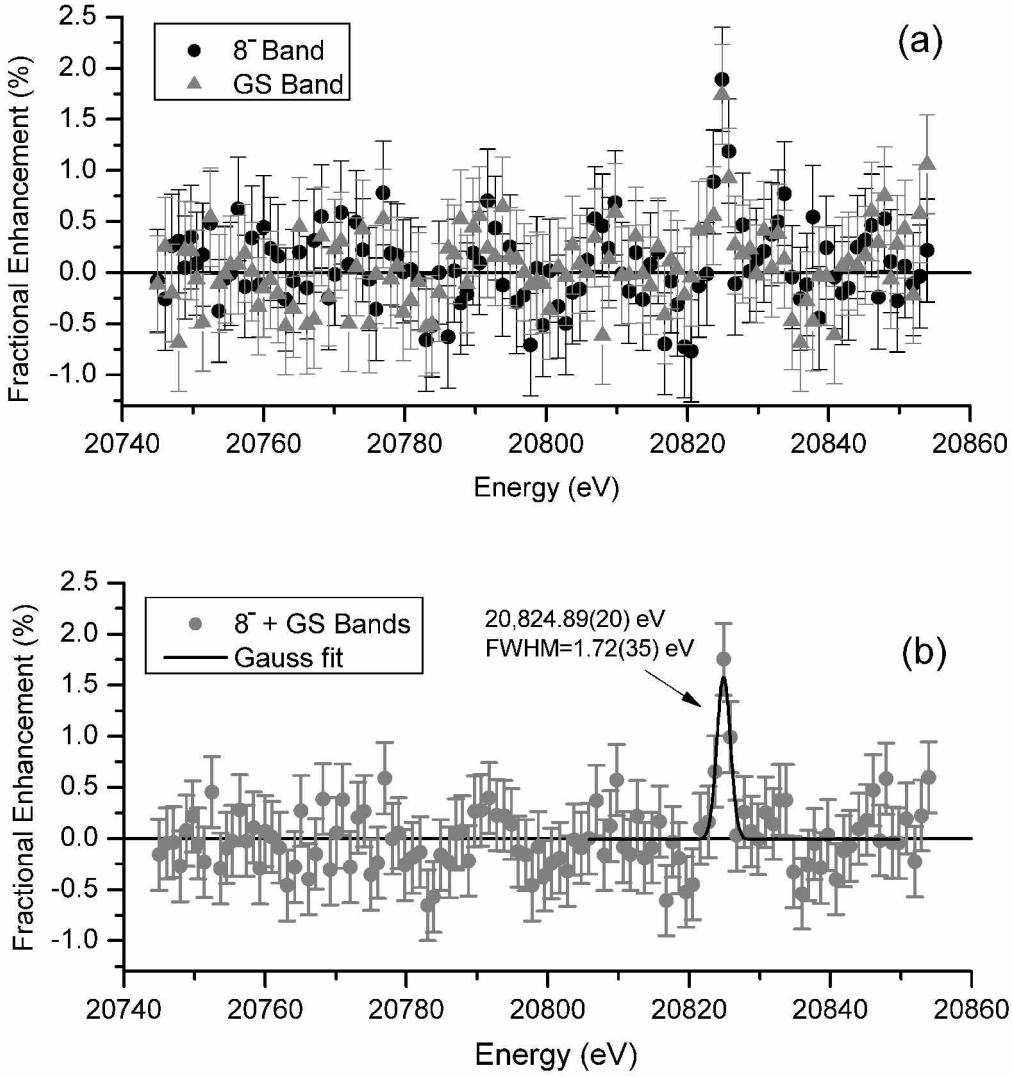

Figure 7.2. (a) The excitation functions of the induced gamma emission of the 8^- and GS band members. They represent the fraction of the extra number of photons detected from the discrete transitions of those two K-bands versus the tuned energy of the monochromatic SR beam incident on the $^{178}Hf^{m2}$ isomeric sample. The excitation functions peak at 20824.89(20) *eV* for both group of transitions.

(b) The excitation function of the induced gamma emission of the 8^- and GS band members compiled together. The gaussian that fits the data is centered at 20824.89(20) *eV* and has FWHM = 1.72(35) *eV*. The peak of the excitation function is identified with a confidence of 4.8 σ

increasing sharply over that range of X-ray energies as figure 7.2 suggests. The time dependence of the ratio of the numbers of induced counts of photons detected in the members of the 8^- band to those collected in the GSB during those times is shown in figure 7.3. An apparent excess of the number of photons detected from the 8^- band relative to the number of photons detected in the GSB in the first seconds of the irradiation can be clearly seen. It is the result of the increased efficiency for inducing the decay of the isomeric nuclei. That excess is reduced with time as the population of the *m1* isomer equilibrates. The time scale for equilibration respects the radioactive decay law of an excited state with half-life of $T_{1/2} = 4\ s$, as the data fit in the figure 7.3 suggests.

The gaussian that fits the peak of the excitation function shown in figure 7.2(b) is centered at 20,824.29(20) *eV* and has a FWHM of about 1.7(3) *eV*, a value which is much smaller than the usual value of the width of the processes involving atomic inner-shell electrons, that should be about $\Delta E/E \sim 10^{-3}$ [71]. It may be concluded that atomic electrons are not mediating the energy transfer from the incident 20,825 *eV* photons to nucleus, but a direct photonuclear excitation process has occurred in this case. There is no known level of ^{178}Hf lying at about 20.8 *keV* above the *m2* isomeric level. In this context, it is necessary to consider that a trigger level should exist at about 2466.8 *keV* from the ground state and that there is at least a decay branch from it to the 8^- band and also a decay branch back to the *m2* isomeric level. In this experiment, only photons with energy between 80 *keV* and 602.2 *keV* were acquired with considerable efficiency as a result of absorption of low energy photons by the multilayer shielding surrounding the detector, and of spectroscopy amplifier threshold and amplification settings. In this range of energy no supplementary γ-lines have been observed. It results that the transition from the 2466.8 *eV* trigger level to the members of the 8^- band is mediated by a cascade of transitions with energies outside of this range. However, the figure 7.1 suggests that there is a stronger enhancement of 495.0 *keV*

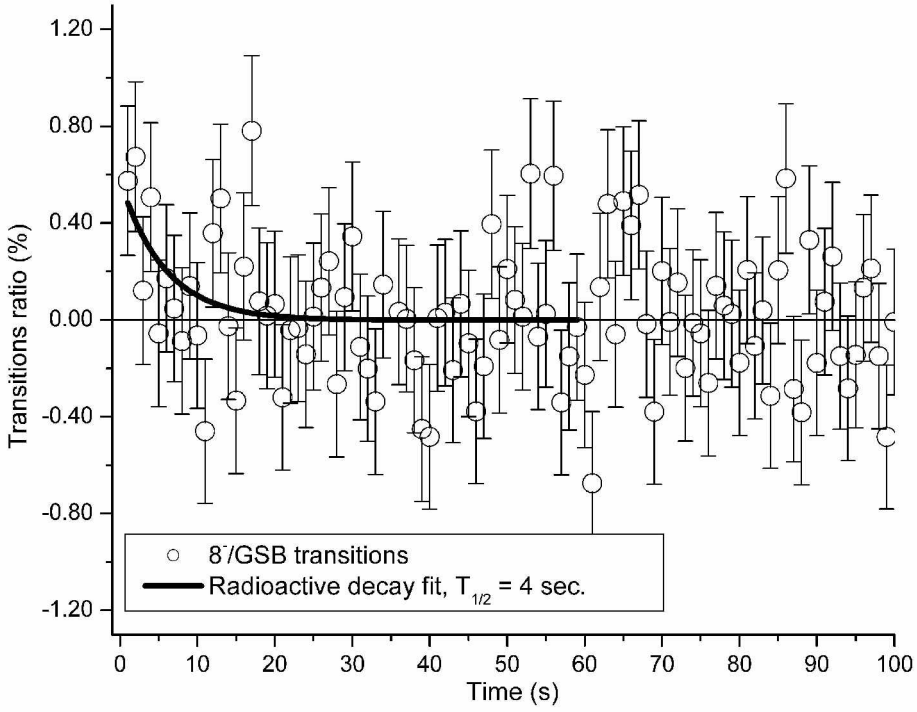

Figure 7.3. Radioactive decay fit ($T_{1/2}$ = 4 *s*) of the time dependence of the ratio of induced γ-emission of the 8^{-} to GS band members during irradiation with 20,820 - 20,825 *eV* X-ray photons

($11^- \rightarrow 9^-$) and 257.6 *keV* ($11^- \rightarrow 10^-$) gamma-lines, which is about 1.6%, than of 574.2 *keV* ($13^- \rightarrow 11^-$) and 296.8 *keV* ($13^- \rightarrow 12^-$) transitions, that is about 0.65%. That means that there is an important decay branch from 2466.8 *keV* trigger level may be feeding the $I^{\pi} = 11^-$ level of the 8^- band, rather than 13^- and 12^- states. The latest two levels are also fed by the natural decay of the 16^+ isomeric state. In this context, the figure 7.4 shows the presumptive triggering mechanism of $^{178}Hf^{m2}$ when the isomeric nucleus was irradiated with 20.825 *keV* photons.

7.2 The 2457.20 *keV* Trigger Level

In 2004, during a set of experiments conducted at the BL09XU, the gain of the spectroscopy amplifier was lowered so that photons with energies up to 2500 *keV* were acquired on 4096 discrete channels by the acquisition system described in the subchapter 3.3. That was the very first time when such large range of γ-energies was investigated. The efficiency of the small physical size of the 10% HPGe detectors available, were drastically decreased to about 1% at 2 *MeV*, but the spectral resolution was still very good. Few trial runs covering the above mentioned γ-energy range included γ-photons accumulation while tuning the SR beam with 1 *eV* spectral linewidth over 20 energy steps of 1 *eV/step*, covering a range of X-rays from 9555 *eV* to 9575 *eV*. A vertical scanning of the isomeric sample with 9567 *eV* X-ray photons was also performed. The average value of the flux was about 2×10^{12} *photons/cm^2/s*.

During this run, initially developed as a test run, but which brought important information, the physical position of the target was moved lower in vertical direction from the Ge detector, in steps of 0.125 *mm/step* with a stepping motor as shown in figure 7.5. The isomeric sample was entirely covered by the spot of the SR beam when it passed by position -0.30 *mm*. This position

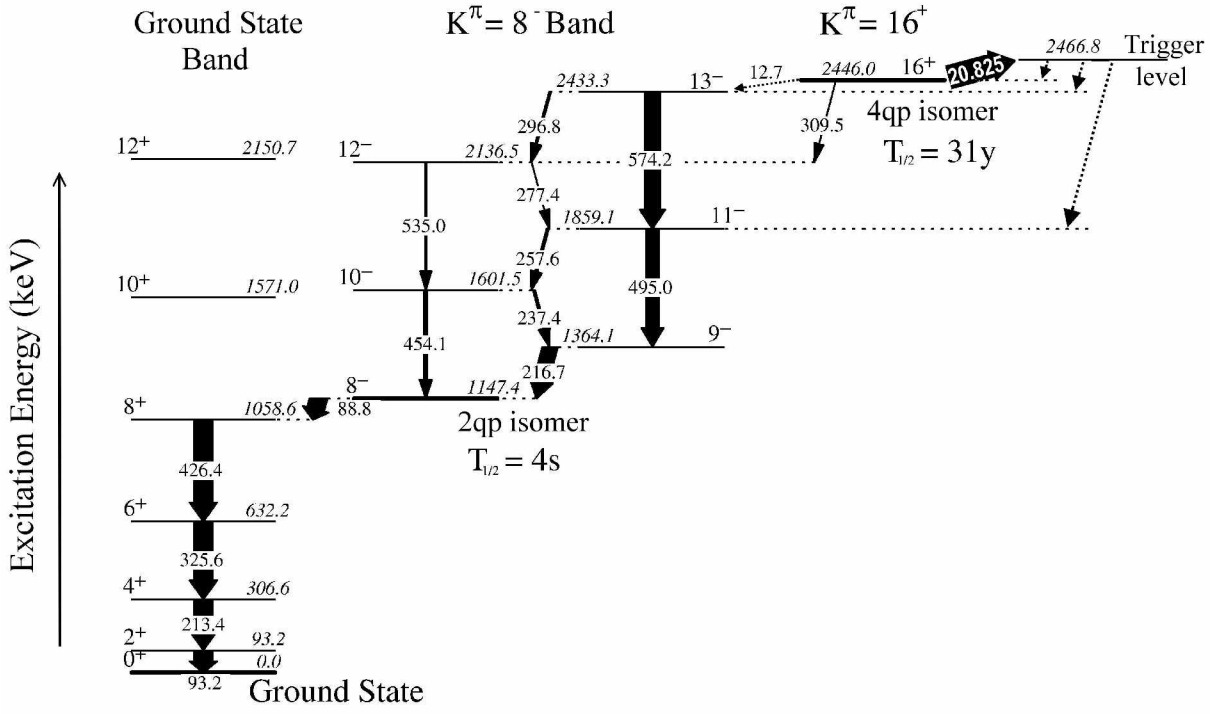

Figure 7.4. The presumptive triggering mechanism of $^{178}Hf^{m2}$ nucleus when the isomeric sample was irradiated with 20.825 *keV* X-ray photons.

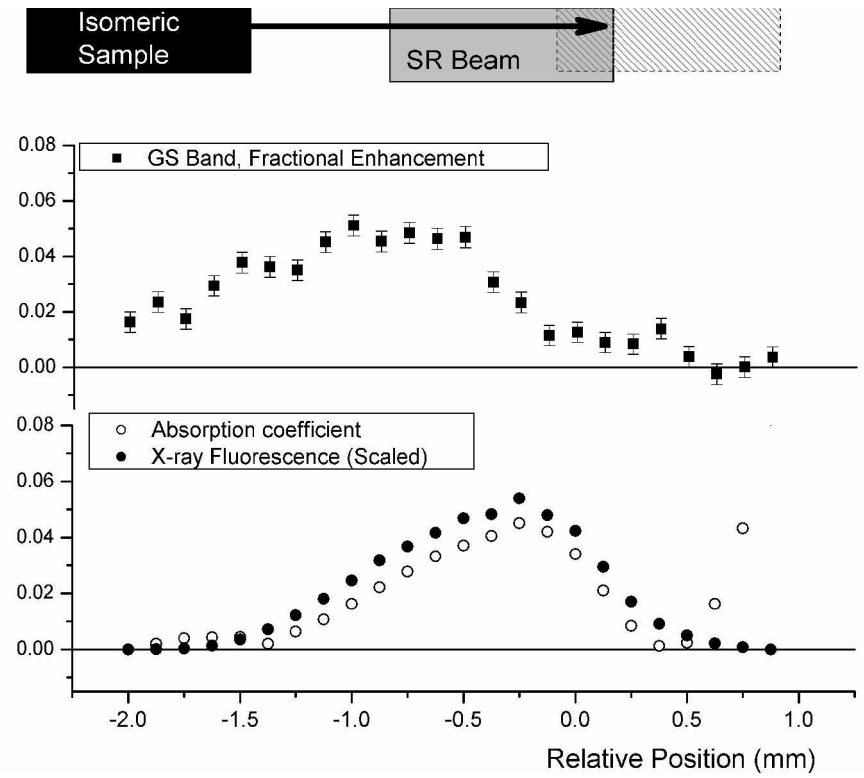

Figure 7.5. Comparison of measured enhancement of the GSB transitions with the coefficient of absorption of the incident 9.567 *keV* X-rays at different positions of the isomeric sample relative to the main axis of the SR beam. Also shown in comparison are the numbers of X-ray photons scattered from the target seen by a SDD detector. The width of the sample is about 1 *mm* same as the width of the SR beam spot. It can be deduced that there is a stronger enhancement of the GSB members in off-axis position of the sample. It results that the off-axis (even-order) SR harmonics have an important role in the induced gamma emission of the $^{178}Hf^{m2}$ isomer. The harmonics comprised 10% of all of the incident photons, during these measurements.

corresponded also to the maximum of the absorption coefficient of the sample that was recorded at the same time by two ionization chambers. Thus it was the usual position of the sample relative to the incident beam during all previous experiments.

At each position of the target the gamma photons were acquired for 300 *s* in two experimental conditions: inbeam (SR beam hitting the target assembly) and baseline (SR beam blocked by a thick absorber). The enhancement of the GSB members is plotted versus the physical position of the sample in figure 7.5, in comparison to the scaled values of the absorption coefficient and of the x-rays scattered by the part of the target assembly being irradiated. It can be seen that the maximum for the induced decay of the isomeric content corresponds to an off-axis position and reached about 5% relative to the spontaneous emission. In the center of the beam the enhancement of the GSB members is about 1% in agreement with previous measurements. It indicates that the off-axis components of the SR beam, such as even-order harmonics, were implied in the triggering process.

Supplementary information has been obtained from the analysis of the γ-spectrum. Figure 7.6 shows the comparison between the spectrum of γ-photons from target assembly when it was irradiated and the baseline spectrum. To improve statistics, the figure 7.6 comprises also the data during which the x-rays were tuned from 9555 *eV* to 9575 *eV*. The line at 2447.86 observed in both spectra arises from the natural background and facilitated the spectrum calibration in that range of γ-energies. A new γ-line at 2457.20(22) *keV* can be identified with a confidence of 6.5 σ only in the inbeam data. Another γ-line was identified in the induced spectrum at about 642.5 *keV* (figure 7.7) with a confidence of 4.4 σ. There is no know transition of the ^{178}Hf nucleus with those energies and also there is no known level lying at 2457.20(22) *keV*. It may be admitted that

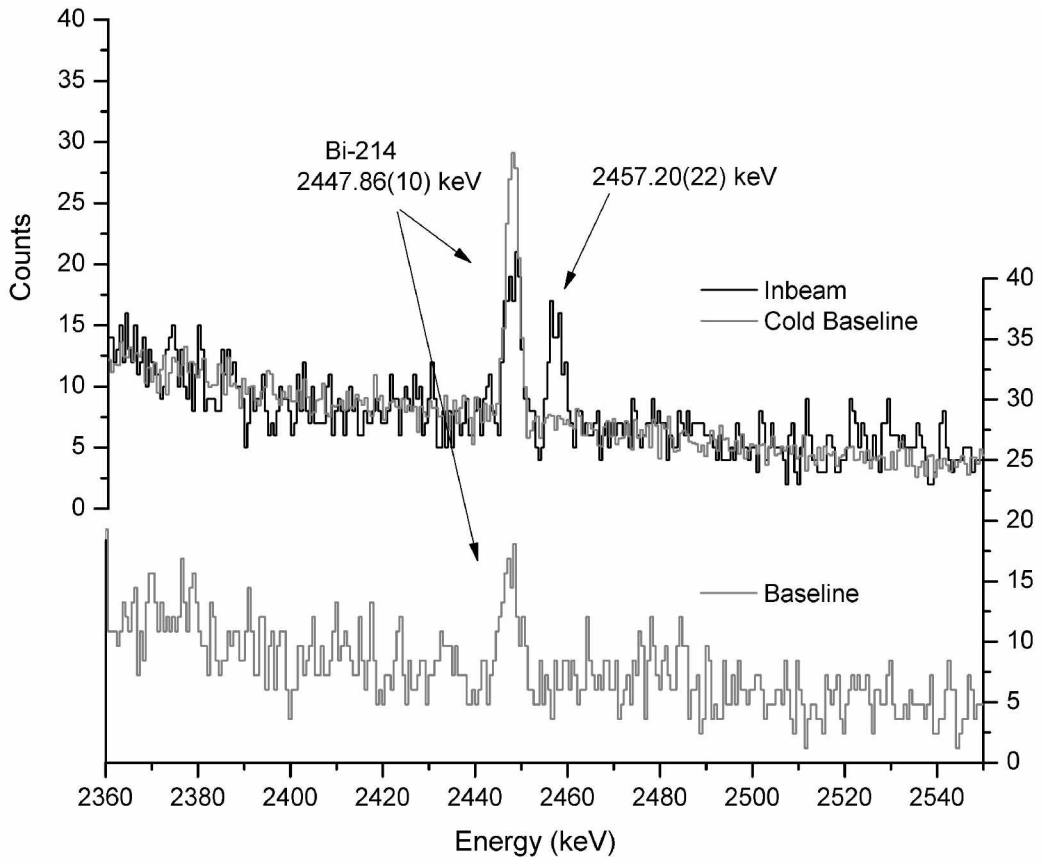

Figure 7.6. Comparison of inbeam and baseline γ-spectrum at energies in the vicinity of the 16^{+} isomeric level of ^{178}Hf. To improve statistics, the data accumulated while scanning the SR beam from 9555 *eV* to 9575 *eV* are included together with the data from the off-axis positions of the isomeric sample. Data identified as *cold baseline* were obtained from the spontaneous decay measured off-site for a much longer period. An unknown γ-line arising only in the inbeam spectrum can be identified with a confidence of 6.5 σ at 2457.20(22) *keV*. It is supposed to be a trigger level which has been excited by higher harmonic components of the SR beam. The 2447.86 *keV* γ-line arise from natural background and served for spectrum calibration at those range of γ-energies.

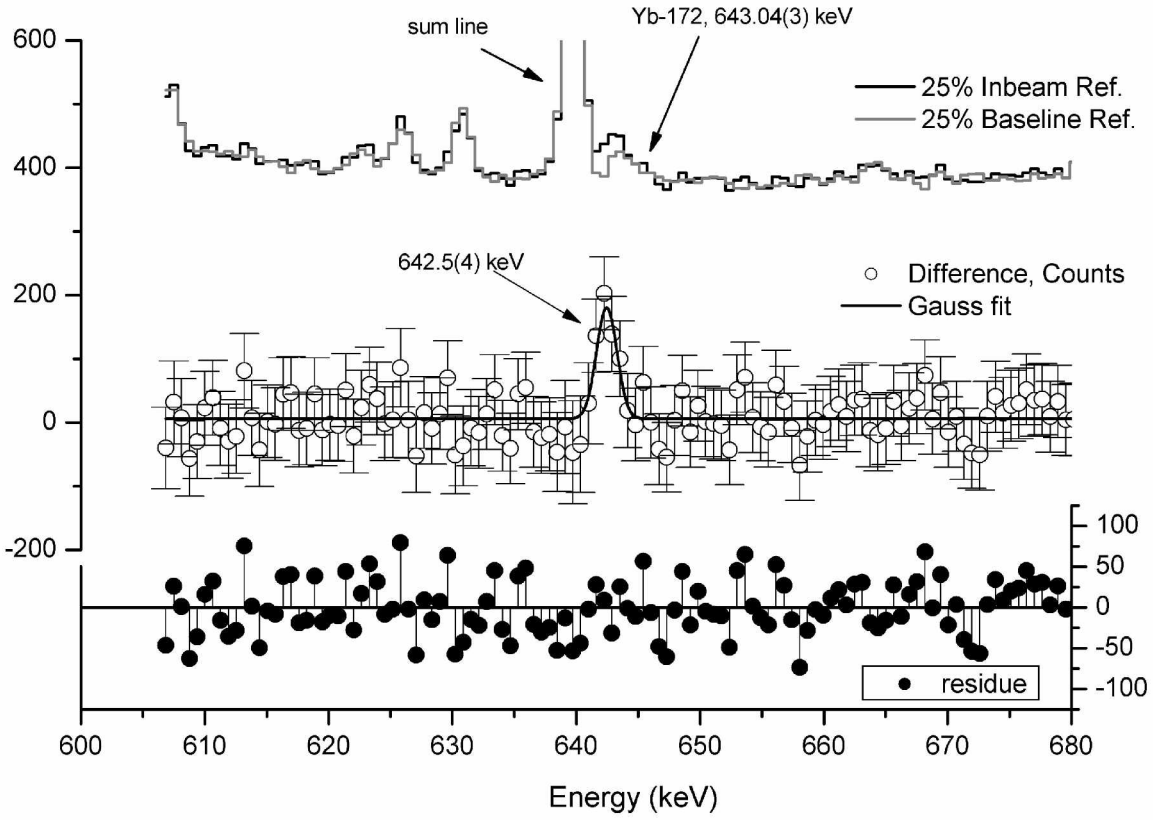

Figure 7.7. A new γ-line, not present in the spontaneous decay of the $^{178}Hf^{m2}$ isomer has been identified in the spectrum of γ-photons collected during irradiation of the isomeric sample with monochromatic SR tuned from 9555 *eV* to 9575 *eV*. The new γ-line arises at 642.5(4) *keV*. The line has a Gaussian shape and a Gauss fitting was performed. There is no evidence for structures in the residue. Also shown are fractions of the inbeam and baseline spectrum which lead to the identification of the 642.5 *keV* line.

this level exist in order to explain the new gamma line in the inbeam spectrum, as a direct transition to the ground state. It could not be a transition to the first excited state - the 2^+ member of the GSB - lying at 93.18 *keV*, because that requires the emitting level to lie at about 104.33 *keV* above the isomeric level, which could be excited by the 11^{th}- or higher-order harmonics of the SR beam, which is very improbable. However, the excitation of the 2457.2 *keV* level can not be explained by making use of fundamental harmonic photons (9.555 – 9.575 *keV*), while its excitation requires 11.15(27) *keV* excitation energy. The difference, 1.42(27) *keV*, is still outside of the errors. The adopted value of the 16^+ isomeric level of ^{178}Hf is 2446.05(15) *keV* [111].

The above observations conduct to the conclusion that the superior-order harmonics were implied in the triggering process, mainly the off-axis harmonics. Only the even-order harmonics propagate off-axis of the main SR beam and the second-order harmonic is the most intense [112]. It covered a range from 19.110 *keV* to 19.150 *keV*. If 11.15(27) *keV* should be used for excitation of the isomeric nucleus to the trigger level, the remaining energy, approximately equals the hafnium $L_{\alpha 1}$ X-ray line (7899 *eV*) or $L_{\alpha 2}$ line (7844 *eV*) [113]. This leads to the idea that coupled Auger-processes or inversed electron-bridge effects are also involved in the excitation mechanism. It may be speculated that a second harmonic photon would initiate a multi-order process. The photon is absorbed and the isomeric nucleus would excite to the intermediate nuclear state at 2457.20(22) *keV* together with the emission of an L-shell electron and coupled Auger-processes that would fill the resonance. Therefore, $L_3M_{4,5}M_5$, $L_3M_{4,5}N_x$, or $L_3M_{4,5}O_x$ Auger-electrons may result. It also may be speculated that an IEB-like process is implied. The second harmonic photon is absorbed and the isomeric nucleus is excited via a virtual transition of $2p_{3/2}$ electron as shown in figure 7.8. In this case, the initial and final electron states coincide and an $L_{\alpha 1}$ photon is also

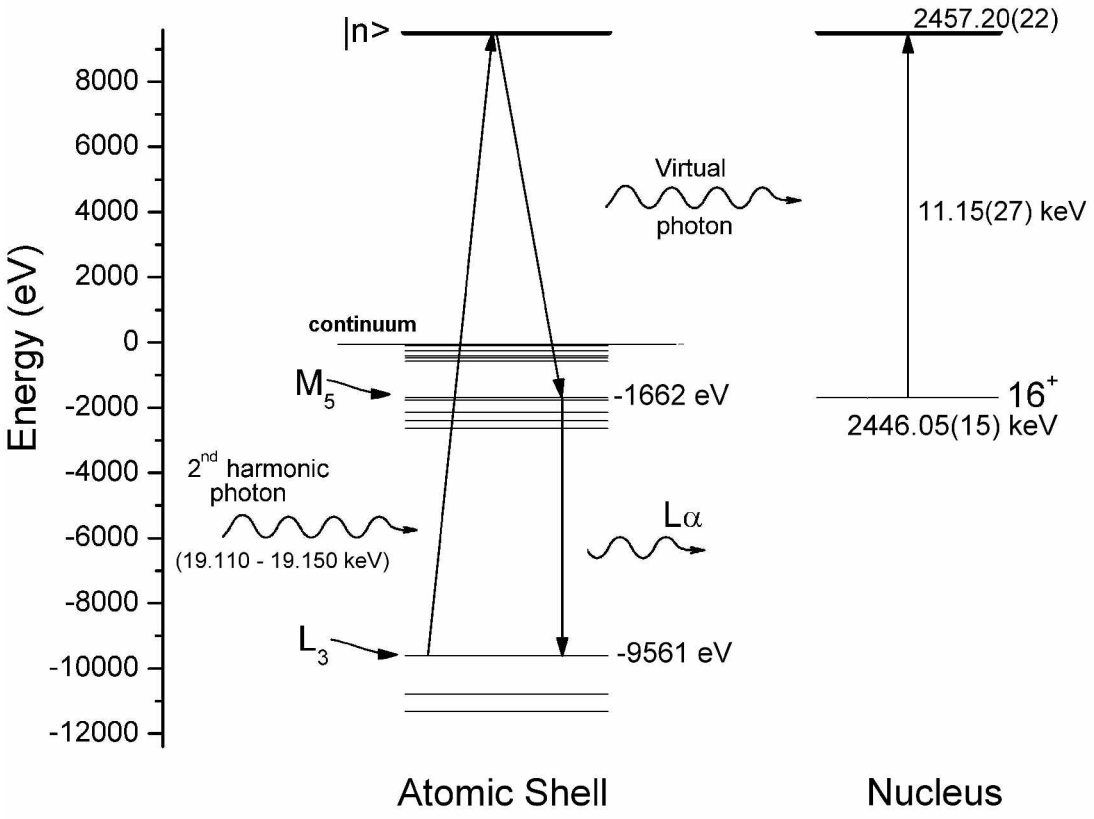

Figure 7.8. A presumptive excitation mechanism of the $^{178}Hf^{m2}$ isomeric nucleus to the 2457.2 *keV* trigger level. Incident second harmonic photons range from 19.110 *keV* to 19.150 *keV*.

emitted. The |n> and M_5 atomic states plays the role of virtual states, so that M_5 does not require to be previously ionized in order to support the virtual transition of the $2p_{3/2}$ electron, as explained in the references [47, 49, 52].

Because the 2457 *keV* transition was excited accidentally in this work, future experimental investigations should include a dedicated nuclear resonance spectroscopy experiment with incident X-ray photons tuned near the 11.15(27) *keV* resonance in order to search for the resonance absorption in the X-ray absorption spectrum that corresponds to the transition of the isomeric nucleus to the trigger level.

CHAPTER 8

CONCLUSIONS

Long-lived high-energy nuclear isomeric states are suitable media for storing the energy in the range of a few *keV* to a few *MeV*. Macroscopic samples of such isomers can store for long period of time large amounts of energy, that usually can represent more than tens of thousands times more energy per gram than what is available from chemical compounds. The stored energy can be released as electromagnetic radiation without implying a nuclear reaction. The deexcited nucleus is the same isotope of the same atomic element in its ground state or into an intermediary lower energy isomeric state.

The controlled release of energy stored in nuclear isomeric samples will produce powerful pulsed-sources of gamma ray radiation. That is why, at present, this field is at the focus of a great scientific and technological interest. In addition, the possibility that the gamma bursts produced to have coherence and directionality (gamma-ray lasers) brings even more attention.

Many efforts and concepts have been put forward to find the best isomeric candidates and solutions to control the release of their energy. The top position of the most interesting candidates list is occupied by $^{178}Hf^{m2}$ isomer [8, 11], and the most promising way to release its energy has been found in employing externally-produced X-rays, the PIGE [10, 11]. Its 4-qp structure explains the long half-life of 31-years of its 16^{+} exited level lying at 2446 *keV* [111]. This means that 1 *g* of macroscopic isomeric sample may store approximately 1 *GJ* of energy, which can be released as electromagnetic transitions. Low energy photons may stimulate the decay of the $^{178}Hf^{m2}$ isomer into a

direct up-conversion scheme [11], because the isomeric level lies at a high excitation energy where high density of states exists. Some of these states may have accentuated K-mixing character, which is the most important requirement of a trigger level.

Following the first experimental demonstration of PIGE employed on $^{180}Ta^{m}$ [13], the experimental efforts in accelerating the decay of $^{178}Hf^{m2}$ started in 1998, in a series of experiments conducted at Center for Quantum Electronics of the University Texas at Dallas [22, 23].

The first investigations used bremsstrahlung radiation to stimulate the decay of $^{178}Hf^{m2}$ and showed a strength of 2% enhancement relative to its spontaneous decay [22, 23, 70], with a global confidence of 5.8 σ for the main GSB members. The irradiation source was working at 40 *mA* peak value of the current with energy endpoints of 90 *keV* and 60 *keV*. Consequently, it was established that only photons with energy smaller than 20 *keV* can accelerate the isomeric decay. For this energy of photons, the integrated cross section was found having a value larger than 2.2×10^{-22} cm^2 *keV*. It was concluded that the decay from the trigger-level proceeds through several parallel cascades of transitions. That is because not all the transitions feeding the GSB were enhanced by the induced decay and unusual increased intensity of several lines that are not part of spontaneous decay have been identified. A γ - γ coincidence measurement was required in order to establish the induced decay path.

In this work, a modern, complex, and flexible multi-parametric list-mode data acquisition system (DAQ) - based on virtual instruments concept - was designed in order to accommodate multi-detector single spectra and multiparameter coincidence measurements. It supplied a large amount of information about the acquisition process, and outputted a complete list of characteristics of each detected event. The DAQ was optimized for collecting data from the 4-fold γ-γ coincidence system, integrating the control of the X-ray device, and monitoring the irradiation [101]. The analysis of

matrix coincidence data was not part of this work. The same data acquisition system has been redesigned and specialized for data logging and analysis for PIGE experiments with synchrotron radiation.

Much higher X-ray flux was required, together with constant emission during each irradiating pulse. The redesigned X-ray device was presented in this work, together with full characterization of the emitted radiation. The flux was doubled during shorter (2.5 *ms*) rectangular pulses of the current through the X-ray tube [101]. It was found that the enhancement was doubled. The same X-ray device was used in year 2000 for irradiation during the investigations by γ–γ coincidence method of the induced decay of $^{178}Hf^{m2}$ isomer. The coincidence experiments identified a new gamma transition at 129.5 *keV* [101], member of a cascade of the induced isomeric decay which feds into the 4^+ state of the GSB. The rest of the cascade members are still unknown and it is assumed that they have energies higher than 1 *MeV* or lower than 80 *keV*.

Based on the increased emission flux of the rebuilt X-ray device, in this work it has been established that the percentage by which the decay was accelerated was proportional to the applied flux at those flux levels around 5×10^{10} *photons/cm^2/s/keV* [102]. That might not be expected to be the case if higher order effects are involved, but cumulative effects of different triggering mechanisms may produce strong effects.

In order to get irradiation with even much higher fluxes and to be able to exactly establish the energy of X-ray photons implied in the triggering process of isomeric $^{178}Hf^{m2}$ nuclei, that is to measure the excitation function of the members of the accelerated decay, tunable monochromatic X-ray photon beams were required. This work made use of the most advanced X-ray photon sources, the 3rd generation synchrotron radiation (SR) sources. During the period 2001-2004 a few induced

gamma emission experimental investigations of $^{178}Hf^{m2}$ have been conducted at the SPring-8 and at the Swiss Light Source (SLS) SR facilities.

The first two SR experiments conducted during year 2001 at the BL01B1 beamline of the SPring-8 facility brought evidences that the subject responsible for the accelerated decay of $^{178}Hf^{m2}$ isomer imply energy transfer from the atomic shell to nucleus when the energy of incident photons were tuned near the L_3 photoionization edges of atomic hafnium [63]. The nuclear excitation by electronic transitions (NEET) process has been considered the main process involved, with a branching ratio estimated at about 0.2% [63] relative to the photoionization processes. This value is approaching the theoretical maxima [39].

Additional structures have been identified in the excitation function of the GSB members [63] and their validation and understanding required repeated experiments with longer time of data accumulation at each tuned energy of SR beam. The existence of additional structures was proved by verifying their consequent appearance in data with higher statistical significance. High resolution scanning was required in order to better describe the excitation function on those ranges. The two experiments conducted in year 2002 at BL01B1 and BL09XU beamlines of SPring-8 synchrotron facility were focused on these tasks. These experiments concluded that additional structures of the GSB excitation function clearly exist above and below the simple ionization edge of the L_3 shell, more exactly at about 9555 *eV*, 9567 *eV*, and 9573 *eV*. These peaks accompany the main peak at 9561 *eV* and they are considered to correspond to nuclear excitations during XAFS-like electronic transitions. This family of processes has been called Nuclear-XAFS [64, 65, 114] effects. Examples may include the two-electron transitions which can add structures above the simple photoionization edge and transitions of inner-shell electrons to the valence and conduction bands at incident photon energies below the simple photoionization edge.

The peak of the excitation function at 9555 *eV* seems to correspond to the L_3 shell ionization as a consequence of the resonant photoexcitation of $2p_{3/2}$ electrons to the partially filled O_4 and O_5 subshells. The binding energy of the 5d electrons is about 6.6 *eV* [116], which justify the 9555 *eV* energy of the $L_3 \rightarrow O_{4,5}$ transition. In the same way, the structure at 9567 *eV*, that represents 6 *eV* above the L_3 edge for photoionization of Hf [116], could be explained as a double transition of $2p_{3/2}$ and $5d_{3/2}$ electrons to the continuum, leading to an enhanced L_3 vacancies production. But the width of the 9567 *eV* peak seems to be small, suggesting a photonuclear resonant absorption process, most probably to the NEET-nuclear level. This level is not yet known and further research would be needed in order to describe the correct mechanism. Also, not well understood is the structure peaking at about 9572 *eV*.

The maximum of the Nuclear-XAFS excitation function of the GSB members is located near 9567 *eV*. Similar structure was identified for the excitation function of a new γ-line near 130 *keV*. Confidence limits of 6.3 σ and 12 σ were established for the observations of the maximum at 9567 *eV* [64, 65]. Over the range of X-ray energies 9555.6 *eV* to 9568.9 *eV* - corresponding to the main peak in photoionization at the L_3 edge - the average enhancement of the GSB members was established to be 0.68% [64, 65]. At the level of irradiation flux of 6.5×10^{10} *photons/cm^2/s* the established enhancement represents a probability of the Nuclear-XAFS of about 1.6×10^{-3} [64] relative to the L_3 photoionization probability, which is in reasonable agreement with the value of 0.2% previously reported [63].

The timing measurements in SR facilities have been strongly hindered by the EMI noises collected by the sensitive timing electronics. In this work was presented only a set of timing data acquired at SLS-PSI SR source, when the level of noises was lower. The data suffers from statistical significance, but still indicates - by comparison with the pattern of the bunches in the ring - that the

induced decay of the 16^+ isomeric level with incident photons having energies near the L_3 photoionization threshold is occurring fast, in the order of few *ns* [64, 65] .

Another mechanism for inducing the gamma emission by X-ray photons was discovered in year 2004 during a set of experiments conducted at the BL09XU beamline. In those experiments the SR beam tuned a range of fundamental harmonic energies from 9.555 *keV* to 9.575 *keV,* with an incident flux at sample of 2×10^{12} *photons/cm*^{2}*/s*. It was the first time when a large subject of γ-energies up to 2500 *keV* was acquired. The experiments, part of the chapter 7 in this dissertation, lead to the discovery of two new γ-transitions at 642.5 *keV* and 2457.20 *keV*. Their detection was established with a confidence limit of 4.4σ and 6.5σ [66], respectively. The 642.5 *keV* transition could have commenced similarly as the 130.2 *keV* γ-line, a member of the induced decay via L_3-shell complex. The 2457.2 *keV* should have been the direct transition to the ground state of a level lying at about 11.15 *keV* above the 16^+ isomeric state, which was excited by a different mechanism than 130.2 *keV* and 642.5 *keV* transitions. That is because the fundamental harmonic photons of the SR beam had not enough energy to induce the 11.15 transition. There are instead evidences that off-axis superior harmonics components played an important role in the triggering process [66], while a 5 times stronger induced gamma emission of the GSB members was observed on off-axis positions of the isomeric target. The supposed mechanism is a multi-order process initiated by a second harmonic photon, leading to the excitation of the isomer to the 2457.2 *keV* level. A decay branch from it consists of a direct transition to the ground state and other decay branches lead to the enhancement of the GSB members. There is also the possibility that the 2457.2 *keV* was populated by a decay branch from a trigger level lying at a higher energy, the latest one could been excited also by a higher harmonic component of the SR beam. Although the 2457 *keV* transition was excited accidentally, the dumping of the *m2* isomer was very efficient. In order to definitely identify the trigger level which was

involved, a future nuclear resonance experiment with incident X-ray photons tuned near 11.15(27) *keV* and higher should search for resonance in the X-ray absorption spectrum that corresponds to the transition of the isomeric nucleus to the trigger level. If so, then almost the entire energy stored by the isomeric nucleus plus the triggering energy could be released by a single transition, such as the 2457 *keV* transition.

One more mechanism for inducing the energy release of the *m2* isomer of ^{178}Hf nucleus has been identified during an experiment conducted in year 2002 at the BL01B1 beamline. The experiment revealed a trigger level lying at about 2466.8 *keV* [115]. This level, not observed before, was excited by the 20,825 *eV* X-ray photons. The gamma emission from the many members of the natural decay path was thus enhanced. The excitation functions of the 8^- and GS band members are similar at those excitation energies, peaking at about 20,825 *eV*. This fact was identified with a confidence limit of 4.8 σ. The FWHM of the gaussian that fits the peak of the excitation function at 20,825 *eV* is about 1.7(3) *eV*, a value which is much smaller than the usual value of the width of the processes involving atomic inner-shell electrons. It may be explained by a direct nuclear photoexcitation process of the isomeric nucleus to the 2466.8 *keV* intermediate state. A decay branch from this gateway is feeding members of the $K^{\pi} = 8^-$ band, especially the 11^- state, resulting in a stronger enhancement of the 495 *keV* and 257 *keV* in comparison with the transitions starting from 13^- level, such as the 574 *keV* transition[115]. The energy release is thus retarded by the 4 second statistical lag of the *m1* isomeric level, member of the induced decay in this case.

It can be stated, as the main conclusion of this work, that there are at least three mechanisms through which the irradiation with X-rays of a sample containing ^{178}Hf^{m2} isomeric nuclei can accelerate the emission of gamma photons from it, and the results depend upon the distributions of energies of the incident X-rays. The energy release can be fast if the incident X-ray photons have

energy near the photoionization threshold of the $2p_{3/2}$ electrons surrounding the isomeric nucleus, and can be retarded by the 4 second statistical lag of the *m1* isomeric level if the $^{178}Hf^{m2}$ isomeric sample is impinged by X-ray photons with energy near the 20,825 *keV* resonance. Fast energy release may be expected also from the 2457.2 *keV* trigger level excited by resonant 11.15 *keV* X-ray photons.

This research offer a much deeper understanding of the processes governing the induced gamma emission by soft X-ray photons of $^{178}Hf^{m2}$ and brings a step forward to the development of a new generation of energy storage devices at the nuclear scale with controlled release of stored energy.

REFERENCES

1. A. S. Eddington, *The Internal Constitution of the Stars*, Cambridge Univ. Press, London (1926).
2. H. Roberts, Hyp. Interact. 107, 91 (1997)
3. S. Soloway et al., Am. Nucl. Soc. Trans. 75, 20 (1996).
4. C. B Collins et al., Laser Phys. 9, 1 (1999).
5. P. M. Walker et al., Nature 399, 35 (1999).
6. P. M. Walker et al., Hyp. Interact. 135, 83 (2001).
7. P. M. Walker, Hyp. Interact. 143, 143 (2002).
8. J. J. Carroll et al., Hyp. Interact. 135, 3 (2001).
9. G. C. Baldwin et al., Rev. Mod. Phys. 53 (4), Part I, 687 (1981).
10. C. B. Collins et al., J. Appl. Phys. 53, 4645 (1982).
11. C. B. Collins, Hyp. Interact. 107, 3 (1997).
12. J. J Carroll et al., Phys. Rev. C 43, 1238 (1991).
13. C. B. Collins et al., Phys. Rev. C 37, 2267 (1988).
14. M. Morita, Prog. Theor. Phys. 49, 1574 (1973).
15. K. Otozoi et al., Nucl. Phys. A 297, 97 (1978).
16. S. Matinyan, Phys. Rep. 298, 199 (1998).
17. M. Breining, et al., Phys. Rev. A 22, 520 (1980).
18. R.G. Helmer et al., Nucl. Phys. A 114, 649 (1968).
19. R.G. Helmer et al., Nucl. Phys. A 211, 1 (1973).
20. C. B. Collins et al., Laser Inter. Related Plasma Phenom. 10, 151 (1995).
21. C. B. Collins et al., Laser Phys. 5, 280 (1995).
22. C. B. Collins et al., Phys. Rev. Lett. 82, 695 (1999).
23. C. B. Collins et al., Laser Phys. 9, 8 (1999).
24. E. Rutherford, Phil. Mag. 21, 669 (1911).

25. M. G. Mayer and J. H. D. Jensen, *Elementary Theory of Nuclear Shell Structure*, John Wiley & Sons Inc., New York (1955).

26. A. Bohr and B. M. Mottelson, *Nuclear Structure Vol. I*, W. A. Benjamin Inc., New York (1969).

27. A. Bohr and B. M. Mottelson, *Nuclear Structure Vol. II*, W. A. Benjamin Inc., New York (1975).

28. K. Siegbahn, *Alpha-, Beta- and Gamma-Ray Spectroscopy*, North-Holland (1965).

29. R. D. Woods et al., Phys. Rev. 95, 577 (1954).

30. K. S. Krane, *Introductory Nuclear Physics*, Wiley (1988).

31. S. G. Nilsson et al., Nucl. Phys. A 131, 1 (1969).

32. R. Bengtsson et al., Phys. Scr. 39, 196 (1989).

33. K. Narimatsu et al., Nucl. Phys. A 601, 69 (1996).

34. F. S. Stephens, Rev. Mod. Phys. 47, 43 (1975).

35. I. I. Sobelman, L. A. Vainshtein, and E. A. Yukov, *Excitation of Atoms and Broadening of Spectral Lines*, Springer, Berlin (1981).

36. V. I. Goldanskii et al., JETP Lett. 23, 451 (1976).

37. V. I. Goldanskii et al., Phys. Lett. B 62, 393 (1976).

38. Y. Ho et al., Phys. Rev. C 44, 1910 (1991).

39. Y. Ho et al., Phys. Rev. C 48, 2277 (1993).

40. K. Okamoto, Nucl. Phys. A 341, 75 (1980).

41. Y. Izawa et al., Phys. Lett. B 88, 59 (1979).

42. V.I. Goldanskii et al., Sov. J. Nucl. Phys. 33, 169 (1981).

43. Z. S Yuan et al., Phys. Rev. C 47, 323 (1993).

44. M. R. Harston, Nucl. Phys. A 690, 447 (2001).

45. T. Carreyre et al., Phys. Rev. C 62, 024311 (2000).

46. E. V. Tkalya, AIP Conf. Proc. 506, 486 (2000).

47. I. S. Batkin, Sov. J. Nucl. Phys. 29, 464 (1979).

48. A. Ljubicic et al., Phys. Rev. C 23, 2238 (1981).

49. R. J. Glauber et al., Phys. Rev. 104, 158 (1956).

50. E. V. Tkalya et al., Phys. Atom. Nucl. 59, 779 (1996).

51. E. V. Tkalya et al., Phys. Scripta 53, 296 (1996).

52. I. S. Batkin et al., Yad. Phys. 32, 972 (1980).

53. K. Pisk et al., Phys. Rev. C 25, 2226 (1982).

54. E. V. Tkalya, Phys. Usp., 46 (3), 315 (2003).

55. D. Kekez et al., Phys. Rev. Lett. 55, 1366 (1985).

56. D. Kekez et al., Phys. Rev. C 34, 1446 (1986).

57. H. Mazaki et al., Phys. Rev. C 5, 1718 (1972).

58. H. Mazaki et al., Phys. Rev. C 21, 344 (1980).

59. J. A. Cooper et al., Phys. Rev. Lett. 15, 680 (1965).

60. K. Aoki et al., Phys. Rev. C 64, 044609 (2001).

61. S. Kishimoto et al., Phys. Rev. Lett. 85, 1831 (2000).

62. H. Fujioka et al., Z. Phys. A 315, 121 (1984).

63. C. B. Collins et al., Europhys. Lett. 57, 677 (2002).

64. C. B. Collins et al., Laser Phys. 14, 154 (2004).

65. C. B. Collins et al., Radiation Phys. and Chem. 71, 619 (2004).

66. C. B. Collins et al., in press, Laser Phys. Lett. (2004).

67. E. V. Tkalya, Sov. Phys. Dolk. 35 (12), 1069 (1990).

68. T. Shizuma et al., J. Nucl. Sci. Tech. 39 (11), 1137 (2002).

69. C. B. Collins et al., Hyp. Interact. 107, 141 (1997).

70. C. B. Collins et al., Phys. Rev. C. 61, 054305 (2000).

71. N. A. Dyson, *X-rays in atomic and nuclear physics*, Longman Group Limited, London (1973).

72. N. Hosoda et al., eConf C011127:TUAP046 (2001).

73. M. Böge et al, *The Swiss Light Source Accelerator Complex: An Overview*, EPAC98, Stockholm (1998).

74. T. Uruga et al., J. Synchrotron Rad. 6, 143 (1999).

75. Y. Yoda et al., Nucl. Inst. and Meth. A 467–468, 715 (2001).

76. SLS-MS beamline web page, *http://sls.web.psi.ch/view.php/beamlines/ms/index.html*.

77. G. Mulhaupt, Hyp. Interact. 123/124, 13 (1999).

78. T. Yoshida et al., J. Phys. Chem. 100, 2302 (1996).

79. K. Nishi et al., J. Phys. Chem. B 102, 10190 (1998).

80. Ortec, *Modular Pulse Processing-Electronics* (2003).

81. G. F. Knoll, *Radiation detection and measurement*, Wiley and Sons, New York (1979)

82. E. M. Gullikson et al., Appl. Opt. 34, 4662 (1995).

83. J. P. Pansart, Nucl. Instr. and Meth. A 387, 186 (1997).

84. A. Q. R. Baron et al., Nucl. Instr. Meth. A 343, 517 (1994).

85. S. Kishimoto, Nucl. Inst. and Meth. A 397, 343 (1997).

86. S. Kishimoto, Rev. Sci. Instrum. 63 (1), 824 (1992).

87. S. Kishimoto, Rev. Sci. Instrum. 66 (2), 2314 (1995).

88. T. S. Toellner et al., Nucl. Inst. and Meth. A 350, 595 (1994).

89. C. M. B. A. Correia et al., Nucl. Instr. and Meth. A 290, 445 (1990).

90. J. B. Simoes, et al., Nucl. Instr. Meth. A 422, 405 (1999).

91. N. Reguigui, et al., Appl. Rad. Isotopes 56, 93 (2002).

92. National Instruments Inc., *Measurement and Automation Catalogue* (2001).

93. C. B. Collins, in *Proc. of the First International Induced Gamma Emission Workshop IGE '97* edited by I. I. Popescu and C. A. Ur (IGE Foundation, Bucharest, Romania, 1999), 1-17.

94. Further exploration of these nuclear analogies is available at the URL: *http://www.utdallas.edu/research/quantum/isomer/tutorial.htm.*

95. I. Ahmad et al., Phys. Rev. Lett., 87, 072503 (2001).

96. E. Browne, Nucl. Data Sheets 72, 221 (1994).

97. C. T. Chantler, J. Phys. Chem. Ref. Data 24, 71 (1995).

98. P. M. Walker et al., Phys. Rev. Lett. 65, 416 (1990).

99. D. Belic et al., Phys. Rev. Lett. 83, 5242 (1999).

100. S. Olariu et al., Hyperfine Interact. 135, 71 (2001).

101. C. B. Collins et al., Hyperfine Interact. 135, 51 (2001).

102. C. B. Collins et al., J. Phys. IV 11, Pr2-437 (2001).

103. S. Olariu et al., Phys. Rev. Lett. 84, 2541 (2000).

104. D. P. McNabb et al., Phys. Rev. Lett. 84, 2542 (2000).

105. P. von Neumann-Cosel et al., Phys. Rev. Lett. 84, 2543 (2000).

106. C. B. Collins et al., Phys. Rev. Lett. 84, 2544 (2000).

107. D. E. Sayers et al., in *X-Ray Absorption:Principles, Applications, and Techniques of EXAFS, SEXAFS, and XANES,* Ed. by D. C. Koningsberger and R. Prins (Wiley, New York, 1988), Vol. 92.

108. W. J. Campell et al., Anal. Chem. B 74, 248R (1970).

109. S. Emura et al., Phys. Rev. B 47, 6918 (1993).

110. I. Ahmad et al., Phys. Rev. C 67, 041305R (2003).

111. S. Y. F. Chu, L. P. Ekström, and R. B. Firestone, *Isotope Explorer*, Version 2.2 (1998).

112. J. C. Sheppard, *Helical Undulator Radiation*, NLC Note LCC-0095 (2002).

113. J. A. Bearden, Rev. Mod. Phys. 39, 78 (1967).

114. S. Emura et al., *Possibility of XAFS Spectra Detection by NEET – Nuclear XAFS* -, 12th Int. Conf. on X-ray Absorption Fine Structure, Malmö, Sweden, June 22 - 27, A9340, 58 (2003).

115. N. C. Zoita et al., *The use of selected monochromatic X-rays to induce a cascade of gamma transitions from the 31-year nuclear isomer to the 4 second isomeric state of Hf-178*, UVX-2004, St-Etienne, France, June 7 - 11 (2004).

116. J. A. Bearden et al., Rev. Mod. Phys. 39, 125 (1967).

VITA

Nicolae Catalin Zoita was born in Falticeni, Suceava County, Romania, on February 16, 1972, the son of Neculai Zoita and Ileana Zoita. He graduated from the “Stefan cel Mare” High School, Suceava, Romania, in June 1990. In July 1990 he entered the University of Bucharest, Faculty of Physics, Romania and he graduated in June 1995. One year later, after satisfying his mandatory military duties, he was employed as researcher in the Institute of Optoelectronics (IOEL-SA), Bucharest, Romania and he transferred in the National Institute for Optoelectronics (INOE-2000), Bucharest, Romania in January 1997. In August 1998 he became scientific researcher at the same institute. In September 1999 he entered the Doctoral Program at the University of Texas at Dallas (UTD), Richardson, Texas. In August 2002 he married Carmen Angela Ionescu. In June 2004 he was employed as Research Associate at the Center for Quantum Electronics of the University of Texas at Dallas.